MODELLING AND SIMULATION OF THIN FILM SEMICONDUCTOR METAL OXIDE GAS SENSOR RESPONSE

A THESIS SUBMITTED TO
THE GRADUATE SCHOOL OF NATURAL AND APPLIED SCIENCES
OF
MIDDLE EAST TECHNICAL UNIVERSITY

BY

BERKAN ATMAN

IN PARTIAL FULFILLMENT OF THE REQUIREMENTS
FOR
THE DEGREE OF MASTER OF SCIENCE
IN
CHEMICAL ENGINEERING

SEPTEMBER 2019

Approval of the thesis:

MODELLING AND SIMULATION OF THIN FILM SEMICONDUCTOR METAL OXIDE GAS SENSOR RESPONSE

submitted by **BERKAN ATMAN** in partial fulfillment of the requirements for the degree of **Master of Science in Chemical Engineering Department, Middle East Technical University** by,

Prof. Dr. Halil Kalıpçılar
Dean, Graduate School of **Natural and Applied Sciences** _____

Prof. Dr. Pınar Çalık
Head of Department, **Chemical Engineering** _____

Prof. Dr. Yusuf Uludağ
Supervisor, **Chemical Engineering, METU** _____

Prof. Dr. Gürkan Karakaş
Co-Supervisor, **Chemical Engineering Dept., METU** _____

Examining Committee Members:

Prof. Dr. Halil Kalıpçılar
Chemical Engineering Dept., METU _____

Prof. Dr. Yusuf Uludağ
Chemical Engineering, METU _____

Prof. Dr. Gürkan Karakaş
Chemical Engineering Dept., METU _____

Assist. Prof. Dr. İnci Ayrancı Tansık
Chemical Engineering Dept., METU _____

Assoc. Prof. Dr. Berna Topuz
Chemical Engineering Dept., Ankara University _____

Date: 09.09.2019

I hereby declare that all information in this document has been obtained and presented in accordance with academic rules and ethical conduct. I also declare that, as required by these rules and conduct, I have fully cited and referenced all material and results that are not original to this work.

Name, Surname: Berkan Atman

Signature:

ABSTRACT

MODELLING AND SIMULATION OF THIN FILM SEMICONDUCTOR METAL OXIDE GAS SENSOR RESPONSE

Atman, Berkan
Master of Science, Chemical Engineering
Supervisor: Prof. Dr. Yusuf Uludağ
Co-Supervisor: Prof. Dr. Gürkan Karakaş

September 2019, 122 pages

Metal oxide based semiconductor gas sensors have attracted attention due to their superior properties. Over past five decades an extensive research had been conducted for understanding the true nature of the sensing mechanism, most suitable material and optimum operating conditions. SnO_2 has received over years a great deal of attention as it can meet most of the necessary requirements of a gas sensor. Although commercially available gas sensors based on tin oxide are available and plenty of studies has been devoted to tin oxide based gas sensors, still there are many questions remained unanswered or have unsatisfactory explanations. In this work by developing a mathematical model with a comprehensive approach it is aimed to address some of those questions in terms of effects of diffusion, kinetic parameters, film thickness on complex dynamic behavior of the n- type semiconductor gas sensors in an environment being CO-air mixture. Furthermore, the constructed model provides an opportunity to analyze response/recovery dynamics in terms of electrical current obtained from current density distribution. The results of the simulations based on the transient model shows that increasing the thickness significantly reduces the sensitivity whereas slightly decreases the response time. The effect of diffusion on concentration profiles and current density distributions and their consequences are

extensively discussed. Elevated temperature resulted in lower response and recovery times of the sensors. The temperature dependence of sensitivity was explained in terms of the competitive effect of activation energies of the surface kinetics and diffusion effect.

Keywords: Semiconductor Gas Sensor, Mathematical Modelling, CO Sensing, Tin Oxide, Dynamic Response

ÖZ

İNCE FİLM METAL OKSİT YARI İLETKEN GAZ SENSÖR TEPKİSİNİN MODELLENMESİ VE SİMÜLASYONU

Atman, Berkan
Yüksek Lisans, Kimya Mühendisliği
Tez Danışmanı: Prof. Dr. Yusuf Uludağ
Ortak Tez Danışmanı: Prof. Dr. Gürkan Karakaş

Eylül 2019, 122 sayfa

Metal oksit bazlı yarı iletken gaz sensörleri üstün özellikleri nedeniyle dikkat çekmiştir. Son elli yılı aşan süredir algılama mekanizmasının gerçek doğasını, en uygun materyali ve optimum çalışma koşullarını anlamak için kapsamlı bir araştırma yapılmıştır. SnO_2, yıllar içinde bir gaz sensörünün gerekli gereksinimlerinin çoğunu karşılayabileceği için büyük ilgi görmüştür. Her ne kadar kalay oksite dayalı ticari olarak temin edilebilen gaz sensörleri mevcut olsa da ve kalay oksit bazlı gaz sensörlerine yönelik birçok çalışma adanmış olmasına rağmen, hala cevaplanmamış ve yetersiz açıklamaları olan birçok soru vardır. Bu çalışmada, kapsamlı bir yaklaşıma sahip matematiksel bir model geliştirerek, CO-hava karışımı ortamında bir n-tipi yarı iletken gaz sensörünün karmaşık dinamik davranışı üzerine difüzyon, kinetik parametreler, film kalınlığı etkileri yönünden o sorulara değinilmesi amaçlanmıştır. Ayrıca oluşturulan model, tepki/geri kazanım dinamiklerini, akım yoğunluğu dağılımından elde edilen elektrik akımı açısından analiz etme imkanı sunar. Zaman bağlı modele dayalı simülasyonların sonuçları, kalınlığın arttırılmasının hassasiyeti önemli ölçüde azalttığını, buna karşılık tepki süresini biraz azalttığını göstermektedir. Difüzyonun konsantrasyon profilleri ve akım yoğunluğu dağılımları üzerindeki etkileri ve bunların neticeleri kapsamlı bir şekilde tartışıldı. Yüksek sıcaklık,

sensörlerin daha düşük tepki ve geri kazanım süreleriyle sonuçlandı. Hassasiyetin sıcaklık bağımlılığı, yüzey kinetiğinin aktivasyon enerjilerinin rekabetçi etkileri ve difüzyon etkisi yönünden açıklanmıştır.

Anahtar Kelimeler: Yarı İletken Gaz Sensör, Matematiksel Modelleme, CO Algılama, Kalay Oksit, Dinamik Tepki

To my beloved family,

ACKNOWLEDGEMENTS

First and foremost, I would like to express my sincere graduates to my advisors. It was a great privilege and honor to study under their supervision. I would like to thank Prof. Dr. Yusuf Uludağ for his patience guidance, encouragements, insight and useful critiques during the research studies. I would like to express my very great appreciation to Prof. Dr. Gürkan Karakaş for his valuable and constructive suggestions during planning and development of this research work.

I would like to thank my dissertation committee: Prof. Dr. Halil Kalıpçılar, Assist. Prof. Dr. İnci Ayrancı Tansık, Assoc. Prof. Dr. Berna Topuz for their valuable suggestions and constructive criticism.

I extend my sincere thanks to my colleagues: Güvenç Oğulgönen, Atalay Çalışan, Mustafa Yasin Aslan, Soner Yaşar, Özge Batır, Ezgi Gözde, Berrak Erkmen, Neslin Güler, Canan Aksoy, Abdullah Keskin, Öznur Doğan, Salih Ermiş and Betül Oflaz. In particular, I would like to thank Ezgi Yavuzyılmaz, Merve Özkutlu, Seda Sivri, Merve Sarıyer, Fatma Şahin and Zeynep Karakaş for their being not only my colleagues but also perfect friends with undeniable trust. I would like to give my special thanks to my dear friend Burak Akdeniz for being a companion during hard times.

I wish to state my thanks to friends with whom I met during my master's study: Nur Ber Emerce, Beril Dumanlılar, Orhun Kahraman and Gökhan Gök. I would like to express my deepest appreciation to my friends from undergraduate years: Umut Arat, Taylan Mor, Ufuk Arat, Seren Alpan, Tayfun Elmalı and Emin Küçük.

Last but never the least, I would like to thank my parents Emine Atman, Tuncay Atman and my big brother Fırat Atman for their endless trust, patience, support and love.

TABLE OF CONTENTS

ABSTRACT v

ÖZ… vii

ACKNOWLEDGEMENTS x

TABLE OF CONTENTS xi

LIST OF TABLES xiii

LIST OF FIGURES xiv

LIST OF ABBREVIATIONS xviii

LIST OF SYMBOLS xix

CHAPTERS

1. INTRODUCTION 1

2. LITERATURE REVIEW 11

3. MODEL DESCRIPTION 29

3.1. The Conductance Model for the Polycrystalline Porous Medium 33

3.2. The Transport of the Target Gas and Reaction Kinetics 36

3.3. Electrical Current Analysis 40

3.4. COMSOL Multiphysics 43

3.4.1. Study and Solver Configurations 44

3.4.2. Mesh Studies 44

3.5. Model Parameters 49

4. RESULTS AND DISCUSSION 51

4.1. Transient Analysis of the CO Sensing of SnO_2 Film in Oxygen Environment 53

4.2. Effect of Temperature 64
4.2.1. Initial Values of Ionixed Oxygen, Conductance and Resistance at the Operating Temperatures 65
4.2.2. Effect of Temperaure on the Conentration, Conductance and Potential Barrier Distributions 66
4.2.3. Temperature Effect On The Dynamic Response and Sensitivity 78
4.3. Film Thickness Effect 84
4.4. Response and Recovery Analysis 97
4.5. Ambient CO Concentration Effect On Response 102
5. CONCLUSION 105
REFERENCES 109

LIST OF TABLES

TABLES

Table 1-1. Environmental aspects of various gases and metal oxide semiconductor materials for their detection.[6–12] 2
Table 1-2. Conductance types, operating temperatures and target gases of common n-type materials and their comparison.[6–9] 6
Table 3-1. List of parameters used in the mathematical model. 50
Table 4-1. Initial values of ionized oxygen, conductance and resistance at different operating temperatures. 66
Table 4-2. Effect of temperature on the response time and the time required to reach steady state of an n-type 10 μm thick SnO_2 film continuously to 0.00814 mol/m^3 CO in an excess oxygen ambient. 81
Table 4-3. Temperature effect on the steady state spatially averaged conductance and normalized response values for SnO_2 film have thickness of 10μm pore diameter of 1nm. (x=500μm) 84
Table 4-4. Film Thickness effect on the response times of SnO_2 sensing films for a step change in CO concentration of 0.00814 mol/m^3 at t=0 in an excess oxygen ambient (T=300°C). 96
Table 4-5. Response and recovery times of SnO_2 film with pore size of 4nm for different temperatures between 300-600°C during step changes in CO concentration in an excess oxygen ambient. 102

LIST OF FIGURES

FIGURES

Figure 1-1. Schematic representation of classical Taguchi-typed gas sensors: a) Planar configuration; b) Cylindrical configuration. 7
Figure 1-2. The schematic of SnO_2 based gas sensor fabricated with CMOS technology on a micro hotplate: a) Side view schematics of the gas sensor; b) Top view of the microhotplate with circular heated area on the dielectric membrane; c)SEM image of the SnO_2 thick film.[33] 8
Figure 2-1. Schematic representation of the potential barrier developed at grain boundary of two adjacent grains in a polycrystalline metal oxide semiconductor. ... 15
Figure 2-2. Synthesis of thin/thick film SnO_2 by sol-gel method and deposition on substrates 20
Figure 2-3. Kinetic mechanisms for the CO interaction with SnO_2: 1) Oxygen vacancy mechanism; 2) Eley-Rideal mechanism; 3) Langmuir-Hinshelwood mechanism; 4) Ionization of CO in the absence of oxygen or low oxygen pressure ambient. 27
Figure 3-1. Simple representation of the polycrystalline metal oxide semiconductor gas sensor exposing to carbon monoxide in air ambient. 30
Figure 3-2. The representation of the rectangular geometry used in the model with the boundary conditions 37
Figure 3-3. Three dimensional representation of the gas sensor device. 41
Figure 3-4. The schematic representation of the cross-sectional area perpendicular to the current direction on a cut plane from the three dimensional representation of the gas sensor. 42
Figure 3-5. The parameters of the mesh element size for free triangular meshes. .. 45
Figure 3-6. Dense construction of free triangular meshes in the rectangular domain. 46

Figure 3-7. Statistical information of the complete mesh for free triangular meshes. 46
Figure 3-8. The parameters of the mesh element sizes for mapped meshes. 47
Figure 3-9. Dense construction of mapped mesh in rectangular domain.....48
Figure 3-10. Statistical information of the complete mesh for mapped meshes.....48
Figure 4-1. Transient analysis of the CO concentration profile development in 15μm thick film at T=300°C. Response to the step change of CO concentration of 0.00814 mol/m^3 in an excess oxygen environment at t=0. 54
Figure 4-2. Transient analysis of the ionized oxygen density [O^-] in 15 μm thick SnO_2 film at T= 300°C. Response to the step change of CO concentration of 0.00814 mol/m^3 at t=0. 56
Figure 4-3. The change in the local conductance (G) with time and its variation along the z (thickness) direction in 15μm SnO_2 sensing film at T=300 °C. Response to the step change of CO concentration of 0.00814 mol/m^3 at t=0 in an excess oxygen ambient. ($Gi = 9.31 \times 10 - 5$) 58
Figure 4-4. The x-component of the current density (J_x) profile development in 15μm thick SnO_2 film at T=300°C. Response to the step change of CO concentration of 0.00814 mol/m^3in an excess oxygen ambient at t=0. ($x = 500$ μm) 59
Figure 4-5. The normalized response of the 15 μm thick SnO_2 film during exposure of carbon monoxide an excess oxygen ambient at T= 300 °C. Step change in CO concentration of 0.00814 mol/m^3 at t=0. (x=500 μm) 61
Figure 4-6. Electric current signal response of the 15 μm thick SnO_2 sensing film to carbon monoxide in excess oxygen ambient at T= 300 °C. Response to the step change of CO concentration of 0.00814 mol/m^3 at t=0.....62
Figure 4-7. The arrow representation of the current density for 15 μm thick SnO_2 film response to the step change of CO concentration of 0.00814 mol/m^3 in an excess oxygen ambient at times: a) t=30 s; b)60 s; c)90 s; d)120s. Note that the scales for the arrows are same. (T=300 °C) 63
Figure 4-8. The steady state CO concentration distributions in the 10 μm SnO_2 film at temperatures between 150-600 °C for pore diameters :a)4nm; b)1nm. 68

Figure 4-9. The steady state ionized oxygen concentration distributions in the 10 μm SnO_2 film at different temperatures for pore diameters: a) 4 nm; b)1nm. 71
Figure 4-10. Temperature effect on the steady state potential barrier profiles for 10 μm thick SnO_2 film which has pore diameter of 1nm. 75
Figure 4-11. Two dimensional representation of the steady state consumption rates of CO at operating temperatures between 423-873K. Results were obtained for a step change of CO concentration of 0.00814 mol/m^3 in an excess oxygen ambient at t=0. 77
Figure 4-12. Effect of temperature on the transient response of the 10 μm SnO_2 sensing film to step change in CO concentration of 0.00814 mol/m^3 in terms of electrical current. (x=500 μm) 79
Figure 4-13. Effect of temperature on the transient normalized response of the 10 μm SnO_2 sensing film to the step change of CO concentration of 0.00814 mol/m^3in an excess oxygen ambient at t=0. (r=1nm). 82
Figure 4-14. Steady state concentration distributions of CO in SnO_2 films have thicknesses of: a) 5μm; b)10 μm; c)15 μm; d)20 μm; e)50 μm f)100 μm. The results were obtained for a step change of 0.00814 mol/m^3 in CO concentration at t=0 and at T=300 °C 86
Figure 4-15. Steady state concentration distribution of ionized oxygen in SnO_2 films have thicknesses of: a) 5μm; b)10 μm; c)15 μm; d)20 μm; e)50 μm; f)100 μm. SnO_2 sensing films were exposed to 0.00814 mol/m^3 CO in an excess oxygen environment at 300 °C. (x=500μm) 87
Figure 4-16. The effect of film thickness on the steady state potential energy barrier distribution for the SnO_2 films at 300 °C exposed to 0.00814 mol/m^3 CO in an excess oxygen environment. (x=500μm) 89
Figure 4-17. Steady state potential energy distributions and arrow representation of the current density for SnO_2 films having thicknesses of: a) 5μm; b)10 μm; c)15 μm; d)20 μm; e)50 μm; f)100 μm. The SnO_2 films were exposed to CO concentration of 0.00814 mol/m^3 in an excess oxygen environment at 300 °C. 5 V DC electric potential

was applied with point electrodes from both sides of the sensing film with DC supplier. 91
Figure 4-18. The effect of film thickness on the dynamic current response to the step change in CO concentration of 0.00814 mol/m^3 in an excess oxygen ambient at 300°C. 5 V DC electric potential applied through point electrodes at both sides of the SnO_2 sensing films. ($x = 500$ μm). 93
Figure 4-19. Effect of film thickness on the normalized response $G - Gi/Gi$ of SnO_2 sensing films for a step change of 0.00814 mol/m^3 in CO concentration in an excess oxygen environment at t=0.(x=500 μm) 95
Figure 4-20. Steady state normalized responses of the SnO_2 films having different thicknesses to exposing CO continuously in an excess oxygen ambient. 97
Figure 4-21. Response/recovery analysis of 10μm thick SnO_2 films having 1 nm pore diameter to step changes of carbon monoxide concentration in an excess oxygen ambient at 350 °C. 99
Figure 4-22. The effect of the temperature on the response/recovery dynamics for 10 μm thick SnO_2 film initially exposed to CO concentration of 0.00814 mol/m^3 in an excess oxygen ambient. 100
Figure 4-23. The effect of the ambient concentration of carbon monoxide on the steady state electric current response of 10 μm thick SnO_2 gas sensor having pores with 4 nm diameter in an excess oxygen environment. 103
Figure 4-24. The effect of the ambient concentration of carbon monoxide on the steady state electric current response of 10 μm thick SnO_2 gas sensor having pores with 1 nm diameter in an excess oxygen environment. 104

LIST OF ABBREVIATIONS

ABBREVIATIONS

AC	Alternating Current
CMOS	Complementary Metal Oxide Semiconductor
DAEs	Differential Algebraic Equations
DC	Direct Current
ODE	Ordinary Differential Equation

LIST OF SYMBOLS

SYMBOLS

a	Specific surface area, $m^2\ g^{-1}$ or m^{-1}
Av	Avogadro number, mol^{-1}
C	Concentration, mol m^{-3}
C_s	Surface concentration of carbon monoxide, mol m^{-3}
D	Grain diameter, nm
$D_{k,eff}$	Effective Knudsen diffusion coefficient, $m^2\ s^{-1}$
E_F	Fermi energy level, eV
E_I	Intrinsic Fermi energy level, eV
$\overline{E}_1$	Activation energy of forward reaction oxygen chemisorption step, J
$\overline{E}_{-1}$	Activation energy of reverse reaction of oxygen chemisorption step, J
$\overline{E}_2$	Activation energy of forward reaction oxygen ionization step, J
$\overline{E}_{-2}$	Activation energy of reverse reaction of ionization of oxygen, J
$\overline{E}_3$	Activation energy of carbon monoxide reaction with ionized oxygen, J
q	Electron charge, C
e^-	Conduction band electron
h	Thickness of the film, μm
I	Current, A
G	Conductance, S

G_n	Carrier generation, m^{-3}
L	Debye length, nm
M	Molecular weight, g mol^{-1}
N	Density of atoms/ions, m^{-2}
N_A	Density of ionized acceptor, m^{-3}
N_D	Density of ionized donors, m^{-3}
N_S	Number of localized surface states, m^{-2}
n_S	Electron density, electron m^{-3}
r	Pore radius, nm
R	Gas constant, J mol^{-1} K^{-1}
$\Re$	CO reaction rate, mol m^{-3} s^{-1}
R_i	Initial resistance, Ω
k_B	Boltzmann's Constant, J K^{-1}
$k_{1,0}$	Pre-exponential constant of forward reaction oxygen chemisorption
$k_{-1,0}$	Pre-exponential constant of reverse reaction oxygen chemisorption
$k_{2,0}$	Pre-exponential constant of forward reaction of ionization of oxygen
$k_{-2,0}$	Pre-exponential constant of reverse reaction of ionization of oxygen
$k_{3,0}$	Pre-exponential constant of carbon monoxide reaction with ionized oxygen
l	Depth of the film, μm
J_n	Current density in n direction, A m^{-2}

J_z	Current density in z direction, A m^{-2}
T	Temperature, K
t_{90}	Response time, s
S	Vacant surface site of SnO_2, m^{-2}
s	Time, s
V	Electric potential, V
V_s	Potential barrier, V
U_n	Carrier recombination, m^{-3}
w	Width of the film, μm
x_0	Depletion layer thickness

Greek Letters

ρ	Charge density, C m^{-3}
ϵ_0	Permittivity in a vacuum, F m^{-1}
ϵ_r	Dielectric constant of the material
ϵ	Permittivity of the material, F m^{-1}
ε	Porosity
τ	Tortuosity
μ	Electron mobility, cm^2 V^{-1} s^{-1}
σ	Conductivity, S m^{-1}
Φ	Potential, V
χ	Non-stoichiometric number

Subscripts

A	Bulk acceptor
b	Bulk electron
CO	Carbon monoxide
D	Bulk donor
i	Initial state for simulations
n	Refers to electrons
st.st	Steady state
O	Oxygen
p	Bulk hole
S	Localized surface state

CHAPTER 1

INTRODUCTION

In industry and everyday life environments detection and monitoring of various gases are critical. There is energy requirement for the heaters that are used at houses, in industry, power plants and vehicles which are mainly based on the combustion processes of fossil-fuels. Thus, emissions from mobile and stationary sources increase day-by-day. Also chemical plants contribute fugitive and stack emissions which include toxic and polluting gases. The necessity of monitoring oxygen for combustion systems, detection and control of flammable gases to prevent undesirable and unpredicted fires and explosions and detection of toxic gases leads significant amounts of gas sensor research and contribute its progress.[1,2] Security in public places such as airports, chemical industries, environmental monitoring, industrial-laboratory safety and breath analysis for diagnosis[3] are the major application fields of gas sensors.[4] These sensors are also used for the emission control of vehicles, humidity and air quality in houses and car ventilation systems[5]. The gas sensors are used for either for single gas detection like CO, NO_x, H_2, NH_3 and CH_4 or odor discrimination[4]. Also chemical warfare agents, volatile organic compounds (VOCs), ozone and SO_2 can also be detected by metal oxide gas sensors. The effects, sources and common materials for detection of the various gases given below in *Table 1-1*.

Table 1-1. Environmental aspects of various gases and metal oxide semiconductor materials for their detection.[6–12]

Gas	Sources	Effects	Sensing Material
CO	Incomplete combustion	Highly toxic	SnO_2, ZnO, TiO_2
NH_3	Agricultural Environment (Animal farms, fertilization)	Highly hazardous NH_4^+ production	ZnO, SnO_2, WO_3, TiO_2
NO_x	Combustion processes Industrial operations Transportation Fertilizers contains nitrogen	Acid rains Photochemical Smog Ozone production Toxic	WO_3, ITO for NO; SnO_2, WO_3 for NO_2; SnO_2, WO_3, ZnO for N_2O
H_2	Occurs in atmosphere naturally Leakage from the storage tanks Production from methane reforming and electrolysis	Leakage of hydrogen into air can cause explosions	ZnO, SnO_2
CH_4	Organic material digestion Storage for internal combustion engine fuel source	Explosive when reach high concentrations in case of trapped in close area	ZnO, SnO_2
H_2S	Crude petroleum & natural gas Volcano activities Organic material decomposition	Inhibit oxygen transport by chemically interacting with hemoglobin	WO_3 (remarkable sensitivity towards low concentrations at room temperature) In_2O_3, SnO_2, ZnO
CO_2	Hydrocarbon and fuel (contains carbon) combustion	Global warming Asphyxiation	SnO_2, ITO, LaOCl

There are different types of gas sensors such as field effect, piezoelectric, electrochemical, catalytic, optical and semiconductor gas sensors[13]. Solid-state semiconductor metal oxide based gas sensors are widely studied because of their advantages such as variety in application fields, low cost, sensitivity to various gases

at ppm or even ppb level concentrations, small size and easy integration, stability, flexibility and on-line operation opportunity. On the other hand, selectivity, long term drift and poisoning are the main problems for metal oxide semiconductors.[7,14]

Selectivity can be improved by membrane filters such as zeolite membranes and porous SiO_2 layers in order to avoid the cross interferences of the undesired gases. Also, the upper part of the membrane can be modified with layers that provide catalytic activity to non-targeted gases.[15] The signal of the semiconductor gas sensor can be obtained as either voltage or electrical current signal due to the resistance/conductance change of the sensing material in the presence of oxygen and target gases. The electron exchange between the bulk and surface states (localized energy levels) of the semiconductor determines this resistance/conductance change. The density of the surface states is influenced by the chemical and electrochemical interactions such as adsorption/desorption of gases and surface reactions. Therefore, the chemical activity of the surface is crucial for the response of the gas sensor. The active sites and activation energies of the chemical interactions have significant effect on the sensitivity and selectivity of the gas sensor. Modification of active sites of the semiconductor sensing material can increase sensitivity of the gas sensor towards specific gases. For this reason, in order to increase the selectivity to desired target gases different doping strategies are used. Also, operating the sensor at different modes and analyzing different sensor properties are other techniques for selective sensing.[6] Temperature modulation is one of those techniques since the surface kinetics are temperature dependent and the response behavior differs for particular species. In sensor arrays (also known as electronic noses) multiple signals from multiple different sensors are examined in simultaneously for a pattern recognition.[16]

Carbon monoxide has serious effects on human health. The irreversible binding of CO to hemoglobin in blood decreases the oxygen transport capacity in human body and leads to death for the high level of exposure. The detection of CO is very hard since it is odorless, nonirritating gas with no color. The incomplete combustion of hydrocarbons in boilers, engines, fires and generators cause lower efficiency and both

VOC and CO pollution.[6,17,18] Therefore, monitoring CO emissions is crucial for environment, safety and energy efficiency. As a result of increase in deaths caused by CO gas, the need for CO gas sensors became more important. Figaro Engineering Inc. released the TGS-203 which is based on tin oxide in 1980 and by 1999 it became one of the mostly used gas sensor.[19] Also in 1990s the metal oxide based CO gas sensor was developed by Motorola which used the technology of silicon micromachinery for the production of these sensor[20].

One of the predominant application area for the solid state chemical sensors is the industries dealing with the combustible and toxic gases. There are variety of dangerous gases in industry. Thus, the gas sensors are crucial for their detection without expensive and complex methods. The prominent gases that need to be monitored for petroleum and petrochemical industries are CO, H_2S, CH_4 and flammable hydrocarbons. In petroleum industry both regulations of the government and potential danger of hazardous and combustible gases brings the progress in gas sensors with it.[20,21] Another important application area for the resistive gas sensors is the automobiles[22]. Gas sensors that are used in exhaust of automobile have significant importance to control efficiency of combustion, engine and pollution abatement system. Measurements need to be accurate in order to get an optimum air to fuel (A/F) ratio[23] for engine and tree way catalyst. Also, toxic gases like CO, NO_x and VOC's in car exhaust. Therefore, it is essential to keep away these gases from the passenger cabin. For this purpose, these sensors are also used in ventilation control systems[20].

The performance of the gas sensors can be evaluated in terms of sensitivity, selectivity and response time. Also stability, drift and interfering gases are the properties that determine the reliability of the sensor. Reproducible and stable responses in 2-3 years of use are the requirements for gas sensors to be long term stable[12]. Long term stability is crucial for the commercial gas sensors. It can be affected from pre-aging which determines microstructure and morphology of the material, irreversible interactions with ambient gases and interaction with the substrate[12]. In general, there are several reasons of instability of the metal oxide gas sensor. Structural changes such as grain

growth with time, poisoning of the surface, change in ambient conditions such as fluctuations in temperature, pressure and humidity and bulk diffusion of oxygen vacancies cause instabilities[24]. Primarily the material selected for the sensing film should possess the following properties[7]:

- Fast and high response
- Selective towards target gas
- Reversible interaction with the ambient gases
- Less dependence on humidity
- Low cost and high reproducibility
- Stable and reliable
- Compatibility with microelectronic technology
- Catalytically active with high surface area
- High sensitivity towards target gases at low temperatures

There are countless studies on different materials used as sensing layer in the semiconductor gas sensors. N-type materials such as SnO_2, WO_3, ZnO, TiO_2 and p-type materials such as CuO, $BaFe_{0.8}Ta_{0.2}O_3$ and La_2O_3 are commonly used as gas sensing layer for the design of the gas sensors.[14] Properties, main target gases and usual operating temperatures of some of the common n-type materials are given in *Table 1-2.*

Table 1-2. Conductance types, operating temperatures and target gases of common n-type materials and their comparison.[6–9]

Material	Conductance	Advantages & Disadvantages	Target Gases	$T_{op.}$ (°C)
SnO_2	Surface Conductance n-type	Sensitivity towards reducing gases and good stability in ambient contains for reducing gases Poor selectivity Cross sensitivity to humidity	Mainly reducing gases like CO, H_2, CH_4	200-400
ZnO	Surface conductance n-type	Mechanical & chemical stability Lower cost and non-toxicity	O_3, NO_X, H_2, CH4, NH_3[25], hydrocarbons[26]	250-350
TiO_2	Bulk conductance n-type	Less dependence towards humidity	O_2, SO_2, CO	350-800
WO_3	n-type	Sensitivity towards oxidizing gases, thermal stability Cross sensitivity to humidity Long recovery times	NO_x[27,28], O_3[29], H_2S, SO_2	300-500
In_2O_3	Bulk conductance n-type	Less dependence towards humidity Sensitivity towards oxidizing gases Fast response/recovery Expensive	NH_3, CO, H_2, CH_4	200-400

A typical gas sensor device has the following components: substrate, electrodes, sensing layer and the heater. The sensing film which is the most crucial part of the device deposited over the substrate with various techniques and it is equipped with the electrodes for the electrical measurements. The heater in general set apart from electrodes and the sensing film by electrically insulating layer.[14] These type of sensors are generally known as Taguchi-typed gas sensors and they are still commercially

dominant. The basic schematic representation of planar and cylindrical configurations of Taguchi-typed gas sensors are given in *Figure 1-1*.

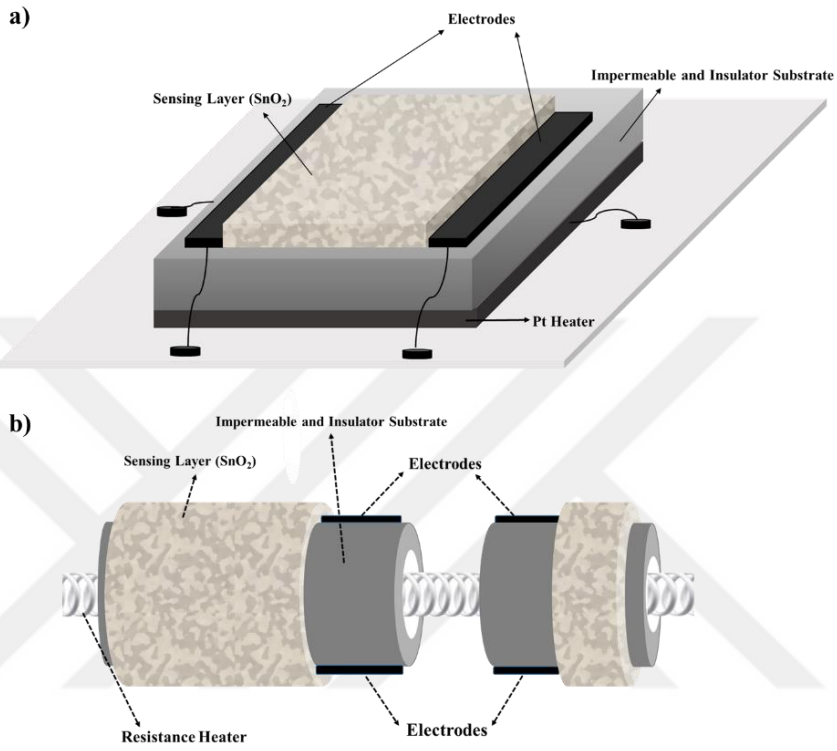


Figure 1-1. Schematic representation of classical Taguchi-typed gas sensors: a) Planar configuration; b) Cylindrical configuration.

High operating temperatures increase the power consumption of the resistive gas sensors. This leads to the miniaturization of the conventional type of gas sensors and integrate them in MEMS (Micro-Electro-Mechanical-Systems) and CMOS (Complementary Metal-Oxide-Semiconductor) technology. In this technology FET (field effect transistor) type devices are used for nanoscale sensing layers.[30] Another type of gas sensor device is the micro hotplate gas sensors. They have three main layers which are resistor based polysilicon, sensing film and a hotplate of aluminum

or tungsten. The resistor is used for heating and the hotplate provides the distribution of the heat. One of the major advantage this type of sensor devices is low thermal time constant. The order of magnitude of the time constant is generally milliseconds therefore this provides chance to operate at temperature programmed sensing mode for operation to increase the selectivity and the sensitivity. Also, easier electronic integration and low consumption of power are other advantages of this type of devices.[31,32] The device structure of a micro hot plate gas sensor fabricated with CMOS process is shown in the *Figure 1-2.*

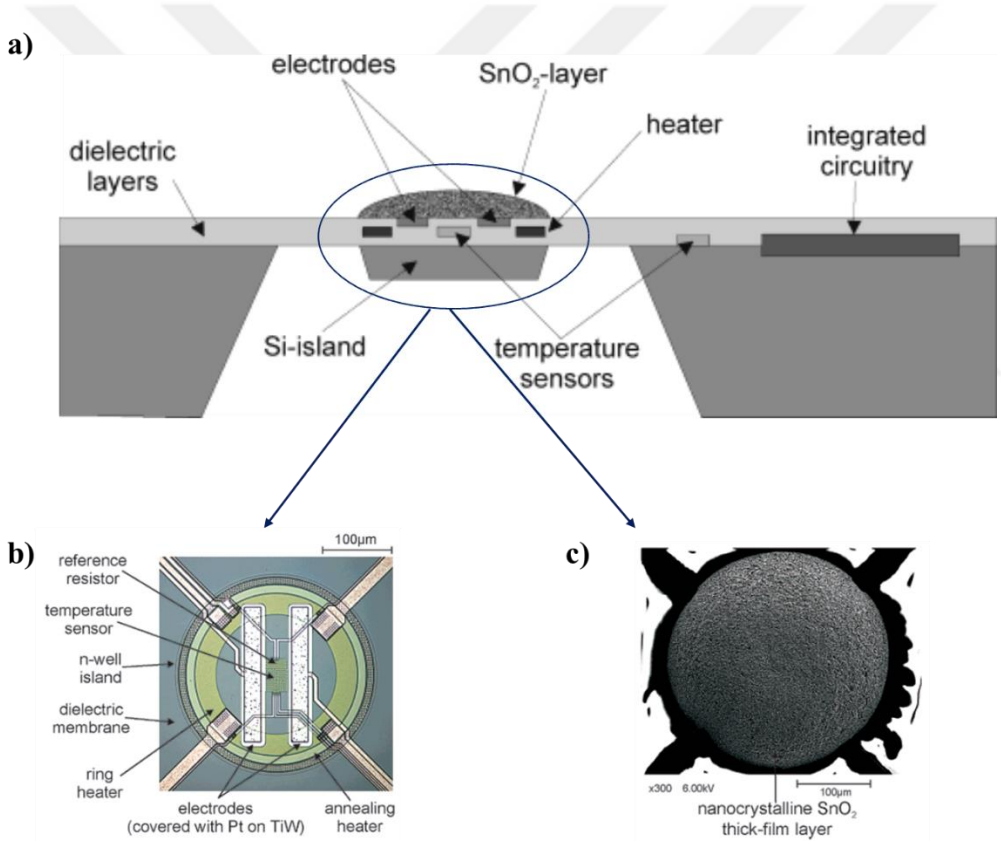


Figure 1-2. The schematic of SnO_2 based gas sensor fabricated with CMOS technology on a micro hotplate: a) Side view schematics of the gas sensor; b) Top view of the microhotplate with circular heated area on the dielectric membrane; c)SEM image of the SnO_2 thick film.[33]

The fundamental theory and the findings of the electro-physical changes due to chemisorption processes and surface chemical interactions, charge transfer between the adsorbed species and the surface go a long way back to studies conducted in the middle of 20th century[30,34–41]. In light of those pioneering studies, the study on ZnO film conducted by Seiyema[42] provided a basis for the practical use of metal oxide semiconductor gas sensor without operating at extreme conditions. At the same years, the commercialization of SnO_2 based gas sensors by Taguchi[30] made the mass production possible. After these developments, extensive research studies were conducted to improve sensitivity, stability, selectivity and reproducibility. Although there are variety of promising materials, SnO_2 is the mostly used and studied material due to its oxidation capability, inert and non-toxic nature, lower cost and exclusive optical property[43,44]. The electrochemical and electrical properties make SnO_2 superior n-type oxide semiconductor for the solid state gas sensor applications.

Over fifty years the metal oxide gas sensors have been extensively researched and yet there is still need for further development and theoretical understanding. Microstructural and morphological parameters influencing the response characteristics of target gas are still unclear. The optimum design of the sensor requires considering many aspects together as the sensing mechanism involves multiple disciplines such as solid-state physics, material science, surface chemistry, reaction engineering and semiconductor electronics. The performance of the sensor depends on complex surface reactions, bulk and surface interactions, electro-physical changes, charge transport, mass and heat transfer, reaction engineering, microstructure/morphology and also the compounds of the whole electronic device. Therefore, it is crucial to investigate the aforementioned effects on the response of the sensor together.

In this study the main aim is to develop a comprehensive mathematical model to analyze the response behavior of the semiconductor metal oxide gas sensors. The developed model takes into account of the detailed surface kinetics, electro-physical changes, diffusion/reaction of the target gas in the sensing film and the electric current

analysis. The current density and voltage distributions were obtained in two dimensional model to analyze the response in terms of electrical current signal for a constant voltage applied to the sensing layer. Carbon monoxide and n-type SnO_2 were selected as probe molecule and model sensing material. The developed model can be used for other gas and sensing materials with appropriate parameters. These parameters were taken from literature considering physical constraints. Some of them were in line with particular studies while other parameters were set by taking into consideration of the recommended ranges in literature. The simulations were performed on the commercial software COMSOL® version 5.3a.

CHAPTER 2

LITERATURE REVIEW

In general, three major factors can be defined for the qualitative description of the gas sensing mechanism of the metal oxide semiconductor gas sensors. These are utility, receptor and the transducer functions. The first one is related with the reaction and diffusion of the target gas within the porous structure. The surface interactions including the adsorption/desorption and surface reactions of the ambient that contains oxygen and the target gas with the porous medium are explained by the receptor function. Transducer function focuses on how those chemical and physical interactions transforms into measurable voltage or current signal. More specifically it is concerned with the transport of carriers between the adjacent grains.[45] The ambient gases and the semiconductor sensing layer interact each other at the grain boundaries. The gas species in ambient can form localized acceptor/donor surface states on the surface of the semiconductor. This surface states either provide electrons to the conduction band or trap electrons from the conduction band. The electron transfer process is influenced by the adsorption/desorption of the gas species and chemical interactions at the semiconductor grain boundary surfaces or on metal dopants. These chemical and electrochemical interactions between the solid and the gas species change electrical conductivity in a reversible manner[12].

The conductance of the semiconductor can be affected by two possible interactions with gases in ambient. One of the interactions includes the oxidation by the molecular oxygen in ambient and removal of the lattice oxygen which changes the stoichiometry of the semiconductor and affects its conductivity. The other one that influence the conductance is related with the adsorption of the ambient gas molecules on the surface.[23] Therefore, for the sensing mechanism primarily two models are used. One of them is known as the oxygen-vacancy model which is based on oxygen

stoichiometry. Diffusion of oxygen vacancies and reduction/re-oxidation mechanisms are the main processes for explaining the sensing operation in those studies. The other one is the chemisorption model which focuses on the chemisorption/ionization of the ambient gases and their interactions with each other and the semiconductor.

Conduction in semiconductors can take place via electrons and holes. Semiconductors can be divided into two types: n- type and p- type. The type of the conductivity of semiconductor can be determined by the relative densities of the acceptor and donor impurities. N- type semiconductors conduct by the conduction band electrons that are resulted from donors, on the other hand valence band holes that are resulted from acceptors provides the conduction in p-type semiconductors.[23] The majority carrier refers to the carrier that has relatively higher density whereas, the minority carrier refers to the carrier that has lower density. In n-type materials the density of the donor impurities is larger than the acceptor impurities. Thus, the dominant carrier is electron which is the majority carrier and minority carrier is hole in an n-type semiconductor.[46] N-type materials have higher thermal stability and they are suitable for low oxygen pressure ambient. Replacement of the oxygen in lattice with the ambient air makes many p-type materials unstable compared to n-type materials. Nevertheless, p-type materials are more appropriate for sensing oxygen or oxidizing gases (e.g. NO_2, Cl_2 etc.) at high operating temperatures. Also conduction of the p-type material is not influenced by the temperature significantly compared with n-type materials thus, one can design the oxygen sensors based on p-type materials without temperature control.[12] When comparing the responses of those two types of material, for the case of all other parameters are same, the response or signal of the p-type material is less than n-type material such that the relation can be given approximately as $S_{n-type} = S_{p-type}^2$[47].

The sensing materials can show n- to p-type transition depending on the changes in ambient environment. For an isothermal case, n- to p- type transition takes place by the change of oxygen partial pressure. When oxygen partial pressure is high, the semiconductor is p-type due to presence of relatively less oxygen ion vacancies

compared to acceptor impurities. The reason of this, at that ambient conditions the metal oxide absorbs oxygen thus p-type conductivity becomes larger and Fermi energy level (E_F) decreases below intrinsic Fermi energy (E_i). Lowering the oxygen pressure will cause oxygen vacancy production and therefore reduce p-type conductivity since each electron that is liberated from each produced oxygen vacancy will eliminate a hole. At a critical value of partial pressure of oxygen, the number of the holes are equal to the number of electrons. Therefore the semiconductor becomes intrinsic and the Fermi energy level (E_F) is equal to intrinsic Fermi energy level (E_i). This critical oxygen concentration is specific to semiconductor material and it is influenced by temperature. Further lowering the oxygen pressure, the semiconductor will turn into n-type as excess electrons are increased as a consequence of the increase in oxygen vacancy formation thus n-type conductivity and Fermi energy increases.[2,23,48]

Barsan and coworkers[47] analyzed the n- to p-type transition for different oxygen concentrations in ambient environment and influence of humidity on this transition[49]. For an n-type material, in the case of no oxygen ambient or relatively high concentration of reducing gas in an oxygen ambient the donors at surface begin to dominate the conduction mechanism thus a switch from the depletion layer to an accumulation layer can be seen. They experimentally observed and theoretically showed this phenomenon for un-doped SnO_2 for CO and H_2 gases in different oxygen concentrations.

When reactive species present over the surface of the semiconductor, they can either transfer electrons to the conduction band or they can accept electrons from the valence band depending on the nature of species. Depletion layer is seen when an acceptor surface state forms due to interaction of oxidizing species with an n-type semiconductor or donor state forms when p-type semiconductor interacts with reducing species. The accumulation layer can form in two ways: for an n-type material if a reducing agent (e.g. CO, H_2, CH_4 etc.) comes into contact with the surface, it transfers electrons into the semiconductor or for a p-type material in the case of

oxidizing agent (e.g. O_2, Cl_2, NO_2 etc.) contact with the solid, it accepts electrons from the valence band and injects holes into the semiconductor.[50] For n-type materials, surface controlled sensing mechanism can be explained as follows. The oxygen present in the ambient environment is adsorbed and ionized on the oxygen vacancies over the semiconductor surface under operating pressures near the atmospheric pressure conditions and usual operating temperatures of $150-400\,^{\circ}C$[4,51]. That interaction of oxygen with surface vacancies creates a depletion layer in the grains since the ionization of the oxygen requires electron from the bulk. The oxygen that binds on the surface by either covalent bonding or electrostatic forces can exists in several charged forms such as O_2^-, O^{2-} and O^-.[43] Oxygen adspecies over the surface traps electrons from the conduction band of the material thus an acceptor surface level is formed. These acceptor surface states capture electrons that are provided by the donor ions. The donor ions which are positively charged present in one side which is called the space charge layer for n-type material. In this space charge layer some of the donor ions (positively charged) are not compensated with the negatively charged acceptor surface states. This region is called as the depletion layer where those uncompensated donors form the charge density which is given by the relation of $N_i=N_D-N_A$. Thus, a potential energy barrier is formed due to the depletion layer formation and the resistance of the material is increased. When the target gas exists in the ambient environment, the depletion layer thickness which is defined by Debye length changes depending on the nature of the target gas. The reaction of the target gas with oxygen on the surface leads to electron transfer therefore, the conductivity of the material changes. When there is reducing gas (CO, H_2 etc.) in the ambient, it reacts with the adsorbed oxygen and releases the trapped electrons and sends them back into the conduction band. This decreases the depletion layer thickness and increases the conductivity of the material. The schematic representation of the mechanism explained above for detection of reducing gas (CO) with an n-type semiconductor can be seen *Figure 2-1*. On the other hand, in the case of oxidizing target gas, reverse phenomenon takes place. The oxidizing gases such as O_2 or NO_2 trap more electrons

from the conduction band and therefore, it causes a decrease in the conductivity and the depletion layer thickness.[4,43,51]

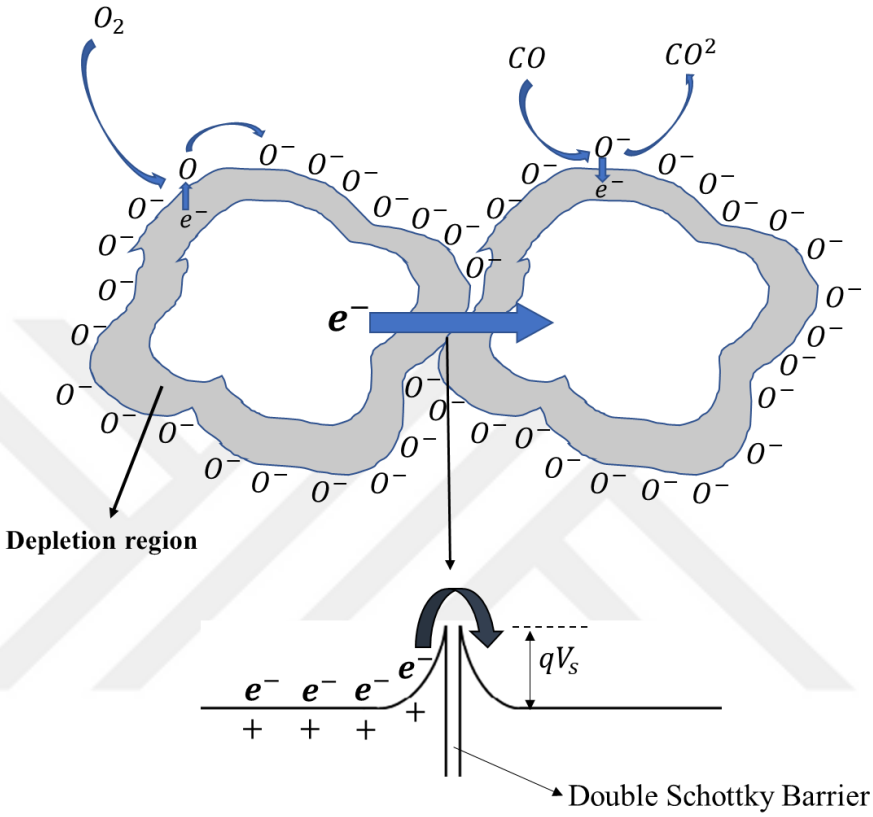


Figure 2-1. Schematic representation of the potential barrier developed at grain boundary of two adjacent grains in a polycrystalline metal oxide semiconductor.

Conductance of SnO_2 at constant temperature is altered mainly by the chemisorption of oxidizing and reducing gases at temperatures close to room temperature since oxygen vacancies are not active[52]. Therefore, reactions on the surface control the sensing mechanism at lower temperatures. Increasing the temperature leads to diffusion of surface oxygen vacancies to the bulk. The surface oxygen vacancies are activated in bulk and act as donor states.[52] However, it is not fast enough to get

equilibrium with the ambient oxygen throughout the sensing time. Also in this temperature range (in between high and low temperatures) the reaction between the bulk lattice of the metal oxide semiconductor and the target gas is possible. This mechanism is known as the redox mechanism. In the high temperature range bulk lattice of the semiconductor and the ambient oxygen quickly reach equilibrium. There are no definite boundaries of temperature for the sensing mechanisms so it is hard to say that in some specific range one of these mechanisms dominates. In general bulk mechanism dominates at temperatures higher than 700 °C and surface kinetics dominates at temperatures lower than 200 °C. Roughly speaking, in between $200 - 500$ °C both redox and surface kinetics and in between 400-700°C both redox and bulk changes influence the sensing.[12]

Oxygen vacancies are the main defects in the bulk of semiconductor metal oxides. Diffusion of oxygen vacancies between grain surface and bulk to reach equilibrium with the oxygen in the ambient can change the bulk conductance of the material.[12] For a non-stoichiometric metal oxide, this equilibration mechanism can be expressed as [48]:

$$O_0^x + 2Sn_{Sn}^x \leftrightarrow \frac{1}{2}O_2 + 2Sn'_{Sn} + V_0^{\cdot\cdot} \qquad 2\text{-}1$$

$$Sn'_{Sn} \leftrightarrow Sn_{Sn}^x + n' \qquad 2\text{-}2$$

The change in the bulk conductivity due to interaction of lattice oxygen and ambient oxygen with each other and the diffusion process of the oxygen vacancy is generally expressed as,

$$G = G_0\, exp\left(-\frac{E_a}{k_B T}\right) P_{O_2}^{\pm\frac{1}{n}} \quad where\ E_a = \Delta G + E_\mu + E_D \qquad 2\text{-}3$$

In the equation *2-3* G_0 is the constant, ΔG is the change in Gibbs free energy of the defect generation reaction, E_μ is the activation energy related with the mobility and required energy for the electron to be excited from the donor state (E_D). The sign in front of the 1/n term depends on the type material, positive for p-type and negative for

n-type. As the 1/n term increases the sensor sensitivity increases. For the case of doubly charged oxygen vacancy formation from the reactions defined above, the n equals to 6.[12,48]

The interaction of the semiconductor with the gaseous oxygen in air have crucial importance on the sensing mechanism. The adsorbed oxygen species can be in different forms on n-type semiconductor depending on temperature. The molecular oxygen needs to be dissociated over the surface since neutral form is not considerably reactive. Both O_2^- (superoxide) and O^- (peroxide) are more reactive than O_2, among them peroxide is the most reactive one and has higher redox potential. Also one other remarkably reactive form of oxygen species is lattice oxygen, O_L^{2-}. When temperature is low, it presents in O_2^- form. The peroxide, O^- begins to dominate as temperature increases due to dissociation of superoxide to peroxide. Although O^- is a reactive form, n-type semiconductors have average activity due to Weisz limitation[39] that is O^- ions can be present about 10^{12} ions per cm^2 of the surface. Formation rate of O^- is also very slow due to energy requirement for electrons to overcome the surface barrier.[23]

Rantala *et al.*[53] investigated the competition of O_2^- and O^-on the surface by constructing a model in which the adsorption/desorption and the electron transfer was concerned. The critical temperature between O_2^- and O^- domination was found as $170°C$. The oxygen species O_2^-, O^- and OH^- on the surface of SnO_2 thin films and their influence on conductivity response were experimentally analyzed for operating temperatures between $25 - 500$ °C[54]. Their observation was that molecular oxygen dominates at temperatures between $25 - 150$ °C, whereas the atomic form starts to dominate for temperatures larger than 450 °C.

S.H. Hahn *et al*[55] examined the effect of the oxygen and carbon monoxide concentrations on the response of the thick films of SnO_2 to carbon monoxide. Their study showed that at very low oxygen concentrations, the conductance signal reached a saturation value for increasing carbon monoxide concentrations due to the complete

coverage or poisoning of SnO_2 surface with carbon monoxide which inhibits oxygen adsorption. However, as the oxygen concentration in ambient increases, the saturation limit becomes no more valid. At higher oxygen concentrations (5 %) in ambient, and sensor shows similar responses as the responses in the excess oxygen environment. Also, decrease in the resistance of the gas sensor and no carbon dioxide formation were observed when the ambient contains only carbon monoxide without any oxygen species. In the light of these observations, they suggested that the competitive adsorption of carbon monoxide with oxygen and the ionization of carbon monoxide over the tin oxide surface determines the response of the gas sensor in an ambient with low oxygen concentrations or no oxygen.

The grain size has significant influence on the sensitivity of the semiconductor materials. The conduction model that describes the electron transport between two adjacent grains depends on the grain diameter. The surface interactions do not affect the large portion of the volume, if the grain diameter is much larger than the depletion layer thickness ($D >> 2L$). In that case, the dominating regions of the grains are the grain boundaries and the sensitivity is independent of the grain diameter. As the size of the grain decreases, the depletion layer becomes comparable with the grain diameter ($D \geq 2L$) therefore, the space charge region (depletion region) expands through the interior parts of the grain. Conduction channel can be seen between the adjacent grains due to the neck formation thus, unlike the previous case, the grain diameter size influences the sensitivity (as diameter decreases sensitivity increases). The other extreme case is the full depletion of the grains ($D < 2L$). Now, the conductivity decreases and it becomes grain-controlled. This situation is also known as the flat-band situation as whole structure acts as interconnected grains.[56] There were some studies investigating the influence of the grain size on the sensitivity. Rotschild and Komen[56] focused on the transducer function for the fully depleted case with a quantative model. The effect of the grain size for range between 5-80 nm, they claimed an inverse relation between the sensitivity and grain size. In another study, Yamazoe and Shimanoe[57,58] theoretically analyzed the influence of shape and size of the grains

on steady state response to oxygen and reducing gases CO, H_2 and NO_2 for a fully depleted or volume depleted case. They found that the square of the sensor response shows linear dependence with the reciprocal of the crytallite size. Later, Kida and coworkers[59] analyzed the crystallite size effect on sensor response to different gases experimentally and simulated for volume depletion case according to the theoretical relation formulated by Simanoe and Yamazoe[45,57,58] in which the response of the sensor proportional to square root of reciprocal of the grain size. Although this relation between sensor response and grain size is verified experimentally for H_2, opposite and nonlinear behavior was observed for CO and H_2S.

The SnO_2 based gas sensors have been commercially available since 1970s. Nevertheless, there is still need for improving performance in terms of sensitivity and the selectivity. Synthesis route, cluster size and the chemical state, distribution of the species and additives influence the performance of the sensor. Using the variety of catalysts, adding metallic active sites, dopants and other additives, modulating the operating temperature are some of the methods to improve selectivity and the sensitivity.[43] The influence of the dopants on the performance of tin oxide based gas sensors have been investigated for a long time. It was discovered that slight addition of noble metals such as Pd and Pt can improve sensitivity of the sensing film towards particular target gases by increasing the catalytic activity thus increases the selectivity and also can enhances stability by lowering the optimum temperature for the operation[43,60–65]. Beside noble metals, transition metal oxides and inert impurities can affect the sensing in terms of electro-physical properties by changing the carrier and surface state densities; chemical activity by influencing the activation energies, active sites and sticking coefficients[66].

There are two major ways for synthesizing SnO_2 gas sensors: thick films and thin films. In general, thick films are prepared by sol-gel method in which precursor that has tin atom and organic ligands (alkoxy and alkyl molecules) is first hydrolyzed by water for polymerization which is followed by condensation-aging and calcination steps[67,68]. Condensation, aging and calcination parameters are critical and enables

grain size control. The colloidal solution obtained by the sol-gel method is deposited on a substrate mainly by spin coating, dip coating and spraying [67]. The deposited liquid film first dried and then calcined. The schematic representation of thin/thick film synthesis by sol-gel method and deposition of synthesized solution on the substrate is demonstrated in *Figure 2-2.*

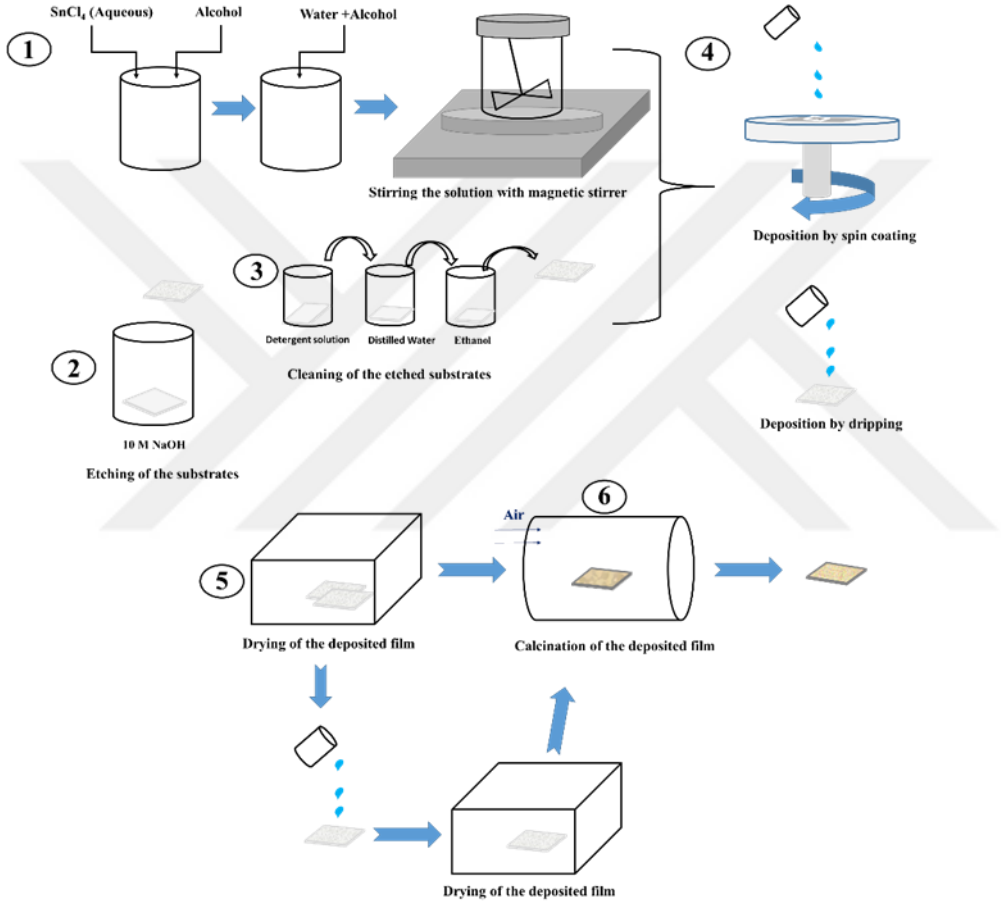


Figure 2-2. Synthesis of thin/thick film SnO_2 by sol-gel method and deposition on substrates.

Sensing layer can be classified as compact and porous layers. The former one is resulted mainly from the deposition techniques for thin films, whereas the latter one

is related with the techniques that are used for thick films. For porous layers, gases can access interior part of volume thus active surface area is superior compared to compact layers in which the volume is not accessible and gas-material interaction can only take place over outer surface.[15] The commercial gas sensors are mostly produced by the thick film technology in which the thickness of the sensing layer changes from few micrometers to 100 micrometers. In thick films, the thickness of the layer does not affect the size of the grains. The grain size can be controlled by the synthesis conditions and the calcination temperature. Thin film technology has various techniques such as evaporation and sputtering which are based on vacuum deposition, spray pyrolysis, pulsed laser deposition, spin coating and different chemical vapor deposition techniques[69]. The unpredictable effect of additives on the grain size, morphology and free charge carriers can be problematic during fabrication for thin film technology. On the other hand, one can overcome with this difficulty in thick film fabrication by introducing additives at the last step of preparation of the paste[66]. Thin films (thickness of 50 to 300 nm) have different response behavior than the thick films[70,71]. The diffusion process is important for the thick films due to their porous structure. According to Korotcenkov *et al.*[72] diffusion can also be critical for the gas sensors based on thin film technology as it can be limiting factor for the response and kinetics. The surface diffusion became important in thin films due to the large contact area between grains. Becker et al.[70] experimentally analyzed the behavior of the temperature dependence of the sensitivity for SnO_2 layer. The different behaviors of thin and thick films were observed and this situation was explained with diffusion effects. Since film thickness affects the grain size in thin films, the effect of the film thickness is more complex compared to the thick films. Therefore, although there are many studies focus on the effect of the film thickness in thin film gas sensors, the complete explanation of the thickness dependency is not a simple task.[72]

Montmeat *et al.*[73] examined the effect of film thickness on the response of SnO_2 thick films have thicknesses between $10 - 80\ \mu m$ and experimentally showed that the

maximum response was obtained with the film have about $40\ \mu m$ for CO and for ethanol the response decreases with the increase in film thickness.

In reality, there are microstructural variations such as the shape and size of the particles in nanostructure and grain size distribution is non-uniform and their connections of adjacent grains can be different. In addition to these, there may exists agglomerations, some dead ends at which no contacts exist between grains and potential barrier distributions throughout the thickness. Synthesis methods, deposition techniques used in thin and thick film technology, film thickness and diffusion effects may cause these irregularities. The percolation theory with effective medium theories were used to take account these variations[74–77]. Also one can consider the contribution of non-depleted parts of grains to the conductivity. The overall behavior of the grains by taking into account of those irregularities can be significantly different from the idealized theoretical considerations[2]. For TiO_{2-x} based CO sensor, a detailed modelling approach for the relation between gas-surface interactions and the grain microstructure was employed[78]. In that study percolative conduction path with the effective medium conductivity that includes the interior parts of the grain was integrated with the surface kinetics.

The mathematical modelling of the metal oxide based gas sensors have crucial importance to understand the integrated behavior of the transducer, receptor and the utility elements. The complete picture of the sensing mechanism requires integrated approach of many fields and needs to be considered in many aspects. In literature, different modeling approaches were used to explain the true nature of the sensing mechanism[78–96]. Mostly, those theoretical works focus on the separate parts of the sensing behavior. The overall behavior in general contains the solid state physics, surface kinetics and diffusion processes and microstructural properties. Also polycrystalline structure, non-uniform grain distribution and different grain contact types lead people to seek effective representations of transport properties such as conductivity and diffusivity. Due to the above explained complex nature of the sensor mechanisms, a few study has detailed and comprehensive theoretical approach. Thus,

the fundamental understanding of the processes takes place in the sensor device is not complete yet.

In early studies, the sensing mechanism was explained by black box approaches in which empirical relations between sensitivity and the partial pressure of the target gas were used and the quantitative description of the operating mechanism was done by simple mathematic relations. In general, those expressions related the concentration of target gases with the sensor response that was obtained experimentally by the power laws[97]. The earliest modelling study for the semiconductor gas sensors was conducted by H.Windischman and P.Mark[86]. In that work steady state response of SnO_x film to CO was explained with ionosorption kinetic model and the square root dependence of conductance to CO partial pressure was suggested. Although this work did not take into the account of the effect of diffusion, surface kinetics and the dynamic behavior of the sensor, it provided a basis for the foregoing theoretical studies. Clifford et al.[98,99] came out with an simple mathematical model for explaining the power law nature of the response of SnO_2 based Taguchi-typed gas sensors for various gases., In these studies, the power law relations for different target gases and combinated effects of multiple gases on the response were derived from the experimental data by using semi-empirical approach. Their model includes the effect of temperature, charge transport and oxygen adsorption kinetics on the conductance which is based on Schottky Barrier model.

The development of theoretical studies continued after that with models having different perspectives as mentioned above. One of the modeling approach focus on the reaction and diffusion of the target gas in the sensing film[95,100–104]. These studies showed that the variation in the concentration of the target gas through the thickness of film have significant effect on the sensor sensitivity. However, these studies employed simple power law expressions and simple kinetics for the conductivity change which briefly provide linear or nonlinear relation between the conductance and target gas concentration without considering detailed surface kinetics with electron transfer and theoretical explanation of conductance change [95,105–110]. Based upon the

effect of the variation of the gas concentration and the conductance through the film thickness, several studies were found in literature focusing on the electrode configurations and influence of that configurations on the response of the sensor[89,111]. Williams and his coworkers[89] numerically solved a simple model that accounts for the diffusion effects and their results showed that variation of the gas concentration in the sensing layer affect the rate of reaction and the conductivity. One of the pioneering work was conducted by Sakai and his coworkers[102]. Responses of the SnO_2 based thin film gas sensors having thicknesses between 80-1000 nm to CO and H_2 gases were investigated by expressing the surface interactions with simple first order reaction. In that study, the steady state diffusion-reaction model is constructed and solved analytically providing the explanation of the bell-shaped temperature dependence of the sensitivity. In their following works[96,112] the un-steady state model was solved analytically for the time dependent case in order to analyze the competitive effect of diffusion and reaction. Based on the same formulation of Sakai[102], T.Kida and S. Fujiyama[59] performed simulations for the SnO_2 responses to CO, H_2S and H_2 for different pore sizes and reaction rates. They explained the increase in the sensitivity for larger pore sizes by the increase in diffusion of the target gas. Also in their simulations they analyzed the competitive effect of the diffusion and reaction of the target gas.

The relationship between sensor response with electron transport through the adjacent grains by considering the grain shape and depth of the depletion/accumulation layer is also subject to theoretical studies[45,57,58,90,113,114]. Barsan and Weimar[115] came out with a comprehensive theoretical model in which grain size, surface reactions and morphology and their influence on the response were taken into account. Later Barsan *et al.* developed a model for the transducer function of a p-type sensing materials[91].

Another group of theoretical studies focus on the detailed surface kinetics and the resulting electron transfer between the bulk and the adspecies on the surface. There are mainly two groups that investigate the kinetics: studies focused on detailed kinetics and charge transfer by phenomenological models[78,83,116–118] and the studies that

contain gray-box models which use relatively simplified surface kinetics models and using these models by estimating the kinetic parameters[82,119–121]. Korotcenkov and coworkers[116] analyzed the time dependent response thin films of un-doped SnO_2 to oxygen by focusing on the surface kinetics. Quantitative behavior of the sensor was explained by a chemisorption model and it was found that the adsorption/desorption steps of the gaseous oxygen controls the dynamics of the sensor instead of the ionization step. A. Setkus[81] developed a general model for the response of the n-type metal oxide gas sensors by focusing on the surface kinetics in which Langmuir-Hinshelwood type mechanism was proposed. In that work the effects of the kinetic parameters, temperature and ambient concentration of CO on the response of thin SnO_2 sensing films to step change in carbon monoxide concentration in oxygen ambient were discussed in detail.

Fort and her co-workers studied[119] dynamic responses of commercial SnO_2 based thick film gas sensors to step changes in temperature in an excess oxygen ambient. They performed parameter estimation for surface kinetics which includes oxygen adsorption, ionization and surface reaction between ionized oxygen and CO. Later they extend their models by taking into account the intrinsic carriers influence on the surface state density[120] and humidity[82].

J.Ding was investigated the effect of intrinsic surface states on the transient response of the SnO_2 based micro-hotplate gas sensor to change in temperature in terms of conductance change[31]. In that work, both intrinsic and extrinsic surface state model was constructed for argon and air ambient respectively and kinetic parameter estimation for the constructed model was done. In the argon ambient, they explained the conductance change by temperature by the electron transfer between the intrinsic surface states and conduction band. On the other hand, in air ambient they analyzed the effect of oxygen chemisorption and ionization kinetics on the response by considering oxygen species as extrinsic acceptor surface states.

CO sensing on tin oxide based semiconductor gas sensor and CO oxidation on tin oxide was extensively researched[65,122–124]. In general the surface interactions of carbon monoxide and oxygen on SnO_2 were given with simple kinetic models which were not consistent with each other. These surface interactions are much more complicated as they involve different charged oxygen species on surface, competitive adsorption of oxygen and carbon monoxide molecules, the interactions with lattice oxygen vacancies and different ionization reactions on the surface. Still, there is no detailed work that provides the kinetic parameters and theoretical comparison between the different mechanisms suggested for CO interaction with SnO_2 in different ambient conditions. In *Figure 2-3* some of the possible mechanisms for the CO and O_2 surface interactions on the SnO_2 are given. For chemisorption models the surface reaction of CO on SnO_2 is described by either Langmuir-Hinshelwood[125] or Eley-Rideal mechanisms[30]. In Mars-Van Krevelen model for carbon monoxide sensing mechanism, surface reduction and its re-oxidation by oxygen determines the detection and the conductance. According to this approach oxygen vacancy is created due the reaction of CO with the lattice surface oxygen. This interaction produces oxygen vacancy due to the removal of the oxygen. The ionized vacancy act as donor and increase the conductivity. The vacancy is filled with the ambient oxygen which captures the conduction band electrons thus leads to decrease in conductivity. One of possible kinetic pathway[30] for the CO detection mechanism by SnO_2 in ambient air according to Mars-Van Krevelen model for is given below by using Kröger-Vink notation[126]:

$$2V_O^{\cdot} + O_{2(g)} + 2e^- \leftrightarrow 2O_O^x \qquad 2\text{-}4$$

$$CO_{(g)} + O_O^x \leftrightarrow CO_{2(g)} + V_O^x \qquad 2\text{-}5$$

$$V_O^x \leftrightarrow V_O^{\cdot} + e^- \qquad 2\text{-}6$$

Fuller and Warwick[127] investigated the kinetics of CO oxidation on SnO_2 which was activated at 450°C for temperatures between 180-210°C in an excess oxygen ambient. They observation is that the rate of reaction does not depend on the concentrations of

CO_2 and O_2. Thus, in their proposed kinetic mechanism which was based on Mars-Van Krevelen mechanism healing of the lattice oxygen with the oxygen in ambient was assumed to be fast. They found kinetic parameters by taking the step describing the adsorption of CO as steady state and the desorption of CO as CO_2 as the rate determining step.

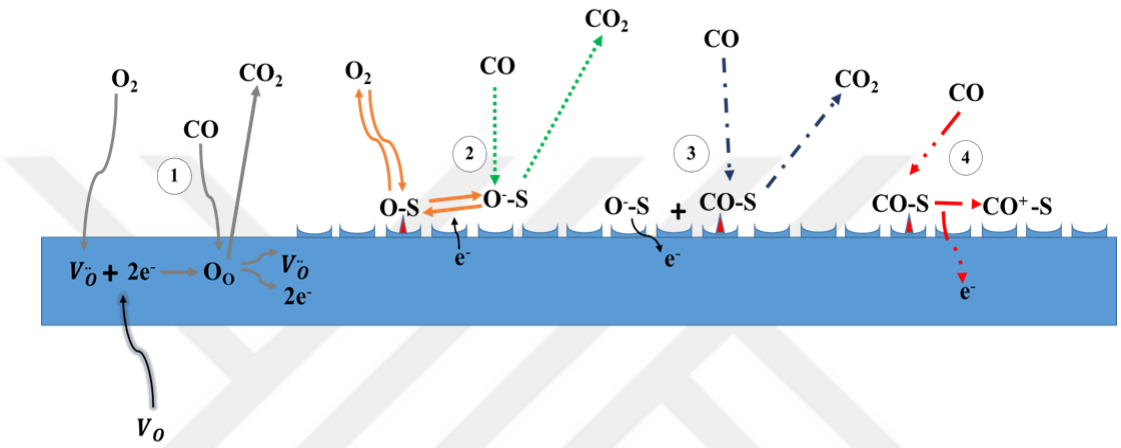


Figure 2-3. Kinetic mechanisms for the CO interaction with SnO_2: 1) Oxygen vacancy mechanism; 2) Eley-Rideal mechanism; 3) Langmuir-Hinshelwood mechanism; 4) Ionization of CO in the absence of oxygen or low oxygen pressure ambient.

In general, theoretical studies focus on the particular components of the sensing mechanism. In this study, our primary aim is to develop a theoretical model that combines the diffusion-reaction approach with a detailed kinetic model that describes the surface interactions including the charge transfer and the resulting conductance/resistance change by considering the potential barrier formation on the boundaries of the adjacent grains. Besides this comprehensive approach, another aim is to integrate reaction kinetics and mass transfer with conduction model to understand the gas sensing dynamics by describing it from microscopic balances to resulting

macroscopic response as an electrical current signal. The lack of such a comprehensive approach in literature shapes the primary motivations of this work which are simulating a gas sensing process by considering many aspects together, to analyze the time dependent response behavior with dynamics affecting in the background and to get fundamental insight from the simultaneous effects of parameters and operating conditions. In order to achieve these goals, the simulations will be performed in commercially available software COMSOL Multiphysics® to investigate the effects of the film thickness, temperature and diffusion processes on the response/recovery dynamics and normalized responses of the gas sensor.

CHAPTER 3

MODEL DESCRIPTION

In this study, a theoretical approach was used to analyze the dynamic response of the semiconductor metal oxide gas sensors to reducing gases in air ambient. A comprehensive mathematical model was developed by taking into consideration of transport of the target gas from the ambient through the film, surface reactions, charge transfer between surface and bulk and consequent conductance/resistance changes. The electrical current analysis was also performed to analyze conductivity change. The main focus is on the thin/thick film as the sensing layer of the metal oxide semiconductor thus, the effects of the other components of the gas sensor device were not considered in the model. It is assumed that, the contacts of the electrodes are ohmic contact with negligible resistance so that the effect of electrode material and resulting potential energy barrier (Schottky contact or the three phase boundary) are negligible. Also, it is assumed that the heater provides spatially uniform temperature in the sensing layer. Chemisorption-ionosorption model for the sensing mechanism was employed for the operating temperature range of the sensing device is in between $150 - 600$ °C.

In this study, the dynamic response of the polycrystalline SnO_2 sensing film to the CO gas in oxygen ambient was analyzed. The composition of ambient environment was tuned for excess oxygen concentration with respect to carbon monoxide so that the effect of ionization of carbon monoxide is negligible. Rectangular geometry of the gas sensor was constructed and the mass transfer of the target gas into this structure was analyzed in one dimension while the equation of continuity for the electrical current was analyzed in two dimensions. The schematic two dimensional representation of the semiconductor gas sensor and the placement of electrodes are given in *Figure 3-1*.

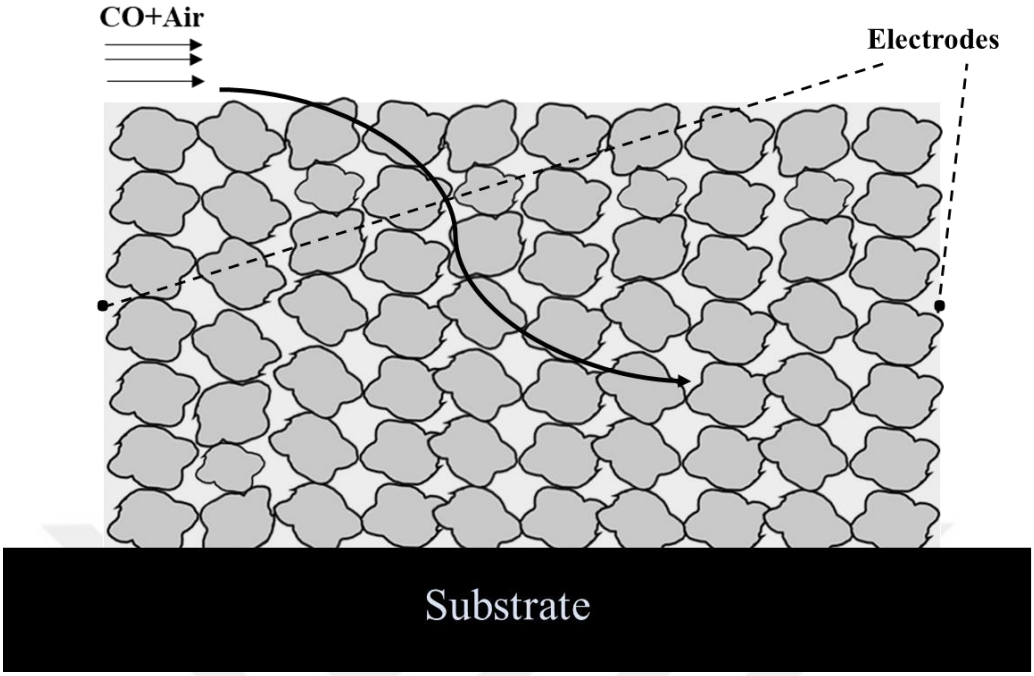


Figure 3-1. Simple representation of the polycrystalline metal oxide semiconductor gas sensor exposing to carbon monoxide in air ambient.

The mathematical model is comprised of four main components:

i- The conductance model that describes the relation between surface states, electron density and the depletion layer formed on the grain boundaries,

ii- One dimensional and time dependent transport equation that describes the mass transfer and reaction of target gas,

iii- The surface reactions which include adsorption and ionization of oxygen on the SnO_2 surface and the reaction between carbon monoxide and ionized oxygen by Eley-Rideal mechanism,

iv- The electrical current analysis based on electric continuity equation which was defined in two dimensions of the film which are width and thickness of the film.

The density of ionized oxygen couples the conduction model with the surface kinetics as it was assumed that the ionized oxygen is the only predominant localized surface states and finally the electric current equations were coupled with the remaining part of the model with the conductivity-conductance relation.

The main assumptions were made to develop the mathematical model are given below:

- The mass transfer of the carbon monoxide is one dimensional in the sensing film as both width and depth of the film are much larger than the thickness.
- Knudsen diffusion prevails and surface diffusion is neglected.
- The external mass transfer resistance is neglected.
- The effect of the humidity is neglected.
- O^- dominates the surface among other possible forms of charged oxygen species.
- The dissociation of the lattice oxygen with temperature is neglected.
- The diffusion of oxygen vacancies was not taken into account as they are assumed to be frozen at the temperature range used in the simulations.
- The effect of intrinsic surface states is neglected as the ionized oxygen dominates the surface states.
- Ionization of carbon monoxide was not taken into account as oxygen pressure is relatively high.
- The grains were assumed to be uniform throughout the medium and percolative effects were not considered.
- The resistance is controlled by the potential energy barrier at the grain boundaries, the neck formation and electron tunneling probabilities were neglected.
- The diffusion of the majority carriers was neglected.
- Oxygen vacancies are the primary defects that forms the shallow donor levels and they are assumed to be completely ionized for the operating temperature range.

- The edge effects are negligible.

Thermal time constant of the gas sensor is assumed to be fast and isothermal operation was considered.

The gas phase reaction of carbon monoxide with oxygen is assumed to be negligible. Although operating temperatures for the simulations can reach up to 600 °C, it is assumed that the reaction of carbon monoxide with gaseous oxygen is not significant compared to the reaction between carbon monoxide and the ionized oxygen. For the comparison purposes, a kinetic rate expression for gas phase carbon monoxide and oxygen reaction was obtained from literature. The activation energy required for the gas phase oxidation of carbon monoxide is about 210000 J/mol[128,129] which is very high compared to the activation energies for the surface reactions in this model. Although the pre-exponential factor of the rate constant of the gas phase oxidation reaction is high compared to the surface reaction, the reaction rate is negligible compared to the surface reactions in the temperature range that was used in the model. The kinetic parameters should be analyzed in detail at such high temperatures since the gas phase reaction may be important which will affect the sensor signal.

In the model diffusion of the gaseous oxygen from ambient through the porous polycrystalline structure was not taken into account. The adsorption of the oxygen over the SnO_2 is assumed to fast. Therefore, there will be no rate term in the transport equation of the oxygen which is given by:

$$\frac{\partial C_{O_2}}{\partial t} = D_{k,eff} * \frac{\partial^2 C_{O_2}}{\partial z^2} \qquad 3\text{-}1$$

For a rough estimation of the characteristic time (t_{ch}), the order of magnitude analysis can be done:

$$t_{ch} = \frac{h^2}{D_{k,eff}} \qquad 3\text{-}2$$

The order of magnitude analysis showed that even for SnO_2 film with thickness of 100 μm the characteristic time is about 1 seconds. Therefore, the oxygen will be uniform

in the sensing film very quickly. However, for the cases when ambient has comparable target gas concentrations with oxygen concentrations or gas sensor system have very fast response, the diffusion of the oxygen should be taken into account. The Knudsen diffusion coefficient is inversely proportional to the molecular weight thus, the selective diffusion of the gases through the porous medium can be important.

3.1. The Conductance Model for the Polycrystalline Porous Medium

Grain diameter is an important parameter that have significant effect on conductance change for polycrystalline metal oxide semiconductors as previously mentioned. In this model it is assumed that grain diameter is large enough that (D>>2L) the resistance of the material is controlled by the potential energy barrier formed at grain boundaries. For an n-type polycrystalline material that have grains with planar geometry, the conductance is derived by relating the majority carrier density and the potential distribution in the depletion layer[23].

Consider a material with bulk electron density n_b and bulk hole density n_p ($n_p \approx 0$). Bulk donors per unit volume N_D and bulk acceptors N_A are assumed to be completely ionized. One can write the charge neutrality in the semiconductor bulk as:

$$N_D + n_p = N_A + n_b \qquad 3\text{-}3$$

It is assumed that there is negligible density of the minority carriers and the majority carriers are captured by the surface states. Since $n_p \approx 0$ for an n-type material and N_A donor electrons are trapped by the surface states (acceptors) there exists $n_b = N_D - N_A$ conduction band electrons. These electrons are captured at the surface sites close to the surface and thus charge of $e(N_D - N_A)$ in the depletion layer forms. The space-charge region or depletion layer corresponds to the region of uncompensated donor/acceptor ions as the predominant charged species. The charge in the depletion layer is given by:

$$\rho = e(N_D - N_A) \quad for\ x < x_0 \qquad 3\text{-}4$$

$$\rho = 0 \qquad for\ x = 0 \tag{3-5}$$

The general form of the Poisson equation is given as:

$$\nabla^2\Phi = -\frac{\rho}{\varepsilon_r\varepsilon_0} \tag{3-6}$$

where ρ is the charge density ((C/m^3) and it is given by:

$$\rho = e\left(n_p(x,y,z) - n_b(x,y,z) + N_D(x,y,z) - N_A(x,y,z)\right) \tag{3-7}$$

In the Poisson equation ε_r is dielectric constant or relative permittivity of the material and ε_0 is the permittivity of the vacuum. The multiplication of the dielectric constant with permittivity in vacuum ($\varepsilon_r\varepsilon_0$) gives the permittivity of the material (ε). Assuming density of donors is homogeneous in the material and x is the direction that is perpendicular to the surface. The potential energy change in the depletion layer can be described by one dimensional Poisson equation,

$$\frac{d^2\Phi}{dx^2} = -\frac{\rho}{\varepsilon_r\varepsilon_0} \tag{3-8}$$

$$\int d\left(\frac{d\Phi}{dx}\right) = \int_{x_0}^{x} -\left(\frac{e(N_D - N_A)}{\varepsilon_r\varepsilon_0}\right) dx \tag{3-9}$$

$$\frac{d\Phi}{dx} = \frac{e(N_D - N_A)}{\varepsilon\varepsilon_0}(x_0 - x) \tag{3-10}$$

$$\Phi = \Phi_b \quad at\ x = x_0 \tag{3-11}$$

$$\frac{d\Phi}{dx} = 0 \quad at\ x = x_0 \tag{3-12}$$

The second boundary condition that is given in equation *3-10* implies that electric field does not exist away from the space charge region in the bulk.

$$\int_{\Phi_b}^{\Phi} d\Phi = \int_{x_0}^{x} \frac{e(N_D - N_A)}{\varepsilon\varepsilon_0}(x_0 - x)\, dx \tag{3-13}$$

Defining $V(x) = \Phi_b - \Phi(x)$ and the integration of the equation *3-9* gives the potential distribution in the depletion layer:

$$V = \frac{e(N_D - N_A)(x - x_0)^2}{2\varepsilon\varepsilon_0} \quad \textit{3-14}$$

The value of the surface barrier V_s can be obtained by the evaluating the V at $x = 0$

$$V_s = \frac{e(N_D - N_A)x_0^2}{2 \cdot \epsilon\epsilon_0} \quad \textit{3-15}$$

The number of charges per unit surface area is defined as:

$$N_s = -(N_D - N_A)x_0 \quad \textit{3-16}$$

where N_s has units of $1/m^2$. Therefore, the potential energy barrier can be expressed as:

$$V_s = \frac{eN_s^2}{2\varepsilon\varepsilon_0(N_D - N_A)} \quad \textit{3-17}$$

This relation which is also known as the Schottky relation which gives the potential energy barrier between bulk and the surface. According to potential energy barrier theory (or double Schottky barrier model) the conductance is given by;

$$G = (gq\mu_s N_d) exp\left(-\frac{q^2 N_s^2}{2k_B\epsilon_r\epsilon_0 N_d T}\right) + G_c \quad \textit{3-18}$$

Where g is related with the geometry, μ_s is the mobility and N_d is the number of ionized donors. The product $gq\mu_s N_d$ is generally expressed with G_0 and taken as constant. G_c is related with the baseline drift.

The electron density and the potential barrier were given as follows:

$$n_s = N_d exp\left(-\frac{q^2 N_s^2}{2k_B\epsilon_r\epsilon_0 N_d T}\right) \quad \textit{3-19}$$

$$V_s = \frac{qN_s^2}{2\epsilon_r\epsilon_0 N_D} \quad \textit{3-20}$$

3.2. The Transport of the Target Gas and Reaction Kinetics

The gas sensing device initially exists in an oxygen ambient. The oxygen species adsorbs on the surface and forms acceptor surface states thus exchange electrons with the material and ionized. This process causes a depletion layer formation and enhanced the potential barrier height. The initial state for the dynamic model is defined as the time at which both chemical and electrochemical equilibrium (Fermi energy level is adjusted) between the adsorption/desorption of the gaseous oxygen and its electron transfer with the semiconductor material are obtained. The transient analysis starts at the moment by introducing CO to the ambient when the surface had reached another equilibrium with the neutral oxygen and the charged oxygen. There were several assumptions done at this moment. First of all, the boundary condition for the surface of sensing film was set to constant concentration of CO. Although there may some external mass transfer resistance, it is also assumed that the external mass transfer of carbon monoxide from ambient to outer surface of SnO_2 film is negligible for sufficiently high flow rates of carbon monoxide and oxygen gas mixture. Therefore, only diffusion of the target gas through the sensing film was considered. The governing transport equation for transient behavior of the mass transfer and reaction with initial and boundary conditions is given as follows:

$$\frac{\partial C_{CO}}{\partial t} = D_{k,eff} * \frac{\partial^2 C_{CO}}{\partial z^2} + \Re \qquad 3\text{-}21$$

$$C_{CO}(z,0) = 0 \quad for\ 0 \le z \le h\ and\ t \le 0 \qquad 3\text{-}22$$

$$\frac{\partial C_{CO}(0,t)}{\partial z} = 0 \quad for\ y = 0 \quad and\ t \ge 0 \qquad 3\text{-}23$$

$$C_{CO}(h,t) = C_{CO,surface} \qquad 3\text{-}24$$

The first boundary condition that is given in equation *3-23* indicates that the net flux is equal to zero at the boundary which represents the impermeable substrate. The second one implies that carbon monoxide concentration is constant at the gas exposed surface of the semiconductor. Since, initially there is no carbon monoxide exist in

ambient, the initial concentration of the carbon monoxide in the sensing film is zero. The two dimensional geometry for the sensing film and the boundary conditions are shown in *Figure 3-2*.

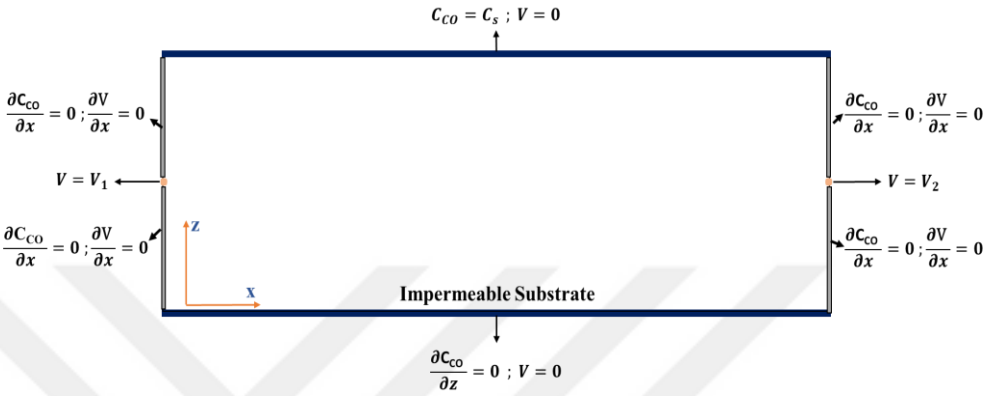


Figure 3-2. The representation of the rectangular geometry used in the model with the boundary conditions.

The effective Knudsen diffusion coefficient with a relation for tortuosity is used for the diffusivity is given below:

$$D_{k,eff} = \frac{\varepsilon}{\tau} \cdot \frac{4r}{3} \cdot \sqrt{\frac{2 \cdot R \cdot T}{M_{CO} \cdot \pi}} \qquad 3\text{-}25$$

Where tortuosity is given with the following relation[130]

$$\tau = \varepsilon^{-0.5} \qquad 3\text{-}26$$

The reaction term in the transport equation couples the surface reactions with transport equation. Since concentrations of surface species is given units of m^{-2}, reaction term was multiplied with specific surface area and divided by Avogadro's number.

$$\Re = -k_{3,0} \cdot exp\left(-\frac{E_3}{R \cdot T}\right) * C_{CO} * N_s * \frac{1}{Av} * a \qquad 3\text{-}27$$

There are two main different kinetic mechanisms as previously mentioned, one is the ionosorption model and the other one is redox (oxygen vacancy) mechanism. In this study ionosorption model was employed by considering the moderate operating temperature. It is assumed that the oxygen vacancies are frozen in that range and diffusion of oxygen vacancies is neglected. To describe surface reaction between carbon monoxide and ionized oxygen, the Eley-Rideal mechanism was used. Overall mechanism contains adsorption of oxygen to the surface of semiconductor and its charging process with the electron and reaction of gaseous CO with the ionized oxygen. Considering the range of the operating temperatures in this model, it is reasonable to assume that atomic form of the charged oxygen dominates the surface such that molecular and doubly charged forms are negligible. The surface reaction mechanism is as follows:

$$\frac{1}{2}O_2(g) + S \underset{k_{-1}}{\overset{k_1}{\leftrightarrow}} 2O - S \qquad \textit{3-28}$$

$$O - S + e^- \underset{k_{-2}}{\overset{k_2}{\leftrightarrow}} O^- — S \qquad \textit{3-29}$$

$$O^- - S + CO(g) \overset{k_3}{\rightarrow} CO_2(g) + S + e^- \qquad \textit{3-30}$$

In the reactions defined above k_1 and k_{-1} are the reaction rate constants of adsorption and desorption of gaseous oxygen on tin oxide surface respectively. The forward and reverse reaction rate constants of oxygen ionization reactions are given by k_2 and k_{-2} respectively. The reaction rate constant of surface reaction between gaseous carbon monoxide and ionized oxygen is denoted by k_3.

The corresponding ODEs that describe the kinetic rates are:

$$\frac{dN_O}{dt} = k_1([S] - N_O - N_s)[O_2]^{1/2} - k_{-1}N_O - k_2 n_s N_0 - k_{-2}N_s \qquad \textit{3-31}$$

$$\frac{dN_s}{dt} = k_2 n_s N_0 - k_{-2}N_s - k_3 N_s C_{CO} \qquad \textit{3-32}$$

$$\frac{dC_{CO_2}}{dt} = k_3 N_s C_{CO} \qquad \textit{3-33}$$

$$\frac{dC_{CO}}{dt} = -k_3 N_s C_{CO} \qquad 3\text{-}34$$

The N_O denotes the density of neutral oxygen that adsorbs on semiconductor surface and N_s is the ionized oxygen density since it is assumed that the charged surface states purely formed by the charged oxygen species. There may also be other components of N_S such as ionized target gas on surface or the charged intrinsic surface states. However, in this model their effects are excluded. At this point one important assumption the chemisorption of the oxygen is fast relative to its ionization was made. Therefore, the steady state surface concentration of neutral oxygen can be found as:

$$\frac{dN_O}{dt} = 0 = k_1([S] - N_0 - N_s)[O_2]^{1/2} - k_{-1}N_0 - k_2 n_s N_O + k_{-2}N_s \qquad 3\text{-}35$$

Assuming number of adsorption sites is much larger than the ionized and chemisorbed oxygen density ($[S] \gg N_s + N_0$)

$$k_1[S][O_2]^{1/2} - k_{-2}N_s = N_O[k_{-1} + k_2 n_s] \qquad 3\text{-}36$$

$$N_{0,st.st.} = \frac{k_1[S][O_2]^{1/2} + k_{-2}N_s}{[k_{-1} + k_2 n_s]} \qquad 3\text{-}37$$

The substitution of steady state expression of N_O into equation *3-32* gives

$$\frac{dN_s}{dt} = k_2 N_{0,st.st.} n_s - k_{-2}N_s - k_3 C_{CO} N_s \qquad 3\text{-}38$$

$$\frac{dN_s}{dt} = k_2 \left(\frac{k_1[S][O_2]^{1/2} + k_{-2}N_s}{[k_{-1} + k_2 n_s]}\right)\left(N_d exp\left(-\frac{q^2 N_s^2}{2k_B \epsilon_r \epsilon_0 N_d T}\right)\right) - k_{-2}N_s - k_3 C_{CO} N_s \qquad 3\text{-}39$$

The rate constants for the reactions are defined by Arrhenius expression.

$$k_i = k_{i,0} * exp\left(-\frac{E_i}{R*T}\right) \qquad 3\text{-}40$$

Thus, if the electron density is expressed with the equation *3-19* , the dynamic behavior of the ionized oxygen density can be expressed with the following equation:

$$\frac{dN_S}{dt} = exp\left(-\frac{q^2N_S^2}{2k_B\epsilon_r\epsilon_0N_dT}\right)\left(\frac{k_{10}exp\left(-\frac{E_1}{RT}\right)[S][O_2]^{1/2}+k_{-20}exp\left(-\frac{E_{-2}}{RT}\right)N_S}{\left(\frac{k_{-10}}{k_{20}N_D}\right)exp\left(-\frac{(E_{-1}-E_2}{RT}\right)+exp\left(-\frac{q^2N_S^2}{2k_B\epsilon_r\epsilon_0N_dT}\right)}\right) -$$

$$k_{-20}exp\left(-\frac{E_{-2}}{RT}\right)N_s - k_{30}exp\left(-\frac{E_3}{RT}\right)N_sC_{CO} \qquad 3\text{-}41$$

Since, our initial condition assumes there is no target gas initially and the surface is covered by ionized oxygen species at equilibrium. The surface concentration of ionized oxygen species depends on the temperature. Therefore, the initial condition of ionized oxygen density is a complex function of operating temperature.

The conductance distribution over the film thickness can be obtained with the simultaneous solution of the equations with the appropriate boundary and initial conditions that are given above. The response in terms of electrical current signal can be obtained by applying voltage drop across the width of the film or by applying current to the film in which voltage response can be analyzed.

3.3. Electrical Current Analysis

The current density and the voltage distribution through the medium was analyzed in two dimensions which are x for the width and z for the thickness of the film. The electrodes are represented in the model as points exists in both sides of the film. It is assumed that the electric potential drop was provided by keeping one point at ground condition, $V = 0$, and the other one at constant potential which is taken as $V = 5\ V$ in this model. The three dimensional representation of the device and the coordinate system is shown in *Figure 3-3*. It is assumed that the grains are identical and uniformly distributed so that they form perfect conductive path.

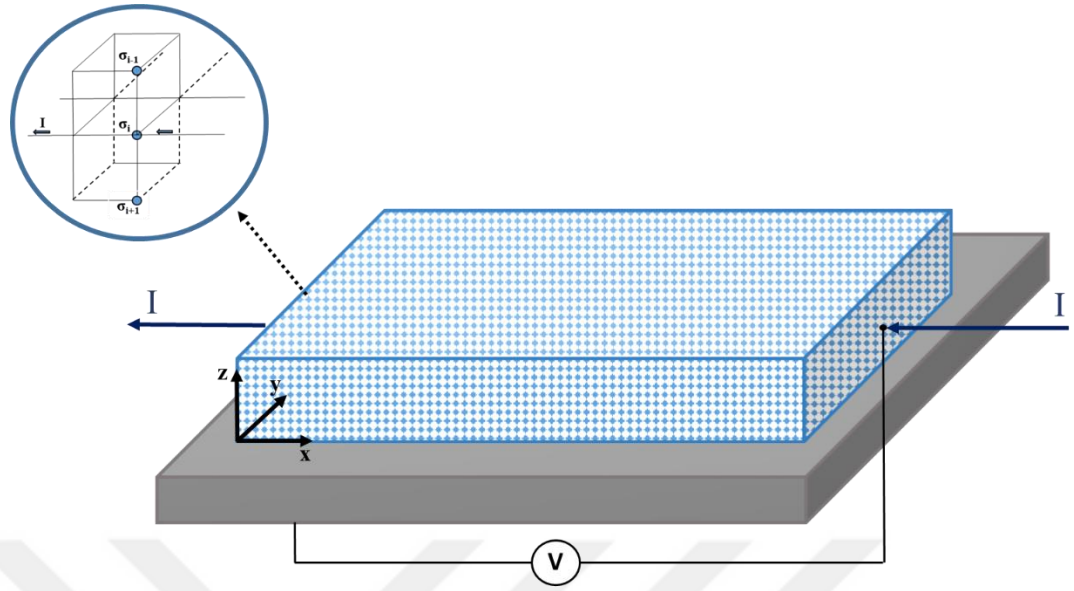


Figure 3-3. Three dimensional representation of the gas sensor device.

For the DC electrical current, the Ohm's law relating the electrical field to the current density is given as:

$$\vec{J} = \sigma \vec{E} \qquad 3\text{-}42$$

$$\vec{E} = -\nabla V \qquad 3\text{-}43$$

in which the total current density is given by the drift-diffusion equation

$$\vec{J} = q \cdot \mu_n . n \cdot \vec{E} + q \cdot D_n \cdot \nabla n \qquad 3\text{-}44$$

Conservation of charge over an elemental volume gives the continuity equation as

$$\frac{\partial n}{\partial t} = \frac{1}{q} \nabla \cdot \vec{J} + (G_n - U_n) \qquad 3\text{-}45$$

or for the case of no generation or recombination, the continuity equation reduces to

$$\nabla \cdot \vec{J} = \frac{\partial \rho}{\partial t} \delta(x - x_s) \delta(y - y_s) \delta(z - z_s) \qquad 3\text{-}46$$

The combination of the equation *3-46* with the Ohm's law gives

$$\nabla \cdot (\sigma \nabla V) = \frac{\partial \rho}{\partial t} \delta(x - x_s)\delta(y - y_s)\delta(z - z_s) \qquad 3\text{-}47$$

The conductivity for the electric current equations was obtained from the conductance that was found from the solutions of surface kinetics, transport equation and potential barrier model. The macroscopic relation between conductance and the conductivity can be obtained as follows:

$$G = \sigma * \frac{l*h}{w} \qquad 3\text{-}48$$

where depth, width and thickness are represented by l, w, h respectively as seen in the *Figure 3-4.*

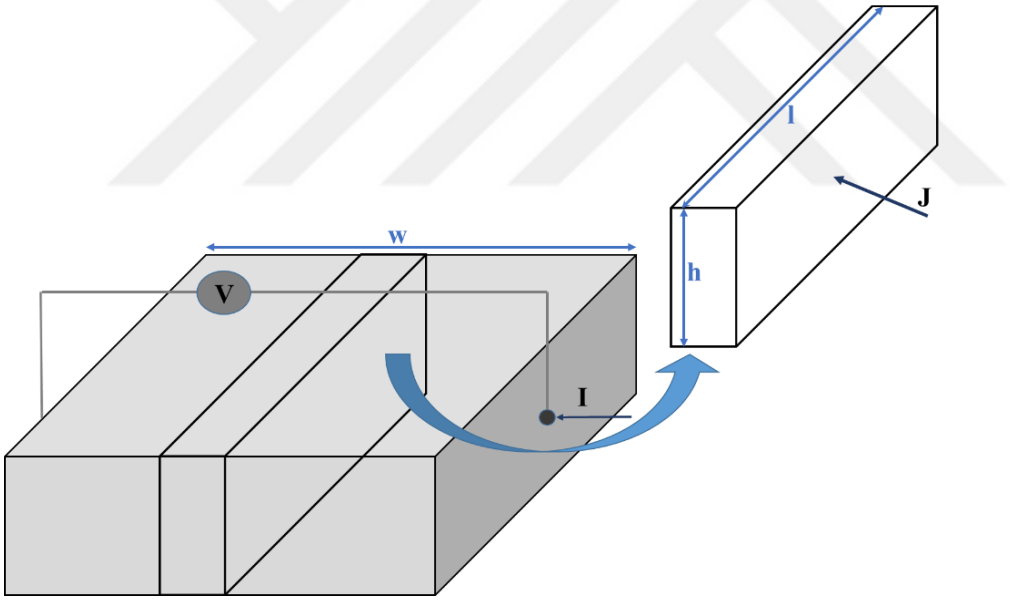


Figure 3-4. The schematic representation of the cross-sectional area perpendicular to the current direction on a cut plane from the three dimensional representation of the gas sensor.

The response of the semiconductor gas sensor is expressed with the averaged conductance and the electrical current. The conductance is spatially averaged over the z direction as follows:

$$G_{avg}(t) = \frac{1}{h} \cdot \int_0^h G(x,t) \cdot dz \qquad 3\text{-}49$$

The electrical current flows in the semiconductor was found by integrating the current density over the cross sectional area that is shown in the *Figure 3-4*.

$$I = \oiint \vec{J} \cdot \vec{n} \cdot dS \qquad 3\text{-}50$$

where $\vec{n}$ is the normal vector perpendicular to surface S.

3.4. COMSOL Multiphysics

The COMSOL Multiphysics® is a commercial software that uses Finite Element Method for numerical analysis and many other linear and nonlinear solvers. Depending on the choice, the numerical analysis can be conducted with adaptive mesh technique or based on error control. It provides a chance to work on multiphysics to solve complex problems.

In general, COMSOL uses following numerical solution scheme to solve transient partial differential equations:

i. Spatial discretization by using finite element method to turn transient partial differential equations into ordinary differential equations.
ii. Discretization of the time to obtain set of algebraic equations.
iii. Automatic linearization of algebraic equations by Newton-like methods.
iv. Solving the linear algebraic set of equations by direct or iterative methods.

The governing equations were solved in COMSOL by using Transport of Diluted Species, Domain ODEs and DAEs in the Mathematics Interface and Electric Currents in AC/DC interfaces. The diffusion and reaction of carbon monoxide is defined in the

Transport of the Diluted Species interface. One dimensional transient diffusion of carbon monoxide was defined in z-direction (along the film thickness). At z=0 the substrate and sensing film interface was defined as impermeable, catalytically inactive and electric insulating by setting diffusive, reactive and current fluxes to zero. The gas exposed surface was defined at z=h (film thickness) by using constant CO concentration on this surface. The rate equations of the surface reactions were defined in the Domain ODEs and DAEs interface. The two dimensional current distribution was obtained by using pointwise constant potential energy boundary conditions which were applied both sides of the film along x direction in the Electric Current Interface.

3.4.1. Study and Solver Configurations

In general, it is suggested to use the automatic adjustments done by the COMSOL Multiphysics® software itself for the solver and work on configurations except for highly ill-conditioned numerical problems or exceptional cases. Therefore, except for several manual adjustments, the configurations and selections that were automatically tuned up by the software were kept. In order to avoid numerical problems due to the variations in order of magnitudes of the dependent variables from different physics, the scales were manually adjusted. For the discretization of the time stepping, BDF (implicit backward differentiation formula) was used which was default method in COMSOL for the physics that involves diffusion and reaction. Settings for the time step sizes were adjusted that the time step sizes were determined by solver which use adaptive time steps based on the local errors. The maximum step size that the solver can take was manually tuned.

3.4.2. Mesh Studies

It is a common approach to start with the coarser mesh and then perform the mesh refinement. Since there are different physics exist in the model and mathematically the dependent variables have values in different order of magnitudes, the numerical instabilities may emerge. In this study, the geometry is not complex and the numerical instabilities and resulting misinterpretations of the results were avoided by working

with finer and high quality meshes. The computer processing time was improved by decreasing the number of elements by monitoring the mesh independency and quality of the results. Here only the denser mesh structures which were used for the starting point of the refinement are given. Free triangular and mapped meshes were used as unstructured and structured mesh strategies respectively. The mesh distribution was applied to all boundaries with fixed number of elements of 120 to enhance the quality of the meshes. Also in some studies the meshes near to the electrodes (pointwise) were constructed in higher quality and smaller sizes relative the remaining part of the domain. For the finer and high quality mesh construction, the extremely fine mesh option was selected. The resulting parameters of the element sizes are given in *Figure 3-5*.

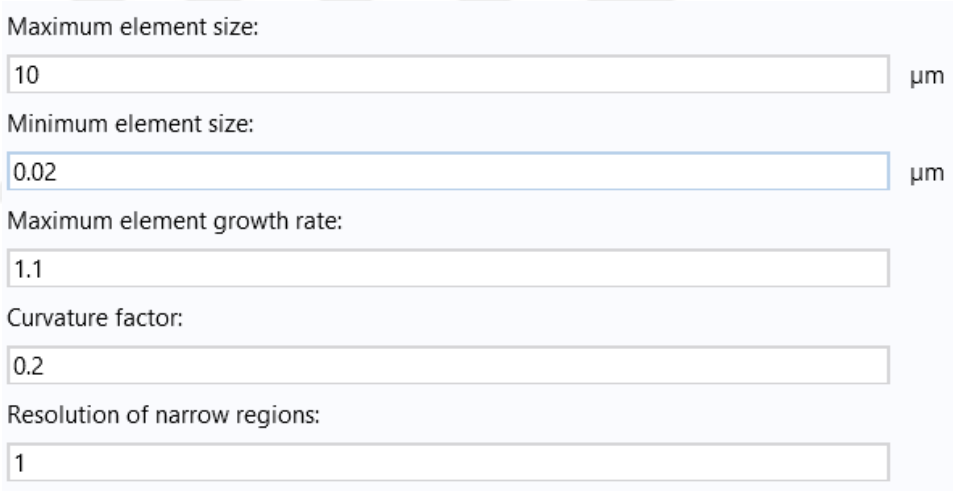


Figure 3-5. The parameters of the mesh element size for free triangular meshes.

The resulted meshes in the rectangular domain can be seen in *Figure 3-6* in which very dense structure of meshes can be seen.

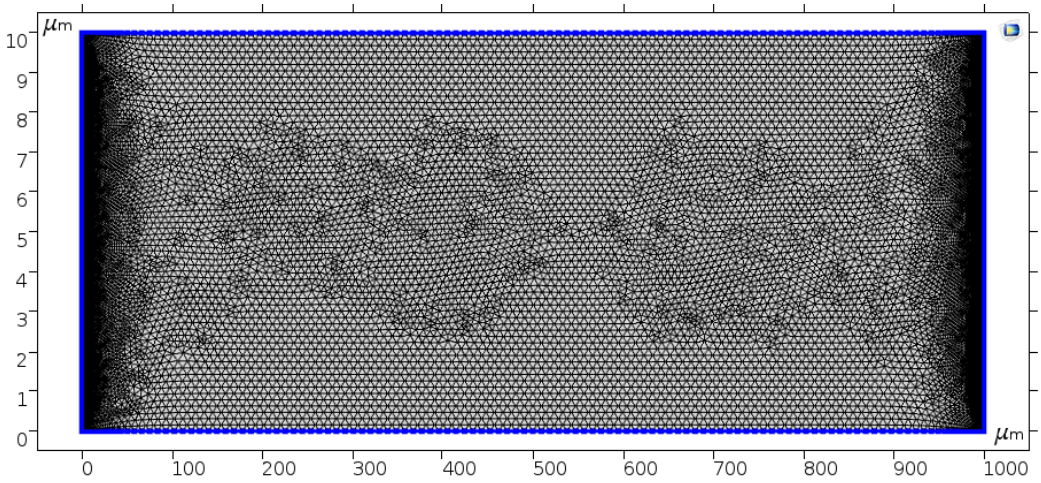


Figure 3-6. Dense construction of free triangular meshes in the rectangular domain.

The information about statistics of the complete mesh is given below in *Figure 3-7.*

Element Quality

Quality measure: Skewness

Statistics

Complete mesh

Mesh vertices: 13167

Element type: All elements

Triangles: 25612

Edge elements: 720

Vertex elements: 6

Domain element statistics

Number of elements: 25612

Minimum element quality: 0.01291

Average element quality: 0.02636

Element area ratio: 0.0205

Mesh area: 10000.0 μm²

Figure 3-7. Statistical information of the complete mesh for free triangular meshes.

The mesh construction on the rectangular domain was also done by using mapped mesh. The construction was adjusted for the elements to be denser and smaller as getting close to the points representing the electrodes. The even distribution was applied to the boundaries and 100 elements were located. The resulting parameters of the elements and mesh sizes are given in *Figure 3-8*.



Figure 3-8. The parameters of the mesh element sizes for mapped meshes.

The *Figure 3-9* shows the dense structure of the mapped meshes.

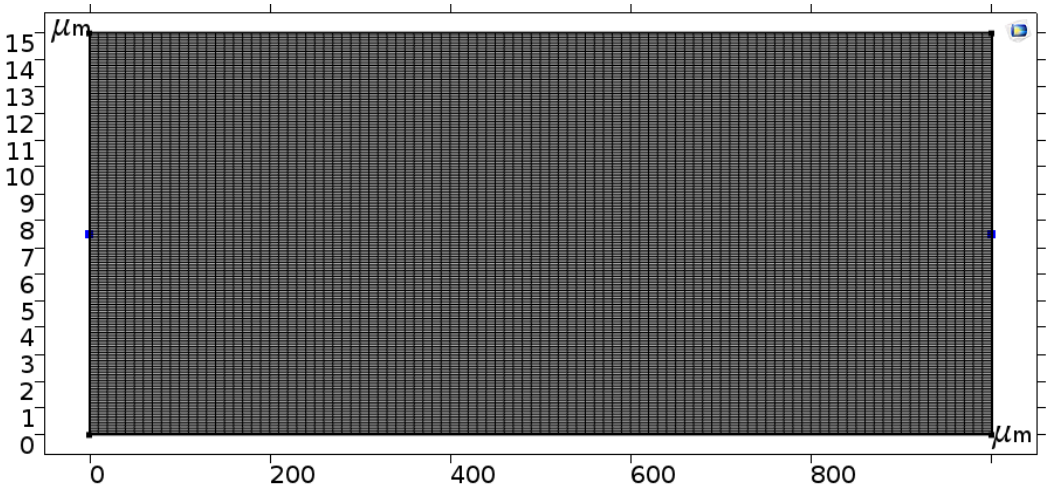


Figure 3-9. Dense construction of mapped mesh in rectangular domain.

The information about the statistics of the complete mesh is given below in *Figure 3-10.*

Element Quality

Quality measure: Skewness

Statistics

Complete mesh

Mesh vertices: 20301

Element type: All elements

Quads: 20000

Edge elements: 600

Vertex elements: 6

Domain element statistics

Number of elements: 20000

Minimum element quality: 1.0

Average element quality: 1.0

Element area ratio: 1.0

Mesh area: 15000.0 μm²

Figure 3-10. Statistical information of the complete mesh for mapped meshes.

3.5. Model Parameters

The constructed mathematical model depends on many physical parameters. The values and ranges of those parameters were taken from literature for the simulations performed in COMSOL Multiphysics®. Also there are other parameters exist that have influence on the theoretical considerations therefore the ranges of those parameters must be determined to ensure the validity of the mathematical model. The parameters and their values or range of parameters are given in *Table 3-1*.

Table 3-1. List of parameters used in the mathematical model.

Parameter	Value or Range	Unit
a	$5-50$ [131]	$m^2 \cdot g$
ε	$0.1-0.5$	-
ϵ_0	8.854×10^{-12}	$F \cdot m^{-1}$
ϵ_r	13.50	-
r	$0.5-5$	nm
q	1.6×10^{-19}	C
Av	6.02×10^{23}	mol^{-1}
k_B	1.38×10^{-23}	$J \cdot K^{-1}$
N_D	$10^{22}-10^{24}$ [132]	m^{-3}
G_c	0	-
G_0	$0-2$ [121]	-
w	$250-5000$	μm
h	$1-100$	μm
l	$1000-5000$	μm
$k_{10}[S][O_2]^{1/2}$	$10^{18}-10^{20}$ [119]	$m^{-2} \cdot s$
$k_{-10}/(k_{20} \cdot N_D)$	$81-93.5$ [119]	-
$k_{30}\langle R \rangle$ **	$0.0001-16.7$ [119]	s^{-1}
k_{-20}	$0.0095-0.106$ [119]	s^{-1}
$\bar{E}_1/k_B$	$3652-8665$ [119]	K
$\bar{E}_{-2}/k_B$	$558.2-2051$ [119]	K
$\bar{E}_3/k_B$	$616-4500$ [119]	K
$(\bar{E}_{-1}-\bar{E}_2)/k_B$	$6656-7227$ [119]	K
V_1	0	V
V_2	5	V
M_{CO}	28.01	$g \cdot mol^{-1}$
M_{O_2}	16	$g \cdot mol^{-1}$
D	>20	nm

** $\langle R \rangle$ corresponds to CO concentration given in ref.

CHAPTER 4

RESULTS AND DISCUSSION

In this work a comprehensive mathematical model was developed for the dynamic response behavior of an n-type tin oxide based metal oxide semiconductor gas sensor to reducing gases (CO) in an excess oxygen environment. The time dependent model was constructed by considering the following physical and chemical processes:

- One dimensional mass transfer of carbon monoxide from surface to the impermeable substrate through porous SnO_2 polycrystalline thin/thick film and its reaction over the surface
- Surface reaction model based on chemisorption and ionization of oxygen.
- The surface reaction of carbon monoxide with the ionized oxygen by Eley-Rideal mechanism.
- The conductance model is based on depletion layer or space charge layer model in which grain boundary controlled resistance is considered.
- Two dimensional electrical current model based on electrical continuity equations.

The constructed theoretical model was defined in commercial software COMSOL Multiphysics® version 5.3a by using Transport of Diluted Species (TDS), Domain ODEs and DAEs interface in Mathematics module and Electric Currents Interface in AC/DC module. The resulting partial differential equations, ODEs and the non-linear algebraic equations were numerically solved in two dimensions which are z direction for the thickness of the film and the x direction corresponds to width of the film. The transient simulations were performed in COMSOL Multiphysics® 5.3a environment to analyze the effects of the geometry of the layer, temperature, surface concentration of carbon monoxide, pore size and response/recovery characteristics. For these

purposes, the effect of these parameters on the dynamic response characteristics and performance of gas sensor in terms of sensitivity and response time were investigated. The results are given for potential energy barrier, conductance, ionized oxygen density, carbon monoxide concentration, current density and time dependent behavior of the current and spatially averaged conductance. The initial conditions for the model were determined from the solution of base case in which only oxygen exist in ambient. The mathematical model developed here depends on many physical and kinetic parameters. The results were obtained by setting the most of the parameters to specific values that were taken directly from the literature or determined from the range suggested in literature. The obtained results are given and discussed in detail in the following sections:

i. Transient response analysis of SnO_2 based gas sensor to CO in oxygen environment.
ii. Effect of temperature on:
    - Initial equilibrium state of oxygen with SnO_2 and initial conductance,
    - Competitive effect of diffusion and surface reactions,
    - Concentration, potential energy barrier, conductance and current density distributions in the SnO_2 sensing film,
    - Dynamic response during exposure of SnO_2 to CO and corresponding response changes,
    - Response time.
iii. Effect of film thickness on:
    - Competitive effect of diffusion and surface reactions,
    - Concentration, potential energy barrier, conductance and current density distributions in the SnO_2 sensing film,
    - Dynamic response during exposure of SnO_2 to CO and corresponding response changes,
    - Response time.

iv. Response/recovery analysis of SnO_2 based gas sensor to step changes in surface concentration of CO and effect of temperature on recovery times.

v. Effect of surface concentration of CO on the steady state response of SnO_2 based gas sensor.

4.1. Transient Analysis of the CO Sensing of SnO_2 Film in Oxygen Environment

The concentration distributions of CO and ionized oxygen, conductance and the current density and their dynamic behavior were analyzed for 15 μm mesoporous thick (pore size 4 nm) at 300°C.

In the Figure *4-1* the transient development of CO concentration profile in z direction can be seen. The ordinate of this figure corresponds to the dimensionless concentration value of the carbon monoxide which is defined as $\theta_{CO} = C_{CO}/C_{CO,surface}$. The abscissa refers to the direction from impermeable substrate (z=0) to gas exposed surface (z=15 μm). The concentration profiles were plotted with respect to time until the steady state profile was reached. Initially (t=0) there is no carbon monoxide in the film and at t=0 the surface concentration of the carbon monoxide is set $0.00814\ mol/m^3$.

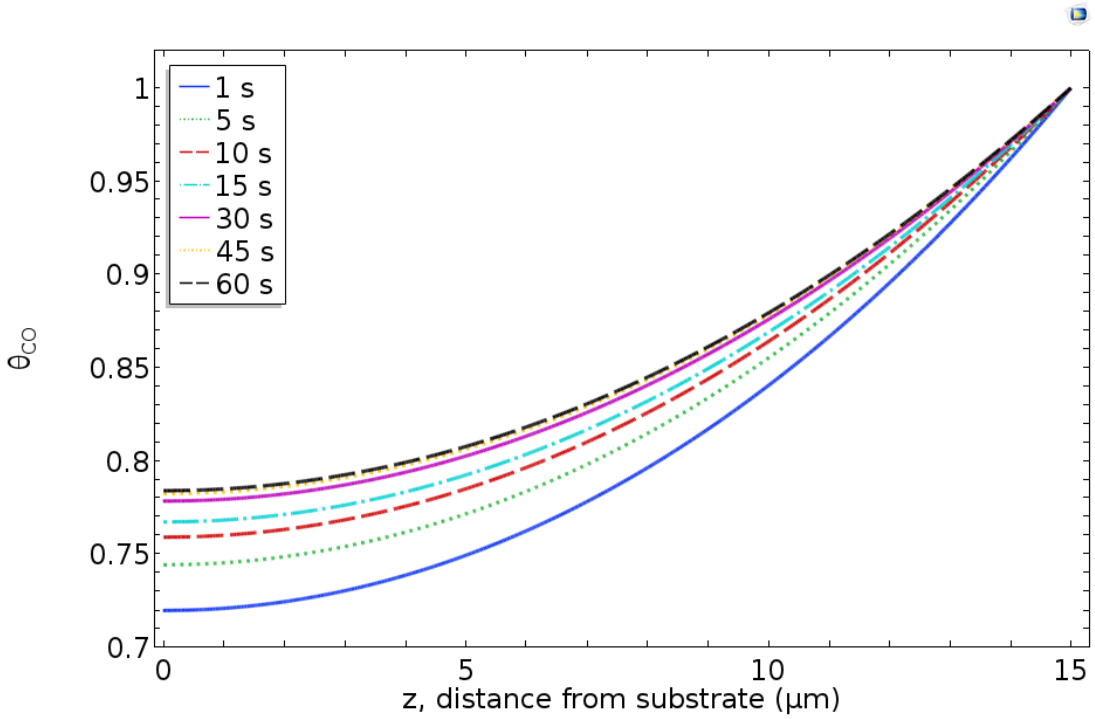


Figure 4-1. Transient analysis of the CO concentration profile development in 15µm thick film at T=300°C. Response to the step change of CO concentration of 0.00814 mol/m^3 in an excess oxygen environment at t=0.

From the curves in *Figure 4-1* fast diffusion of CO is apparent. Within a second CO concentration at the substrate interphase becomes 72 percent of the surface concentration. The time course of concentration change along the z direction of thin/thick film indicates the penetration of carbon monoxide from surface to the substrate and convergence towards steady state concentration. In addition, the reaction of carbon monoxide is evidenced by the decrease of carbon monoxide with z direction at steady state which also indicates the conversion of carbon monoxide with a comparable reaction rate with mass transfer rate. The concentration difference between the gas exposed outer surface and substrate surface depends on the relative magnitudes of the reaction rate and mass transfer rate.

The transient analysis of the concentration profile of ionized oxygen to the step change of concentration of carbon monoxide is given in *Figure 4-2.* As it is seen, the ionized oxygen concentration over the exterior surface (z=15μm) decreases drastically indicating the reaction of ionized oxygen with carbon monoxide and the rate of formation of ionized oxygen is slower than the rate of consumption. On the other hand, the reaction of ionized oxygen with carbon monoxide is slower within the film due to the lower concentration of CO. The ionized oxygen density in the film decreases with time towards to new steady state. Although this change in ionized oxygen density with time is not very large, the reaction rate between carbon monoxide and ionized oxygen slightly decreases. Therefore, due to the competitive effect of diffusion and the reaction, the concentration profile changes and getting slightly more uniform with time as seen in *Figure 4-1*. The reason is that reaction rate decreases slightly and therefore the effect of mass transfer become less pronounced.

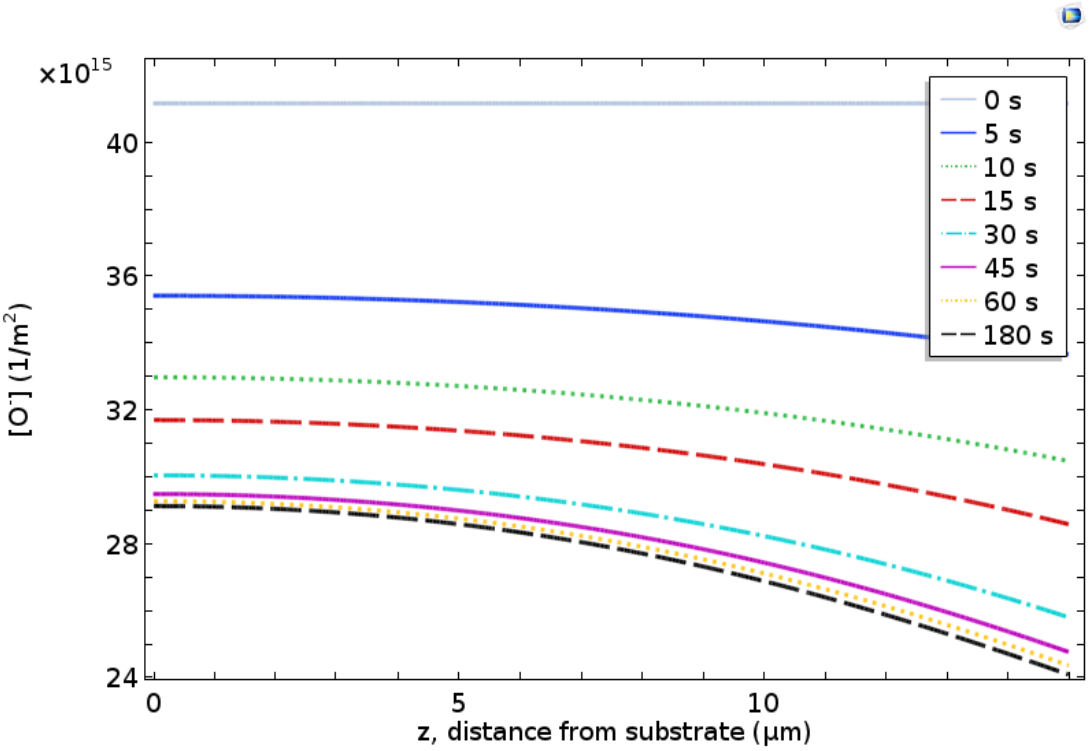


Figure 4-2. Transient analysis of the ionized oxygen density [O^-] in 15 µm thick SnO_2 film at T = 300°C. Response to the step change of CO concentration of 0.00814 mol/m^3 at t=0.

The local conductance variation along the sensing film thickness with time are given in the *Figure 4-3*. For an n-type semiconductor the potential barrier theory states the inverse relation of the conductance with acceptor surface state density. The acceptor surface states decrease the number of electrons in the conduction band. Since electrons are the majority carriers for an n-type semiconductor, the conductance decreases as the acceptor surface states increases. The conductance was given in equation *3-18* as:

$$G = G_0 exp\left(-\frac{q^2 N_s^2}{2k_B \epsilon_r \epsilon_0 N_d T}\right)$$

Where N_s $(= (N_A - N_D)x_0)$ refers to the charge density in the space charge region with thickness of x_0 and it is in inverse relation with the conductance. Since, only the

ionization of the oxygen was taken into account in this model, the acceptor surface states are related with the ionized oxygen density. The oxygen species that are ionized on the surface by creating a depletion layer by trapping electron from the conduction band. Therefore, ionized oxygen density is equal to the charge density in the space charge region ($N_s = [O^-]$). It means that, higher local conductance should be observed for lower ionized oxygen concentrations. As it was seen from the *Figure 4-3* conductance of the film is more uniform at the beginning (i.e. $t = 5$ s) and with time, the exterior surface becomes more conductive with time due to the electrons donored to oxygen by carbon monoxide. The ionized oxygen transfers the electrons that was trapped before to the conduction band of the SnO_2. Therefore, the conductance increases as the ionized oxygen density decreases. This explains the upward shift in the conductance profiles.

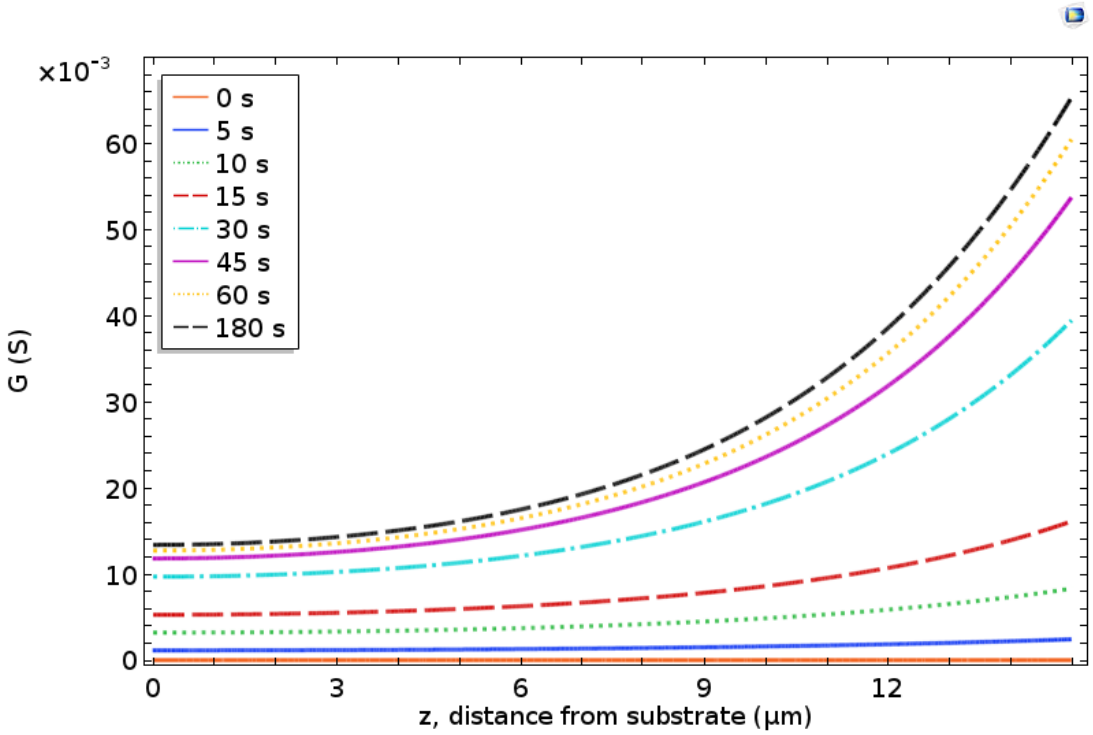


Figure 4-3. The change in the local conductance (G) with time and its variation along the z (thickness) direction in 15µm SnO_2 sensing film at T=300 °C. Response to the step change of CO concentration of 0.00814 mol/m³ at t=0 in an excess oxygen ambient. ($G_i = 9.31 \times 10^{-5}$)

When a potential energy difference is provided by applying constant pointwise potential to the both sides of the film, an electric field and thus a current density is constituted in x and z directions in two dimensional model. The conductance variation causes a current variation through the film thickness (z direction). This causes a distribution of x-component of the current density (J_x) through the thickness of the film. The dynamic behavior of the current density along the z axis is shown in *Figure 4-4* in which the ordinate represents the current density with units of amperes per unit cross-sectional area (thickness×length) at $x = 500$ µm. As time increases the distribution profiles of J_x get closer and shift upward since conductance increases.

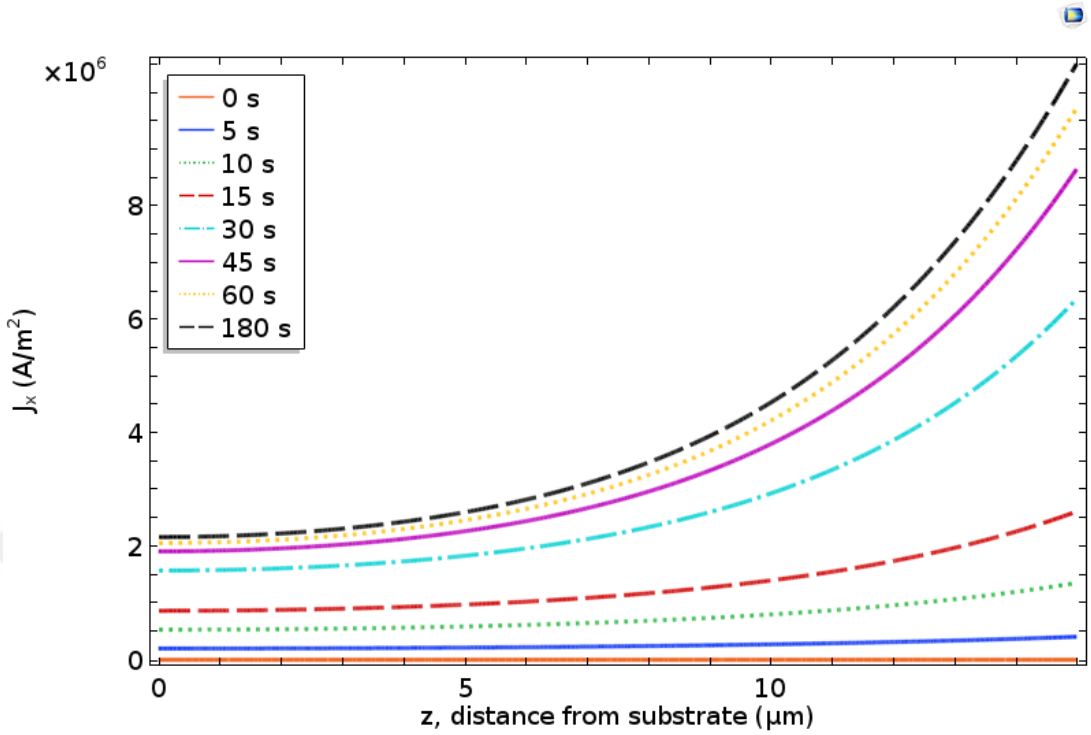


Figure 4-4. The x-component of the current density (J_x) profile development in 15µm thick SnO_2 film at T=300°C. Response to the step change of CO concentration of 0.00814 mol/m³ in an excess oxygen ambient at t=0. ($x = 500\ \mu m$)

In order to analyze the response of the semiconductor gas sensor, the local conductance was spatially averaged in z direction and the resulting time course of conductance is shown in *Figure 4-5*. It should be noted that spatially averaged conductance changes only in z direction. The abscissa shows the time in seconds and $t = 0$ corresponds to the beginning of exposure of surface to carbon monoxide introduced to the system and the ordinate shows the value of spatially averaged conductance which was found by integrating the local conductance over z direction and dividing it by the thickness of the film:

$$G_{avg}(t) = \frac{1}{h} \cdot \int_0^h G(x,t) \cdot dz$$

The average conductance increases with time because of the mass transfer and reaction of carbon monoxide takes place through the film and the concentration of ionized oxygen decreases by reaction. Ionized oxygen is consumed with time due to the reaction between ionized oxygen and carbon monoxide. Since the replenish rate of ionized oxygen is slow, the consumption reaction of ionized oxygen is getting slower with time due to the decrease in its concentration with time until the new equilibrium state is achieved. The conductance increase can be explained by the slower replenishment of O^- species over the surface as a result of slower ionization rate. Therefore, new equilibrium concentration of ionized oxygen species is achieved. Since the equilibrium concentration of the ionized oxygen is lowered compared to its initial state, the potential energy barrier decreases. Thus, the conductivity of the sensing film increases. The change in conductance decreases with time as approaching to new equilibrium of ionized oxygen species on the surface. At lower times $[O^-]$ has high values thus, the rate of consumption of $[O^-]$ is high. As concentration of O^- decreases with time, the rate of reaction between CO and O^- decreases. Therefore, the decrease in change of averaged conductance continues until the replenishment and consumption rates of ionized oxygen equalize and conductance becomes constant once the steady state is established.

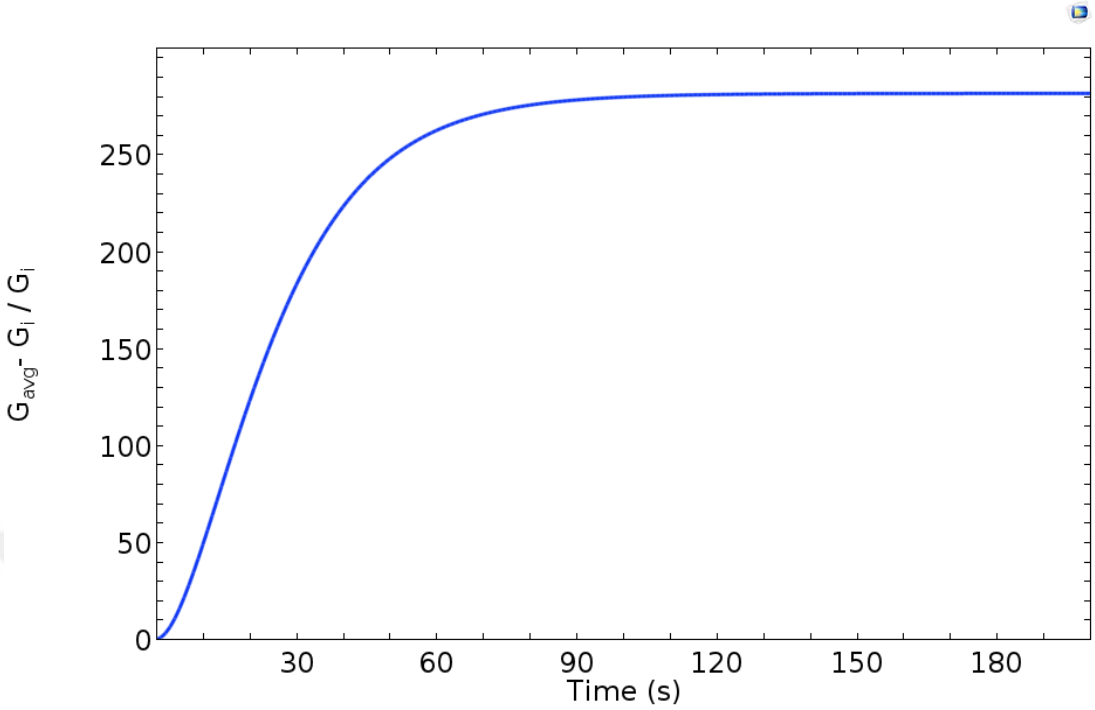


Figure 4-5. The normalized response of the 15 µm thick SnO_2 film during exposure of carbon monoxide an excess oxygen ambient at T= 300 °C. Step change in CO concentration of 0.00814 mol/m^3 at t=0. (x=500 µm)

The transient response of the sensor is also expressed in terms of electrical current in *Figure 4-6*. The direct current provided to the system by applying 5V constant electrical potential difference from both sides of the sensing film. As expected, it exhibits almost the same dynamic behavior of the average conductance. As conductance increases the current also increases.

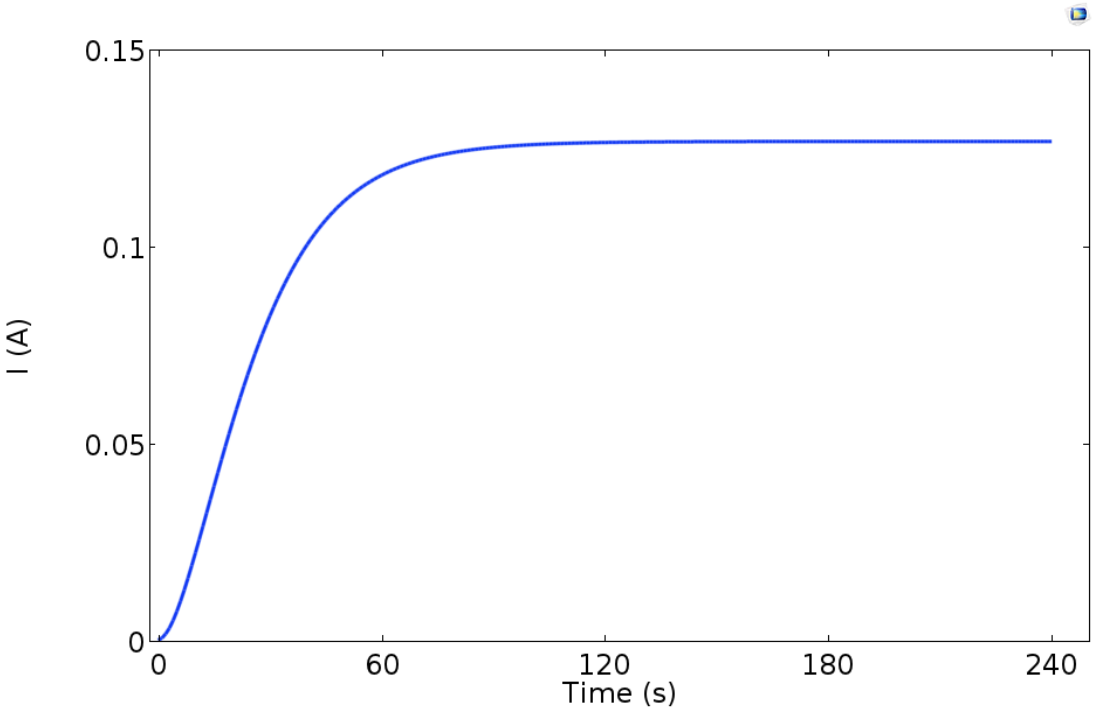


Figure 4-6. Electric current signal response of the 15 µm thick SnO_2 sensing film to carbon monoxide in excess oxygen ambient at T= 300 °C. Response to the step change of CO concentration of 0.00814 mol/m^3 at t=0.

In overall as explained in the literature review part, the oxygen species has uniform initial distribution in the SnO_2 giving rise to high resistance. As carbon monoxide diffuses through the film and it reacts with previously ionized oxygen species. The electrons donored by CO are transferred into the conduction band of semiconductor and the resistance of the material decreases as seen in *Figure 4-5*. The concentration profile of carbon monoxide developed by the mass transfer and reaction rate. The ionized oxygen concentration is determined by the reaction rates of CO oxidation, O_2 ionization and oxygen mass transfer which affects the current density. Thus, close to the surface which is exposed to the carbon monoxide gas the higher values of conductance and current density should be observed and this behavior can be obviously seen in *Figure 4-4*. Also the response behaviors are consistent with the

current density evolution with time which is faster at smaller times and getting slower as time increases. The same observation can be made from the *Figure 4-6.*

The sensing mechanism that is explained previously can be seen more clearly in *Figure 4-7* in which the two dimensional plots of current density are included. These plots show the current density behavior which is expressed with arrow representation with time. 5 V DC electrical potential applied to the system from the pointwise electrodes which are located on both sides of the sensing film at 7.5 μm depth from the gas exposed surface and the electrode spacing is 1 mm. The z direction (direction perpendicular to the substrate or surface) corresponds to ordinate and the x direction in which the electric field was applied corresponds to the abscissa. The arrows were plotted in the same scale which means the sizes of the arrows can be compared for each case and the direction of the arrows shows the flow direction of the current.

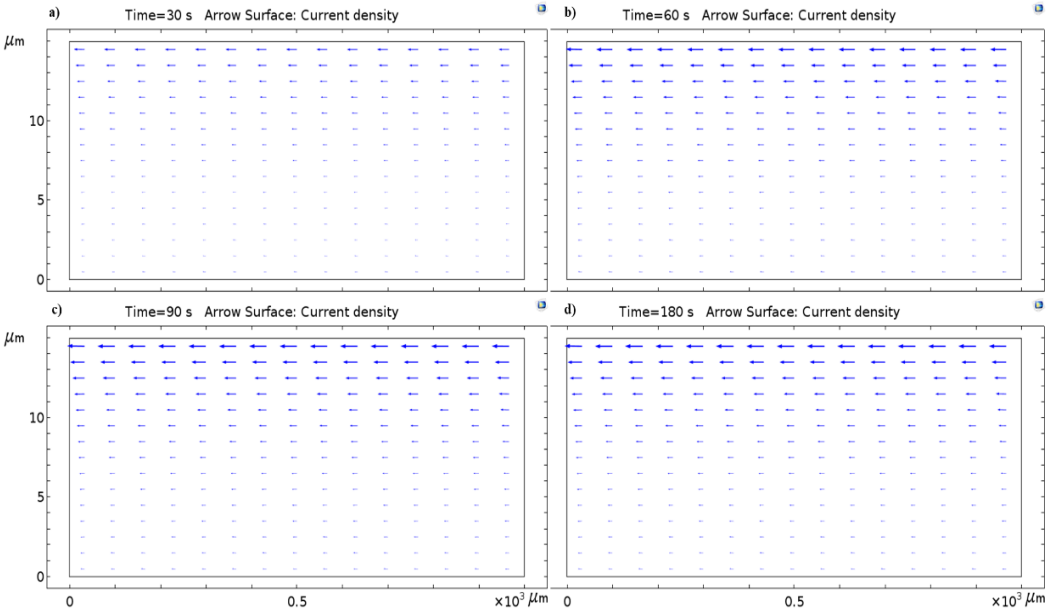


Figure 4-7. The arrow representation of the current density for 15 μm thick SnO_2 film response to the step change of CO concentration of 0.00814 mol/m^3 in an excess oxygen ambient at times: a) t=30 s; b)60 s; c)90 s; d)120s. Note that the scales for the arrows are same. (T=300 °C)

The orientation of the arrows shows that the x component of the current density is much larger than the z component of the current density. It is an expected situation since there is a small potential difference that is resulted from the potential energy barrier height distribution in z direction. The variation of J_x in z direction become more apparent as time increases because of the variation of the carbon monoxide concentration and the ionized oxygen density over the surface. Also the size of arrows getting larger as from t=0 to t=180s which means magnitude of the current density increases. The reason is that as the reaction between ionized oxygen and carbon monoxide continues, more electrons can release from the acceptor surface sites and return back to the conduction band. This charge transfer process increase conductivity of the film and therefore, the current density increases. As it can be from the four images given at different times, for 60s the arrows are getting larger and the distribution become more pronounced whereas after 60s this change in magnitude becomes very small as system approaches new steady state. Apparently, most of the current flows upper half of the gas sensor due to the competitive effect of diffusion and reaction of carbon monoxide. Thus, positioning the electrodes at upper parts will provide higher signals. It can be said that electrode position is important for getting higher current signals when the effect of diffusion is significant.

4.2. Effect of Temperature

The effect of temperature on the dynamic behavior of sensing layer was examined in 150-600 °C temperature range with 50°C intervals. Before dynamic simulations, initial conditions and parameters for the model for each temperature were determined. The simulations at this part were performed for 10 μm thick film with 1000 μm electrode spacing and for two different pore diameters (1nm and 4nm) which only affect the diffusion coefficient.

4.2.1. Initial Values of Ionixed Oxygen, Conductance and Resistance at the Operating Temperatures

The initial values of the ionized oxygen density ($N_{s,i}$), conductance (G_i) and the resistance (R_i) for each temperature were determined by solving the rate equations that describe oxygen chemisorption and ionization steps before introduction of CO to the ambient environment. The values of the $N_{s,i}$, G_i and R_i for different operating temperatures are given in *Table 4-1* in which the steady state value of the ionized oxygen density increases as temperature increases. That means the acceptor surface states trap more electrons from the bulk when initial equilibrium of the oxygen with SnO_2 was established. This increase in acceptor surface states (the ionized oxygen density in this case) will decrease the conductance of the material. On the other hand, temperature enhances the material conductance due to the thermally excited electrons from valence band to the conduction band. It can be seen from *Table 4-1*, at the initial equilibrium state higher conductance values are obtained at high temperatures. That means that when there is only oxygen species present in the ambient, the conductance is more sensitive to temperature compared to surface kinetics of oxygen.

Table 4-1. Initial values of ionized oxygen, conductance and resistance at different operating temperatures.

$T\ (°C)$	$N_{s,i} \times 10^{-16}\ (m^{-2})$	$G_i \times 10^{5}\ (S)$	$R_i \times 10^{-5}\ (\Omega)$
150	3.9135	0.9901	1.010
200	4.0021	2.1845	0.4578
250	4.0608	4.7980	0.2084
300	4.1183	9.3053	0.1075
350	4.1716	16.146	0.0619
400	4.2281	25.642	0.0390
450	4.284	38.2	0.0262
500	4.337	54.4	0.0183
550	4.39	74.4	0.0134
600	4.44	98.2	0.0102

The mobility of the electrons is also inversly proportional to temperature which can be expressed as $\mu \sim T^{-1.5}$. Therefore, resistance decreases with the increasing temperature due to higher mobility of electrons (or holes for p-type). In the present work, the mobility was lumped in the pre-exponential factor of the conductance term and taken as constant value and its variation with temperature was neglected due to its weak dependence of temperature when compared to the density of surface states. However, it may still be important for the comparison of cases that have large temperature differences.

4.2.2. Effect of Temperaure on the Conentration, Conductance and Potential Barrier Distributions

The steady state CO concentration profiles were examined for a temperature range of 150-600 °C which is exposed to 0.00814 mol/m^3 of CO continously in an excess oxygen ambient. In order to analyze the effect of temperature and pore size on the

competitive effect of mass transfer and reaction rate and resulting concentration distribution, two different 10 μm thick mesoporous sensing films having different pore size values (1nm and 4nm) were examined and the results are compared. The effect of temperature on the concentration profiles for 4 nm and 1 nm pore size are shown in *Figure 4-8a* and *Figure 4-8b* respectively . In both graphs z=0 and z=10 correspond to the impermeable substrate and gas exposed surface respectively for the 10 μm thick sensing film.

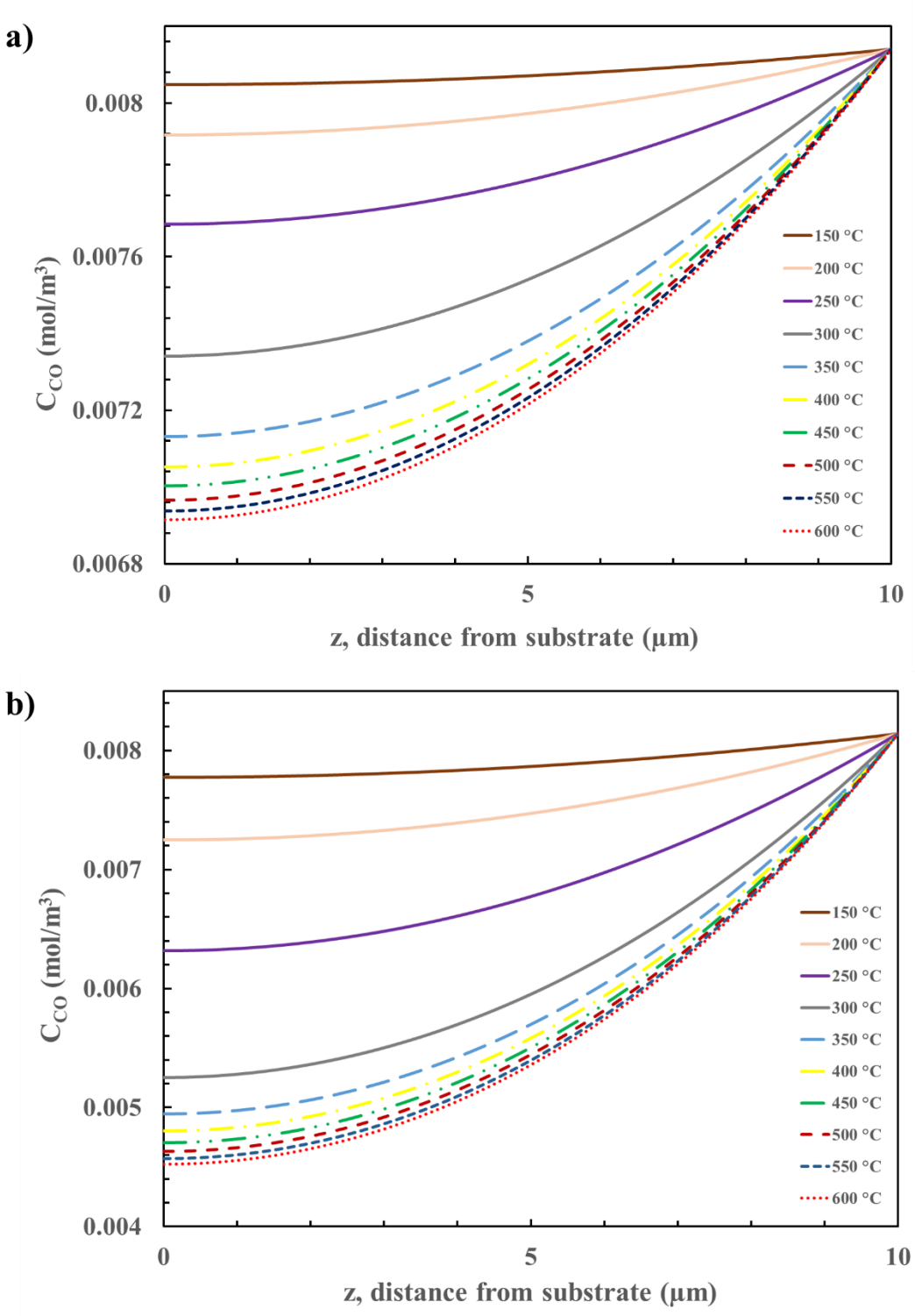


Figure 4-8. The steady state CO concentration distributions in the 10 µm SnO_2 film at temperatures between 150-600 °C for pore diameters :a)4nm; b)1nm.

At low temperature range (150-200 °C), the concentration change with depth (z direction) is small compared with moderate (250-300 °C) and high temperature ranges (350-600°C) which can be explained by the exponential increase of reaction rate with temperature. At low temperature change, the reaction rate is slow and more comparable with mass transfer rate which results with small change in concentration in z direction (*Figure 4-8a* and *Figure 4-8b).* However, the effect of temperature on reaction rate is more pronounced in moderate temperature range and more competitive with mass transfer rate. Temperature affects both reaction and the diffusion however there is an exponential dependence of temperature on the reaction rate constants which were defined by the Arrhenius relation. On the other hand, the Knudsen diffusion coefficient only affected by the square root of the temperature as seen in equation that is given below:

$$D_{k,eff} = \frac{\varepsilon}{\tau} \cdot \frac{4r}{3} \cdot \sqrt{\frac{2 \cdot R \cdot T}{M_{CO} \cdot \pi}}$$

Therefore, increase in temperature enhances the reaction rate more significantly than diffusion coefficient. These general observations that were obtained for 4 nm pore size are also in line with the results obtained for 1 nm pore size. However there are some important differences between two cases. The decrease in the pore diameter should cause a decrease in mass transfer rate due to the decrease in Knudsen diffusion coefficient. Therefore, the mass transfer rate is expected to be more critical in 1 nm pore size case. Knudsen diffusion coefficient values slightly change with temperature. These values are in between $4.42 \times 10^{-8} - 4.42 \times 10^{-8}\ m^2/s$ and between $1.11 \times 10^{-8} - 1.58 \times 10^{-8}\ m^2/s$ for 4nm and 1nm pore diameter respectively. As it is seen from *Figure 4-8*, the concentration of carbon monoxide within the moderate and high temperature ranges are significantly lower than the 4 nm case which indicates the lower rate of diffusion. However, the effect of temperate becomes less significant at high temperature range as the concentration of carbon monoxide is still significantly high even on the substrate surface (z=0). In order to understand the effect of

temperature on the reaction kinetics, the concentration profiles of ionized oxygen within the same temperature range were analyzed.

In *Figure 4-9a* and *Figure 4-9b* the steady state concentration profiles of the ionized oxygen were plotted with respect to temperature for two different pore diameters that were studied. The ordinate shows the number of ionized oxygen per square meter and the abscissa shows the distance from the impermeable substrate. The smaller graphs placed on the right top of the figures provides a closer look for convenience.

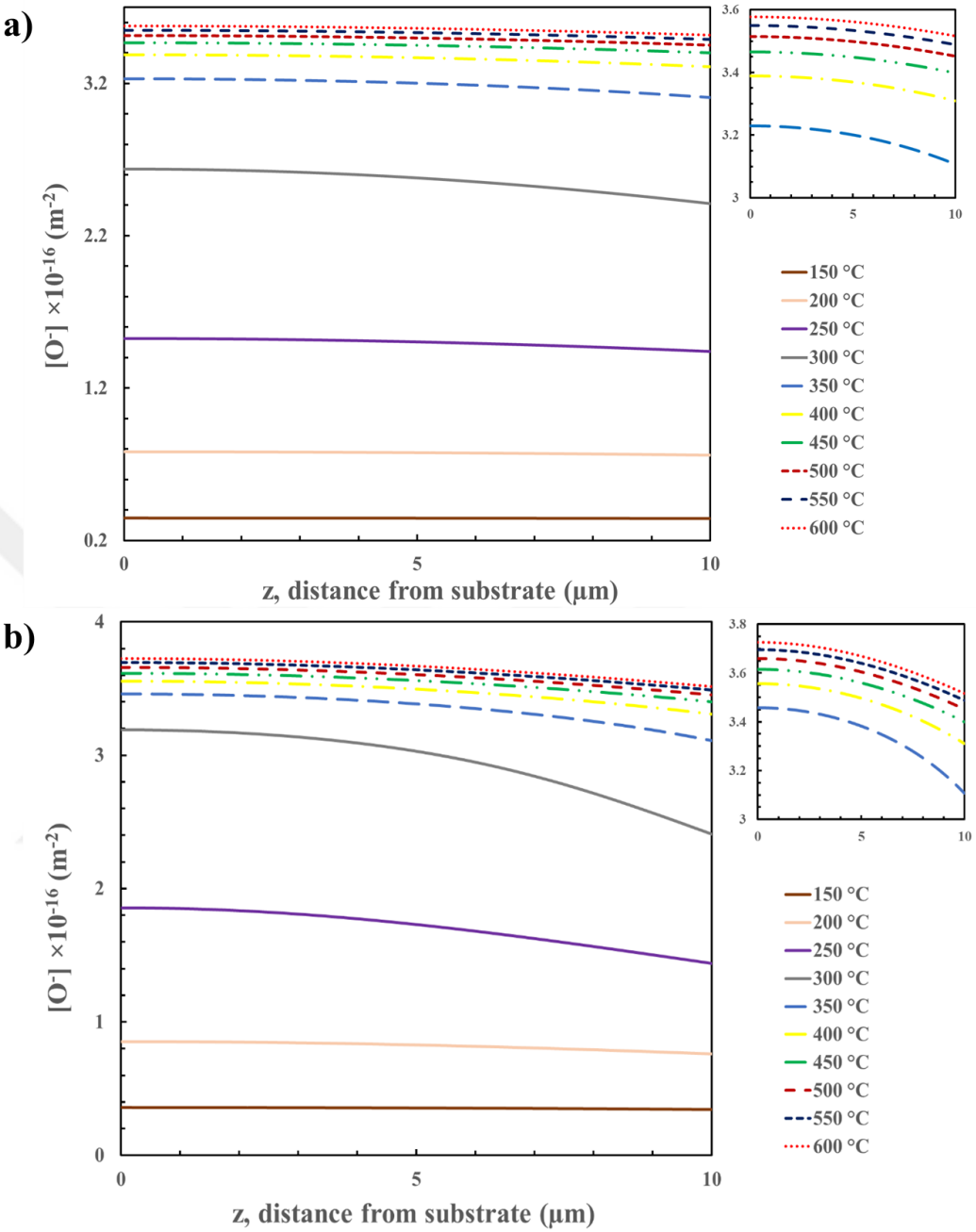


Figure 4-9. The steady state ionized oxygen concentration distributions in the 10 µm SnO_2 film at different temperatures for pore diameters: a) 4 nm; b)1nm.

As stated earlier the reaction with carbon monoxide determines the surface density of ionized oxygen. For convenience the reaction mechanism for the simulated model is given below as:

$$\frac{1}{2}O_2 + S \underset{k_{-1}}{\overset{k_1}{\leftrightarrow}} 2O - S$$

$$O - S + e^- \underset{k_{-2}}{\overset{k_2}{\leftrightarrow}} O^- — S$$

$$O^- - S + CO \overset{k_3}{\rightarrow} CO_2 + S + e^-$$

The ionized oxygen over the semiconductor surface is consumed by the reaction with CO and replenished by oxygen diffusion and ionization over the surface. The decrease of ionized oxygen density in the sensing film from its initial state shows that the ionization rate is smaller than the oxidation reaction of carbon monoxide with ionized oxygen. As it can be seen from the *Figure 4-9*, the ionized oxygen surface concentration is almost constant along the depth of sensing layer and increases with temperature. It is clear that at low and moderate temperature range, the equilibrium surface concentration of ionized oxygen is low and favored by temperature. The ambient environment is comprised of excess oxygen and contains 0.00814 mol/m^3 CO. These results show that surface oxygen ion concentration is almost constant along the sensing layer depth and it changes with temperature only. Therefore, the oxygen concentration over the sensing layer surface can be assumed as at equilibrium under the simulation conditions. The adsorption and ionization reactions of oxygen are given as:

$$\frac{1}{2}O_2 + S \underset{k_{-1}}{\overset{k_1}{\leftrightarrow}} 2O - S$$

$$O - S + e^- \underset{k_{-2}}{\overset{k_2}{\leftrightarrow}} O^- — S$$

It can be clearly seen from *Figure 4-9* that the change in ionized oxygen density much larger at low operating temperatures. From *Table 4-1* the initial value of the ionized oxygen density is about 3.9×10^{16} m^{-2} at 150 °C and the change in ionized oxygen is larger than 3×10^{16} m^{-2} whereas, at 600 °C change in number of ionized oxygen

is not even larger than 1×10^{16} m^{-2}. This change in ionized oxygen density in the sensing film also decreases with decrease in pore size. That means that for smaller pore size the Knudsen diffusion coefficient is smaller and diffusion is relatively small compared to the consumption reaction. Therefore, the diffusion effect is more pronounced. Due to the less carbon monoxide concentrations in the sensing film for 1nm pore radius the change in ionized oxygen is not very large as in the 4nm pore diameter case. Among the activation energies the E_1 $(31427.7\, J/mol)$ and the parameter $E_{-1} - E_2$ $(58535.35\, J/mol)$ have larger values and they have opposite influence on the ionized oxygen density. Both of them are appeared in the rate equation that describes the transient change in ionized oxygen which is given below for convenience:

$$\frac{dN_s}{dt} = exp\left(-\frac{q^2 N_s^2}{2k_B \epsilon_r \epsilon_0 N_d T}\right)\left(\frac{k_{1,0} exp\left(-\frac{E_1}{RT}\right)[S][O_2]^{1/2} + k_{-2,0} exp\left(-\frac{E_{-2}}{RT}\right)N_s}{\left(\frac{k_{-1,0}}{k_{2,0}N_D}\right) exp\left(-\frac{(E_{-1}-E_2)}{RT}\right) + exp\left(-\frac{q^2 N_s^2}{2k_B \epsilon_r \epsilon_0 N_d T}\right)}\right)$$
$$- k_{-2,0} exp\left(-\frac{E_{-2}}{RT}\right)N_s - k_{3,0} exp\left(-\frac{E_3}{RT}\right)N_s C_{CO}$$

Since they have large values, at lower temperatures the effects of those parameters are significantly reduced. E_3 $(5121.42\, J/mol)$ and E_{-2} $(4637.3\, J/mol)$ have very low activation energies compared to those given above therefore, at low temperatures their effects are relatively large. The effect of consumption reaction is large compared to the reverse reaction of ionization. The term $(k_{-2,0} exp\left(-\frac{E_{-2}}{RT}\right)N_s)$ that describe the reverse reaction of ionization affects both formation and consumption of ionized oxygen. And also, the multiplier of consumption reaction ($k_{3,0}N_s C_{CO} \sim 10^{15}\, m^{-2} \cdot s^{-1}$) is larger than the multiplier of the reverse reaction of ionization ($k_{-2,0}N_s \sim 10^{14}\, m^{-2} \cdot s^{-1}$). The oxygen consumption rate is relatively higher than replenishment rate at low temperatures. Among two large activation energies, the effect of E_1 is more pronounced since its multiplier ($k_{1,0}[S][O_2]^{1/2} \sim 10^{18}\, m^{-2} \cdot s^{-1}$) is very large compared to the multiplier of $(E_{-1} - E_2)$ which is $k_{-1,0}/\left(k_{2,0}N_D\right) = 92.44$. This explains the significant change of ionized oxygen

density at low temperatures due to the slow replenishment. Although activation energy required for the chemisorption step of oxygen is high, at high temperatures its effect become important since it has very large multiplier. Thus, the replenishment rate of ionized oxygen become comparable with the rate of consumption of ionized oxygen with carbon monoxide. This also reveals the reason of sharp variations in CO concentration in sensing film at temperatures higher than 300°C. Since, the replenish of ionized oxygen become faster at high temperatures higher ionized oxygen densities in the film is seen. Therefore, the surface reaction rate of carbon monoxide with ionized oxygen increases and the CO diffusion becomes relatively slow and its effect become more pronounced. It means that more carbon monoxide is consumed before diffusing deeper regions of the sensing film. In high temperature region (higher than 350 °C) the concentration profile curves in *Figure 4-8* get closer, the effect of the temperature on relative rates of mass transfer and reaction is not as high as the low temperature region. This can be explained by Φ, Thiele modulus, (dimensionless number that is used for the comparison of internal mass transfer and the reaction) and effectiveness factor relation. The effectiveness factor can be defined as:

$$\eta = \frac{rate\ of\ whole\ sensing\ film}{rate\ of\ the\ outer\ gas\ exposed\ surface\ of\ the\ sensing\ film}$$

As Thiele modulus increases the effectiveness factor decreases and for the larger values of Thiele modulus Φ, relation between them can be approximated as reciprocal relation. Therefore, as Thiele modulus increases, the effectiveness factor will decrease. However, this decrease will get smaller for larger values of Φ. At high temperatures the Thiele modulus has large values due to high reaction rates. Since, in this range change in η is less compared to lower values of Φ (low temperature range), the CO concentration profiles get closer in *Figure 4-8*.

The ionized oxygen concentration demonstrate similar trend with the smaller 1 nm pore size *Figure 4-9*. However, significantly higher oxygen ion concentrations were observed at all temperatures. Since the mass transfer is slower due to smaller pore size and the effect of the reaction become more dominant as mentioned for the carbon

monoxide concentration distribution profiles. Therefore, the mass transfer influence on rate is more pronounced and more carbon monoxide is consumed before penetrating deeper regions of the film. At high temperatures this effect become more clear and it causes smaller changes in ionized oxygen in deeper regions. This is why the ionized oxygen densities at the new established equilibrium is higher in the SnO_2 sensing film with 1 nm pore diameter.

The steady state variations of the potential energy barrier through the thickness (z-direction) of sensing layer were presented in *Figure 4-10* for the examined temperature interval. The ordinate of the figure shows the magnitude of the potential energy barrier (V) that is formed between the adjacent grains and abscissa shows the distance from the impermeable substrate. The simulations for all cases of different operating temperatures were carried out for 1 nm pore diameter case.

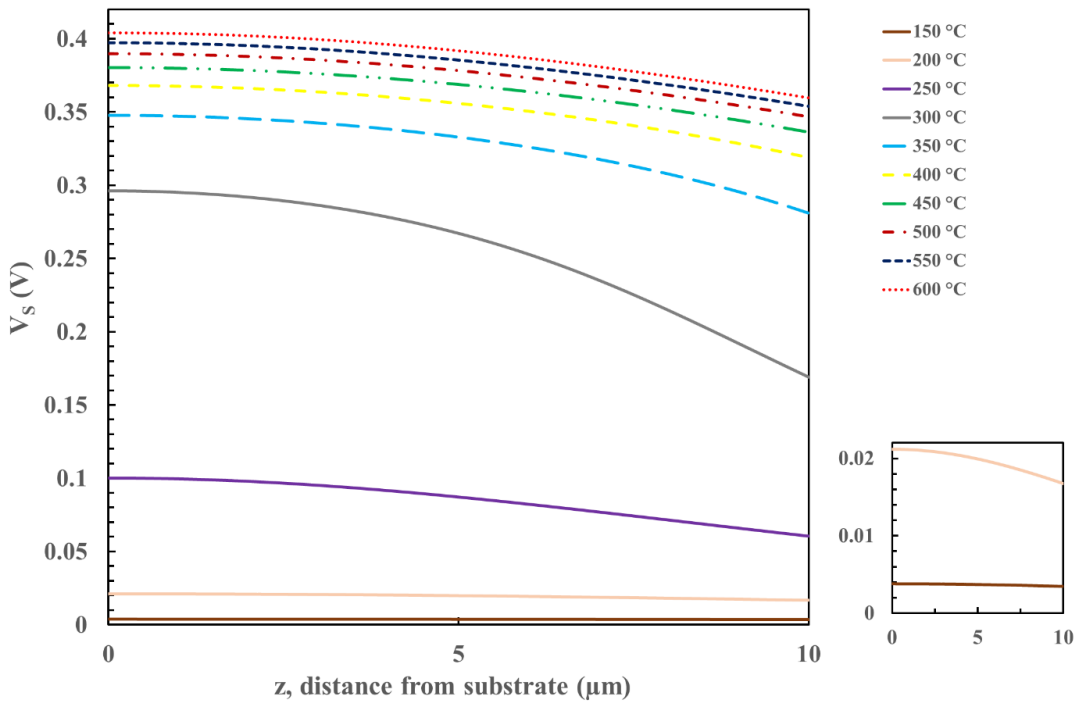


Figure 4-10. Temperature effect on the steady state potential barrier profiles for 10 µm thick SnO_2 film which has pore diameter of 1nm.

Since the gas exposed to outer surface (z=10 μm) the lowest values of the potential barrier can be seen at that boundary. The reason of this is as carbon monoxide gas reacts with the ionized oxygen which previously formed a potential energy barrier by acting as acceptor surface site, more electrons transferred from carbon monoxide to the conduction band so that the magnitude of the potential energy barrier decreases. As mentioned before due to the effect of mass transfer and reaction, carbon monoxide concentration decreases through the film thickness and the highest carbon monoxide concentration is observed over the outer surface. At low temperature range, the potential energy barrier is uniform and almost constant along the sensing layer depth. As the temperature increases the variation become more pronounced and the curves getting closer to each other. The increase in temperature increases the rate of carbon monoxide oxidation reaction and due to competitive effect of reaction and mass transfer, the carbon monoxide concentration through the film increases as the temperature increases. Also in conjunction with the *Figure 4-9* the largest change in potential drop from initial state to the steady state is seen at lowest temperature due to slow replenishment of the ionized oxygen and this change is getting smaller as temperature increases.

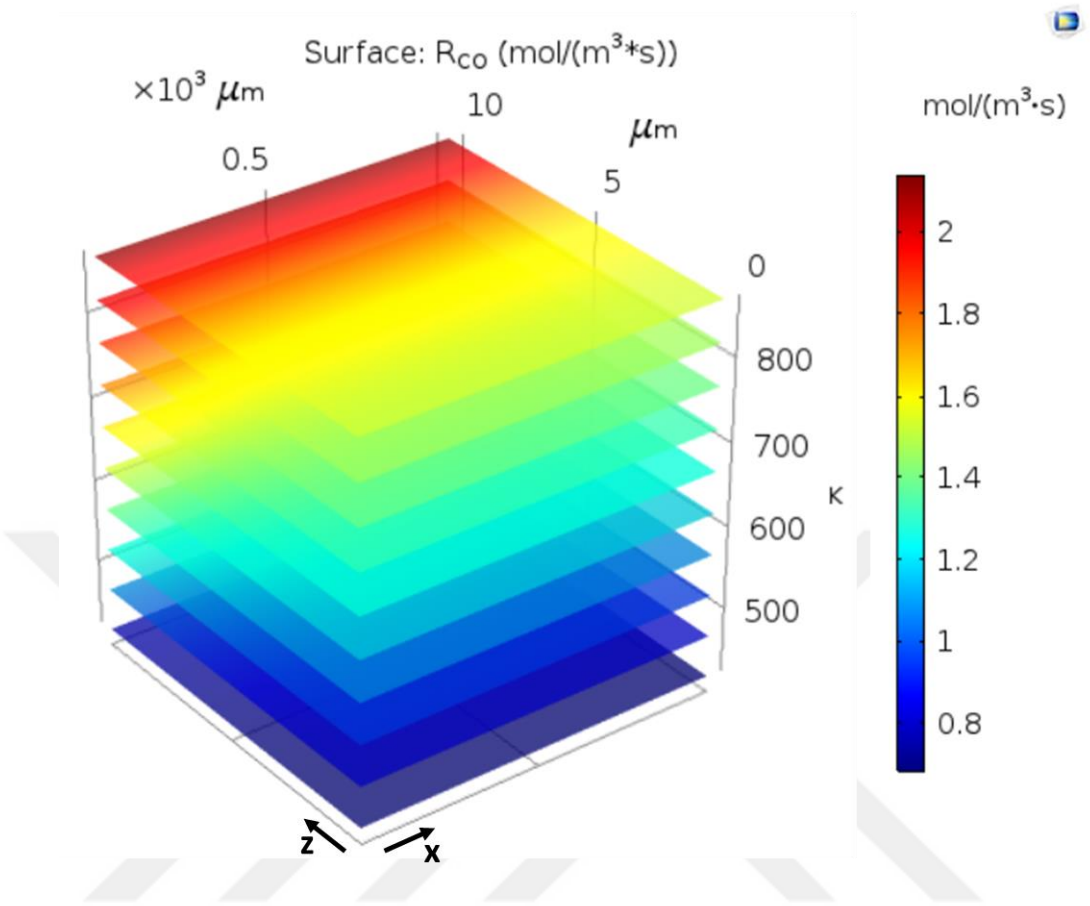


Figure 4-11. Two dimensional representation of the steady state consumption rates of CO at operating temperatures between 423-873K. Results were obtained for a step change of CO concentration of 0.00814 mol/m^3 in an excess oxygen ambient at t=0.

The effect of mass transfer and the temperature on the rate of reaction between carbon monoxide and ionized oxygen can be seen in *Figure 4-11* in which z direction represents the thickness of the film, x represents the electrode spacing. The surface plots show that in high temperatures the variation of the reaction rate along the z direction is more pronounced. On the other hand, as temperature decreases more uniform distribution of the rate can be seen which is in good agreement with the concentration distribution of the carbon monoxide. Also the surface plots show that

higher reaction rates were obtained at higher temperatures which is an expected result due to the temperature dependence of the reaction rate constant.

4.2.3. Temperature Effect On The Dynamic Response and Sensitivity

The temperature have remarkable effects on the reaction kinetics, thermodynamics and conductance. So the sensitivity, response time and dynamic response behavior of sensing layer should be carefully analyzed for operating temperature. In the *Figure 4-12.* Effect of temperature on the transient response of the 10 μm SnO2 sensing film to step change in CO concentration of 0.00814 mol/m3 in terms of electrical current. (x=500 μm) the effect of temperature on the time dependent current signals as a response to the step change of carbon monoxide concentration in ambient enviroment containing excess oxygen under 5V DC potential difference between two point electrodes . The simulations for this results were performed for 10 μm mesoporous thick film having 4 nm pore diameter in the temperature range of $150 - 600$ °C . The ordinate was plotted in logarithmic scale and it corresponds to the electrical current and the abscissa of the graph shows the time of the response. It should be noted that the initial current values for each case are different due to initial equilibrium states of ionized oxygen at different temperatures.

At low temperatures the current is much larger than the current values at high temperatures. As mentioned before, when temperature is low, the ionized oxygen is consumed with carbon monoxide faster and the rate of reverse direction ionizateion reaction is more pronounced. Because, activation energies for the reverse reaction of ionization and consumption reaction of ionized oxygen with carbon monoxide have lower values. This cause large changes in ionized oxygen density. On the other hand increase in temperature cause larger changes in the exponential terms that are $exp(-(E_{-1} - E_2)/RT)$ and $exp(-E_1/RT)$ due to large values of $(E_{-1} - E_2)$ and E_1. Therefore replenish of ionized oxygen increses, and new equikbrium value of ionized oxygen get closer to initial state which means that changes in current also decreases. Since reaction rates increases with temperature, the new equilbrium states

are established at high temperatures which can seen in *Figure 4-12*. It demeonstrates that at high temperatures the current flows in the semiconductor has very small values compared to the current values in lower temperature case. Although this temperature change can either increase or decrease ionized oxygen density by maximum of factor of three but conductance change will be much higher than that change due to exponential dependence of conductance to square of ionized oxygen density. Therefore small disturbances in ionized oxygen equilbrium cause high changes in current signal. In literature one of the solution to the selectivity problem is taking advantage of this competitive effects of kinetic parameters. This large difference in current with the change of temperature explains this. As it is seen from the *Figure 4-12* after $400\,°C$ the current signal starts to increase again with increasing temperature since the effect of temperature on reaction rates become less pronunced and its effect on conductance become predominant.

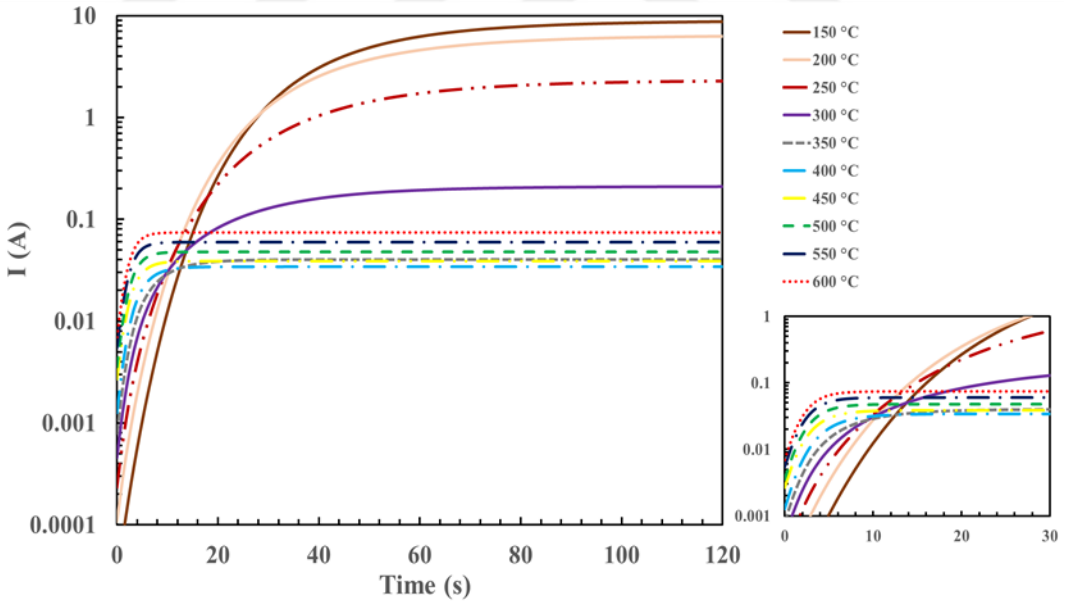


Figure 4-12. Effect of temperature on the transient response of the 10 µm SnO_2 sensing film to step change in CO concentration of 0.00814 mol/m^3 in terms of electrical current. (x=500 µm)

The response time is generally defined as the time corresponds to 90% of the steady state value of current or average conductance response following the step input of carbon monoxide concentration from zero to 0.00814 mol/m^3mol/m3 at t=0 in an excess oxygen environment. In *Table 4-2*, response time and time necessary to reach steady state current values are given for 10 μm mesoporous thick SnO_2 films having pores with 4 nm diameter for the temperature interval studied. The response time decreases with temperature as expected and which is favored kinetically. The staeady state is delayed at low temperatures because of the lower forward and backward reaction rates of oxygen ionization. When comparing two cases in which operating temperatures are 250 and 350 °C, the time required to reach steady state at 350°C is about 5 times faster than the sensor operated at 250°C. However, response time is not improved significantly above 350°C.

Table 4-2. Effect of temperature on the response time and the time required to reach steady state of an n-type 10 μm thick SnO_2 film continuously to 0.00814 mol/m^3 CO in an excess oxygen ambient.

Operating Temperature °C	**Response Time, t_{90} (s)**	**$t_{steady\text{-}state}$ (s)**
150	87	350
200	85	300
250	82	250
300	56	195
350	16	47
400	9	34
450	7	20
500	7	19
550	6	18
600	6	17

The temperature influence on the change in the response in terms of the normalized conductance (spatially averaged) for a 10 μm thick SnO_2 film with 4 nm pore radius was analyzed and the results are given in *Figure 4-13.* The ordinate was plotted in logarithmic scale due to large differences in the values of normalized responses obtained at different temperatures. The abscissa shows the response time which starts with exposure to 0.00814 mol/m^3 of carbon monoxide at t=0 in an excess oxygen environment. At lower temperatures normalized response values reach very high values. Initial equilibrium value of the ionized oxygen density and the resulting initial conductance depends on temperature. The initial conductance values are much higher at high temperature range than the values of initial conductance at low temperature range. As discussed before, the ionized oxygen species are replenished very slowly at low temperature range due to relatively higher activation energy than the oxidation of carbon monoxide. The change in ionized oxygen density (consumption with the

CO) is therefore large compared to higher temperatures which is the main reason of such large values of sensitivity. Same behavior was also observed in response times as given in *Table 4-2*. Until 300 °C the replenish of the ionized oxygen is very slow and as temperature starts to increase the effect of this replenishment becomes more prominent since it depends exponentially on temperature and also the variation in ionized oxygen become significant due to the competition between diffusion and reaction. Thus, the conductance changes exponentially decrease while at higher temperatures that exponential effect diminishes and very close values of normalized responses were obtained.

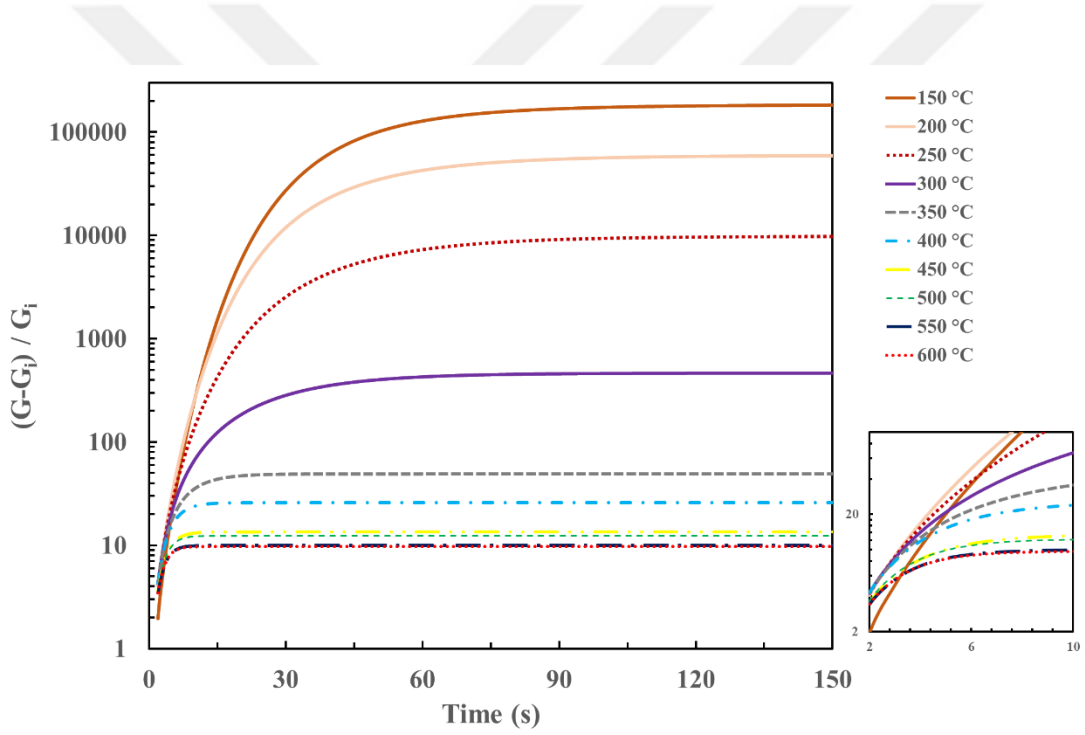


Figure 4-13. Effect of temperature on the transient normalized response of the 10 µm SnO_2 sensing film to the step change of CO concentration of 0.00814 mol/m^{3}in an excess oxygen ambient at t=0. (r=1nm).

The normalized response was defined as the ratio of change in average conductance during the exposure to the carbon monoxide to the initial conductance and it is given with $(G - G_i)/G_i$. In *Figure 4-13* at different temperatures the normalized responses and steady state averaged conductane values are given for an n-type SnO_2 film to the step response to the exposure of 0.00814 mol/m^3 carbon monoxide over mesoporous 10 μm thick sensing layer of SnO_2 having 1 nm pore size. The final averaged conductane values decreases as temperature increases until 400 °C with a high slope at lower temperatures and after 400 °C the final average conductance increases again. This behavior was also observed in the *Figure 4-12* in which the current signal was also increased after $400\,°C$ for the case of 4 nm pore diameter. The reason of this behavior may also be due to the effect of temperature getting predominont on conductance rather than effect on the kinetics. The same observation for the current behavior on both cases of pore diameters also can be interpreted as diffusion effect does not determine the dynamic behavior of the current but rather the competition between temperature effect on the kinetics and conductance is decisive. On the other hand, the normalized response decreases as temperature increases.

Table 4-3. Temperature effect on the steady state spatially averaged conductance and normalized response values for SnO_2 film have thickness of 10μm pore diameter of 1nm. (x=500μm)

$T_{op}(°C)$	$G_{avg}(S)$	$Normalized\ Response\ (G-G_i)/G_i$
150	1.8088	182684.9
200	1.2375	56647.35
250	0.3177	6620.729
300	0.01616	174.601
350	0.0049	29.23339
400	0.0048	17.8448
450	0.0058	9.687789
500	0.0073	9.142726
550	0.0093	7.445218
600	0.0117	7.296885

4.3. Film Thickness Effect

The effect of the film thickness on the sensor response in terms of current, concentration distribution, sensitivity and the current density were analyzed. For better comparison, simulations were conducted for SnO_2 films having 5, 10, 15, 20, 50, 100 μm thickness with 4 nm of pore diameter at $300\ °C$. The responses were obtained step change of CO concentration of 0.00814 mol/m^3 at t=0 in an excess oxygen environment. Since, the temperature is same the initial condition for ionized oxygen ($N_{s,i}$) density is applied for all thicknesses.

The influence of film thickness on carbon monoxide concentration in z direction is presented in *Figure 4-14*. The steady state concentration distribution of carbon monoxide was plotted for SnO_2 films having thicknesses of 5-100 μm and in all cases z=0 corresponds to the impermeable substrate. The variation of carbon monoxide

concentration along film thickness indicates the significance of mass transfer with increasing film thickness. Almost uniform distribution was obtained for 5 μm thick film, whereas in 100 μm thick film, almost half of the film deprived from carbon monoxide. The competitive effect of diffusion and reaction rate can be analyzed by Thiele modulus. As thickness, h, increases Φ increases which means the effect of the mass transfer on the rate become significant. The diffusion rate is relatively slower compared to the reaction rate in thicker films, thus CO consumed before penetrating deeper regions of the film. Although in all films carbon monoxide have the highest concentration value at the exposed surface, inner regions this value decreases and this decrease more pronounced as thickness increase. Thus, in regions far from the exposed surface of the film the rate of reaction decreases and most of the film is not effective as the exposed surface.

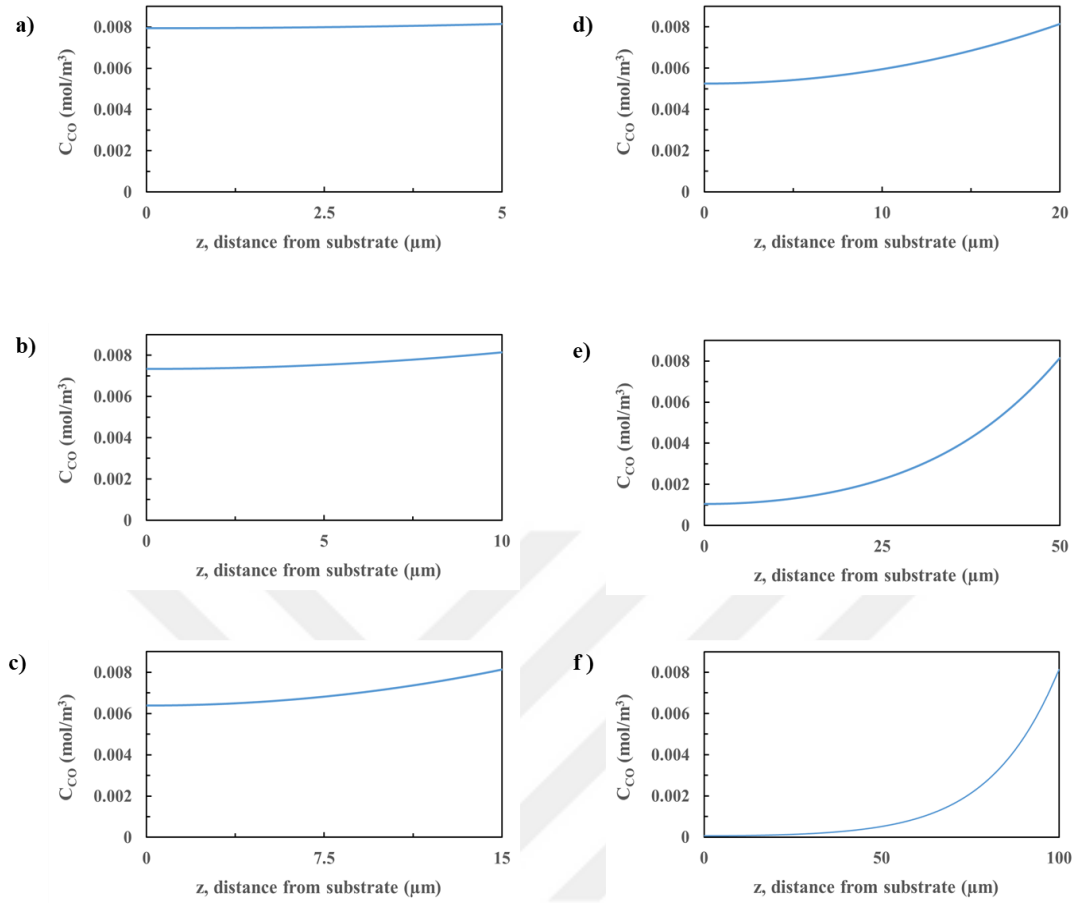


Figure 4-14. Steady state concentration distributions of CO in SnO_2 films have thicknesses of: a) 5µm; b)10 µm; c)15 µm; d)20 µm; e)50 µm f)100 µm. The results were obtained for a step change of 0.00814 mol/m^3 in CO concentration at t=0 and at T=300 °C

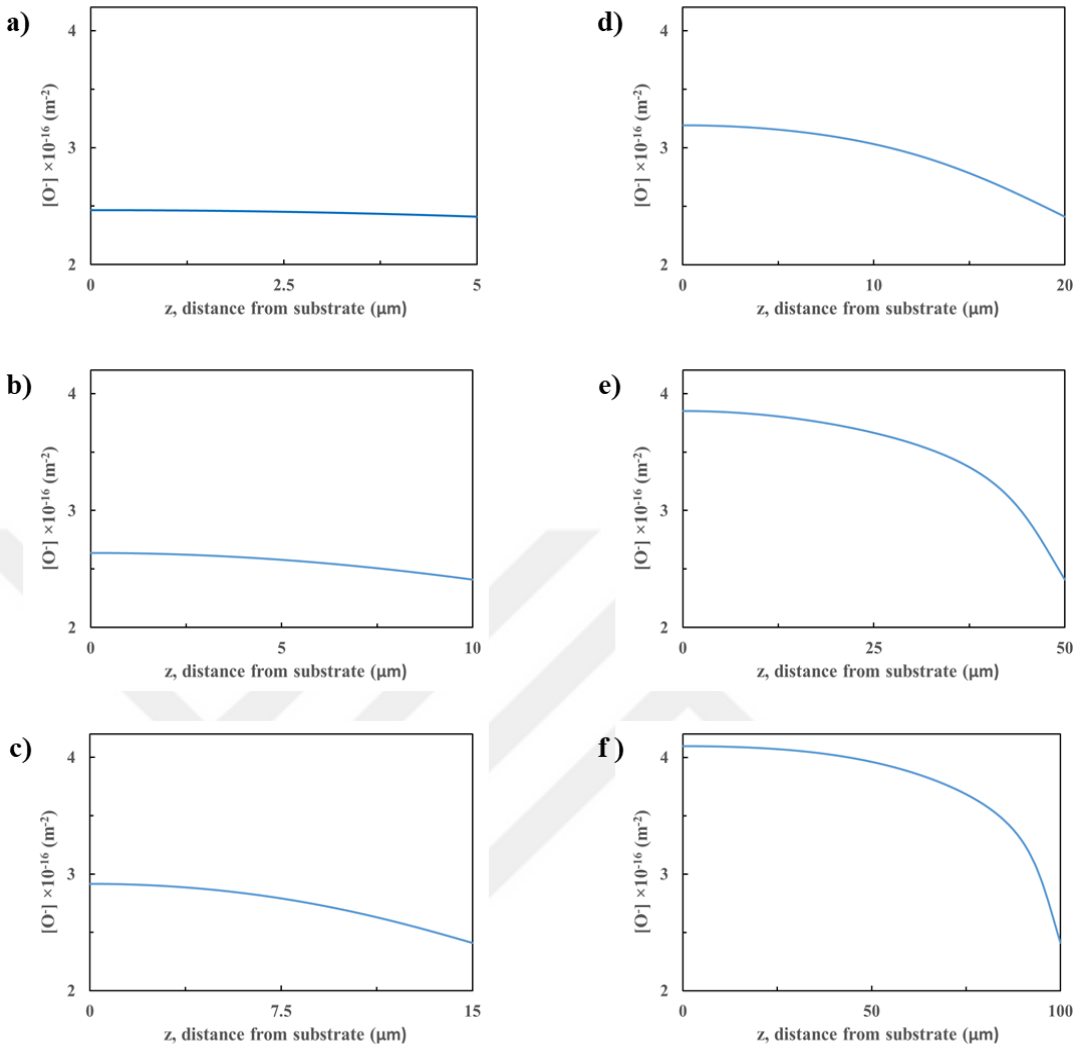


Figure 4-15. Steady state concentration distribution of ionized oxygen in SnO_2 films have thicknesses of: a) 5µm; b)10 µm; c)15 µm; d)20 µm; e)50 µm; f)100 µm. SnO_2 sensing films were exposed to 0.00814 mol/m^3 CO in an excess oxygen environment at 300 °C. (x=500µm)

The steady state ionized oxygen density distributions in SnO_2 films having thicknesses 5, 10, 15, 20 ,50, 100 µm are shown in the *Figure 4-15*. It is clearly seen that the variation become more apparent as thickness increases. Highest variation in ionized oxygen density is observed for 100 µm film thickness and almost uniform distribution

is seen in the film that has 5 μm thickness which is shown in *Figure 4-15a*. As the thickness increases the variation become more apparent since as thickness increases the diffusion effect become predominant for both carbon monoxide and oxygen. Therefore, larger variation in ionized oxygen is observed due to the reaction with carbon monoxide which causes consumption of ionized oxygen species. In regions close to the exposed surface, lower ionized oxygen density is seen for all cases since the carbon monoxide exist at those regions at higher concentrations which means higher oxidation rate of both carbon monoxide and ionized oxygen species. It means that the ionized oxygen density at the exposed surfaces cannot replenish to its initial value which is $4.1183 \times 10^{16}\ m^{-2}$. Although there is an excess amount of oxygen in ambient and it was assumed that adsorption step of the oxygen is fast, the ionization reaction of oxygen adspecies is relatively slow compared to its consumption rate.

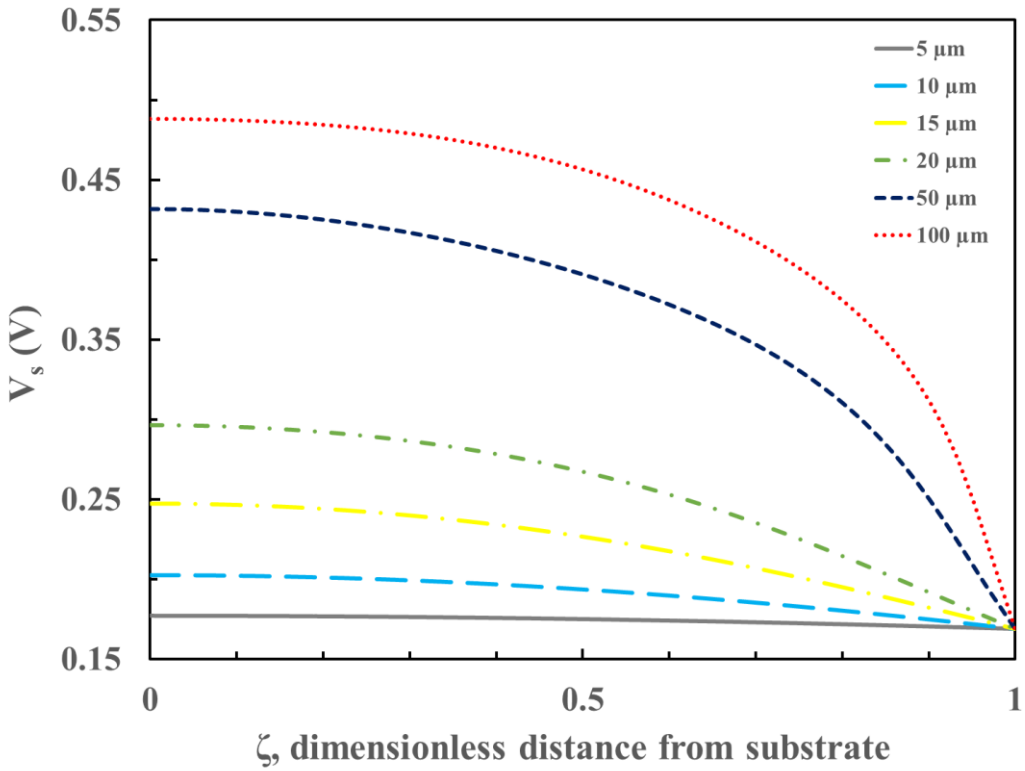


Figure 4-16. The effect of film thickness on the steady state potential energy barrier distribution for the SnO_2 films at 300 °C exposed to 0.00814 mol/m^3 CO in an excess oxygen environment. (x=500µm)

The steady state profiles of potential energy barrier between adjacent grains along the film thicknesses are shown in the *Figure 4-16* in which the abscissa represents the dimensionless distance from the substrate. The dimensionless distance was defined as the ratio of the distance to the film thickness ($\zeta = z/h$). Almost uniform profile was obtained for the 5 µm thick film case and the variation in potential energy barrier becomes larger as the thickness of the film increases which reveals that the electrons at inner regions of the grains cannot be easily transferred into adjacent grains. Therefore, there is significant difference in conductivity between the inner region and the exterior surface that the carbon monoxide is exposed. Ionized oxygen consumption is less at deeper regions in which carbon monoxide has low concentrations due to the

effect of the diffusion. Therefore, the potential energy barrier has higher values at deeper regions for thicker films. Doubling the film thickness in both thin films (10 μm to 20 μm) and thick films (50 μm to 100 μm) have similar effects on change of the carbon monoxide and ionized concentration distributions. However, the potential barrier change is larger in between thinner films. For example, increasing thickness 10 μm of 10 μm film increase the potential energy barrier with a value of about 0.1 V at the impermeable substrate surface, on the other hand 50 μm increase results about 0.05 V difference in potential barrier when compared 50 μm and 100 μm films. This means that effect of diffusion on the potential barrier is more pronounced as in thinner films.

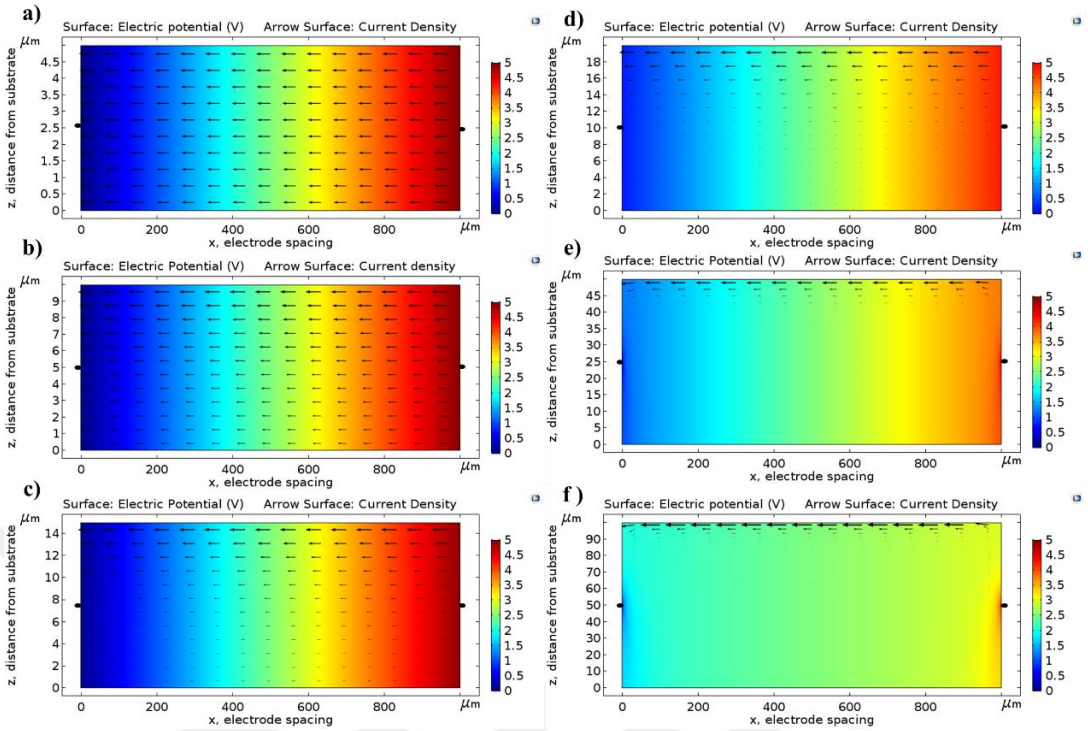


Figure 4-17. Steady state potential energy distributions and arrow representation of the current density for SnO_2 films having thicknesses of: a) 5μm; b)10 μm; c)15 μm; d)20 μm; e)50 μm; f)100 μm. The SnO_2 films were exposed to CO concentration of 0.00814 mol/m^3 in an excess oxygen environment at 300 °C. 5 V DC electric potential was applied with point electrodes from both sides of the sensing film with DC supplier.

In *Figure 4-17*, the effect of sensing layer thickness on the current density and electric potential value is illustrated for the 0.00814 mol/m^3 CO and excess oxygen exposure and 5 V DC electric potential applied through point electrodes. The arrows represent the current density and the colored surface plot indicates the value of electric potential value. The two dimensional graphs that represents each thickness case are plotted for different scales in arrow sizes so the size of the arrows should be compared in each graph in itself. The reason of the different scale selection is due to the order of magnitude difference in current density between the different film thickness cases. It

is clearly seen that, variation in current density shows remarkable increase with sensing film thickness which is related with the power requirement of the sensor. At 20 μm case, it can be said that current flows through the upper half of the film preferentially and for 50 and 100 μm cases, there is almost no current flowing through the bulk of the sensing layer and the upper exposed layer is the only the active part of the film. Thus, it is required higher potential energy drop to get same current signal with fully active sensing layer and there will be significant energy loss due to non-active part of the sensing film. Moreover, energy requirement for heater in thick films is higher compared to thin films. Since, large portion of the sensor is non-active the energy usage for heating will go to waste. Relatively smaller variations in concentration results with larger variations in current. Also one other observation can be made from those graphs that the voltage distribution changes as thickness increases. In thinner films, unidirectional (x) voltage variation was observed. However, two dimensional voltage variation (x,z) was observed in thicker films as expected. Therefore, the current density in z direction becomes comparable with the current density in x direction as film thickness increase.

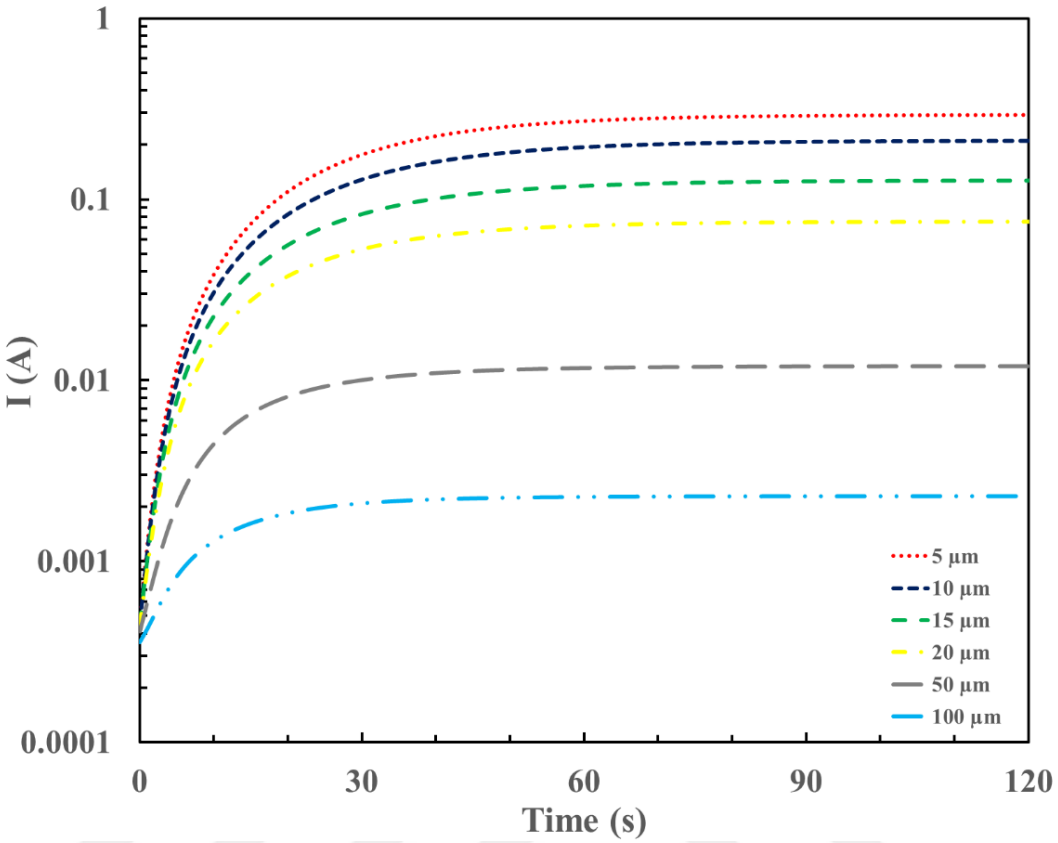


Figure 4-18. The effect of film thickness on the dynamic current response to the step change in CO concentration of 0.00814 mol/m^3 in an excess oxygen ambient at 300°C. 5 V DC electric potential applied through point electrodes at both sides of the SnO_2 sensing films. ($x = 500$ µm).

The effect of the film thickness of sensing layer on the dynamic response behavior of current following the step change of carbon monoxide concentration from 0 to 0.00814 mol/m^3 of at t=0 and at 300 °C was also investigated in *Figure 4-18*. Since the temperature is same for all cases the initial value of the conductance and the current are same for all film thicknesses. It can be seen that the current change is larger in thinner films and lower current signals were obtained as the thickness of the film increases. Since, in thinner films less mass transfer influence on the rate was observed, most of the film can be effectively used and potential energy barrier reduced even in

deeper regions. This means that conductivity of the inner regions of the film increases during the exposure to CO while in thicker films most of the inner region was remained unchanged compared to its gas exposed surface. Therefore, higher current signals were obtained in thin films.

The normalized current response ($(G - G_i)/G_i$) of SnO_2 sensing films (r=2nm) having thicknesses between 5-100 μm to step change in CO concentration in an excess oxygen ambient at 300°C is given in Figure 4-19. The ordinate which is given in logarithmic scale corresponds to the normalized response in terms of conductance and the abscissa shows the operating time at which the CO introduced to oxygen ambient at $t = 0$. In thicker SnO_2 films become thinner, the effect of diffusion on the rate of the film becomes insignificant and surface reaction controls the rate as previously discussed. Therefore, highest value of normalized response was obtained in 5 μm thick sensing film and as films are getting thicker the sensitivity decreases as seen from the *Figure 4-19.*

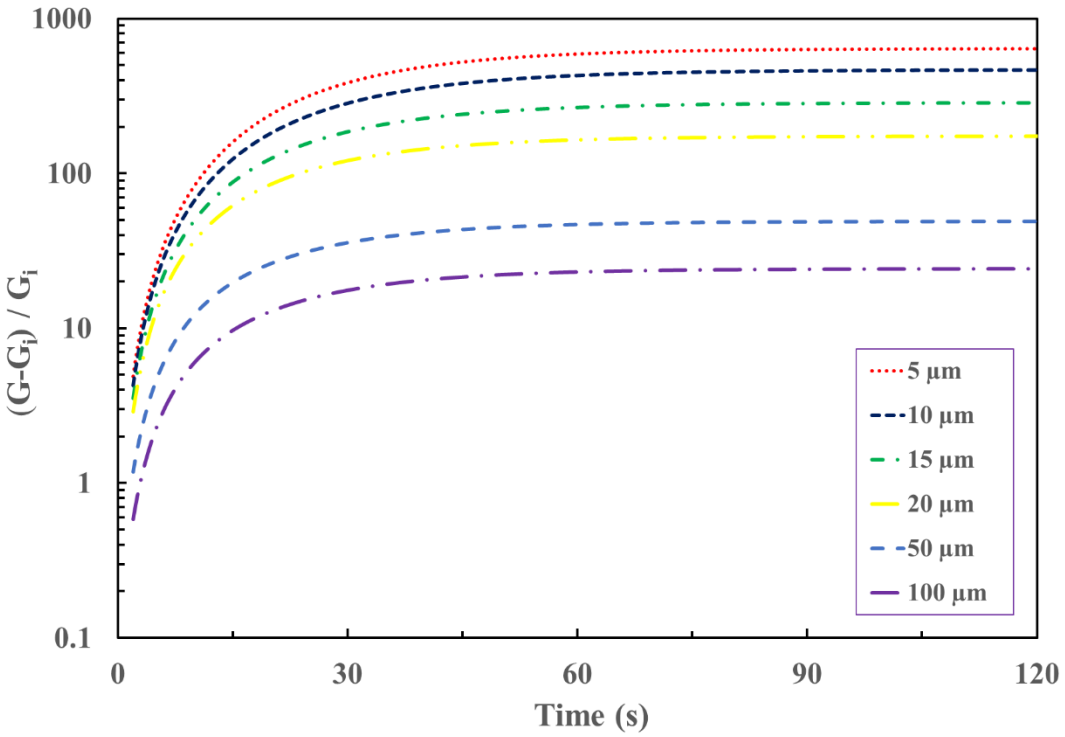


Figure 4-19. Effect of film thickness on the normalized response $(G - G_i)/G_i$ of SnO_2 sensing films for a step change of 0.00814 mol/m^3 in CO concentration in an excess oxygen environment at t=0.(x=500 µm)

Moreover, the influence of film thickness on the response time was analyzed and the results are shown in the *Table 4-4*. The operating temperature for the simulations was $300\,°C$ and pore diameter is 4nm. The response time was defined as the time corresponding to 90% of the total change in response in terms of electrical current. It can be seen from *Table 4-4* differences in response times are not as high as in the case seen that of temperature. Although the diffusion time is comparable with the surface reaction rate of carbon monoxide,the replenishment of the ionized oxygen (the ionization reaction) is relatively slow. So, the surface kinetics determine the response time. This is the reason for higher differences in response times were seen in different temperatures which significantly effect the surface kinetics. The effect of the diffusion

of carbon monoxide cause variations in ionized oxygen density and this effect is pronounced at thicker films. In thinner film on the other hand the reaction rate is also effective in deeper regions where more carbon monoxide could penetrate compared to thicker films. Therefore ionized oxygen is also significantly consumed in deeper regions in thinner films which may be the reason difference in response times since it takes more time to reach a new steady state for higher concentrations of ionized oxygen and carbon monoxide in the film.

Table 4-4. Film Thickness effect on the response times of SnO_2 sensing films for a step change in CO concentration of 0.00814 mol/m^3 at t=0 in an excess oxygen ambient (T=300°C).

Film Thickness (µm)	**Response Time (t_{90}) (s)**
5	56
10	56
15	53
20	49
50	38
100	31

The steady state normalized responses of SnO_2 sensing films with different thicknesses to 0.00814 mol/m^3 concentration of CO in an excess oxygen envirnoment is given in *Figure 4-20.* It is clearly seen that in the SnO_2 film with 5 µm thickness the conductance change is much higher than the conductance change in with a thickness of 100 µm. As previously discussed the conductance change with thickness shows an exponential behavior. In thinner films the effect of film thickness is more pronounced.

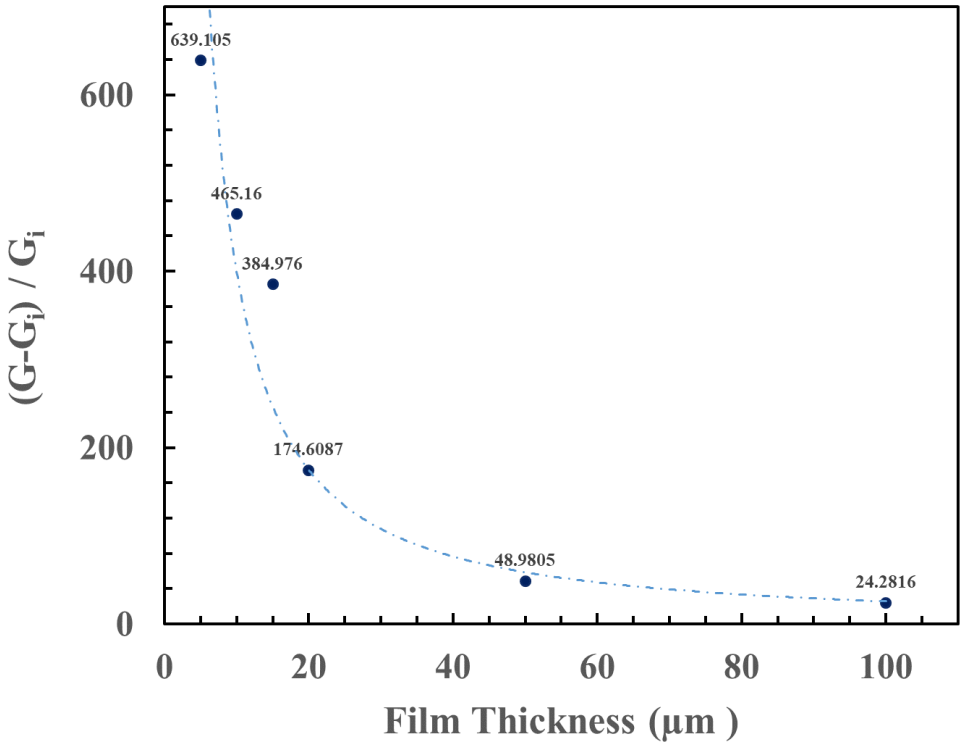


Figure 4-20. Steady state normalized responses of the SnO_2 films having different thicknesses to exposing CO continuously in an excess oxygen ambient.

4.4. Response and Recovery Analysis

The response/recovery analysis for step changes in surface concentration of carbon monoxide was performed for 10 µm thick SnO_2 film with 4 nm pore diameter. Recovery corresponds to gas sensor to return back its initial state where the step change was applied.

Results of the simulations that were performed for the response/recovery cycles at $350°C$ were given in *Figure 4-21* in which C_s refers to the concentration of carbon monoxide in ambient and it has value of 0.00814 mol/m^3 that was used in all simulations of which results are given until this section. In *Figure 4-21b* the ordinate corresponds to the surface concentration of carbon monoxide and the abscissa shows

the time in seconds. Step changes that were applied to surface concentration of carbon monoxide with time can be seen from this plot in which in certain times step changes of $C = C_s; C = 0.5C_s; C = 0.25C_s$ and $C = 0.125C_s$ were applied for response curves and their negative step changes to C=0 were applied for the recovery analysis. In *Figure 4-21a* the response of the metal oxide to applied step changes in terms of electrical current can be seen. Higher current outputs were obtained for higher exposure concentration of carbon monoxide which can be explained by the increase of the rate of consumption of surface ionized oxygen species and the transfer of higher number of electrons to the conduction band of SnO_2 surface. Beside this qualitative analysis also quantitative observation can be made from this plot for the relation between the exposure concentration of carbon monoxide and the current output or sensor response. Taking into considerations of two responses of the sensing film to $C = C_s$ and $C = 0.5C_s$ one can clearly see that the current output does not fall by half but instead lower value and also if one analyzes the other values for different surface concentrations it can be said that there is an exponential relation between the carbon monoxide concentration and the current output.

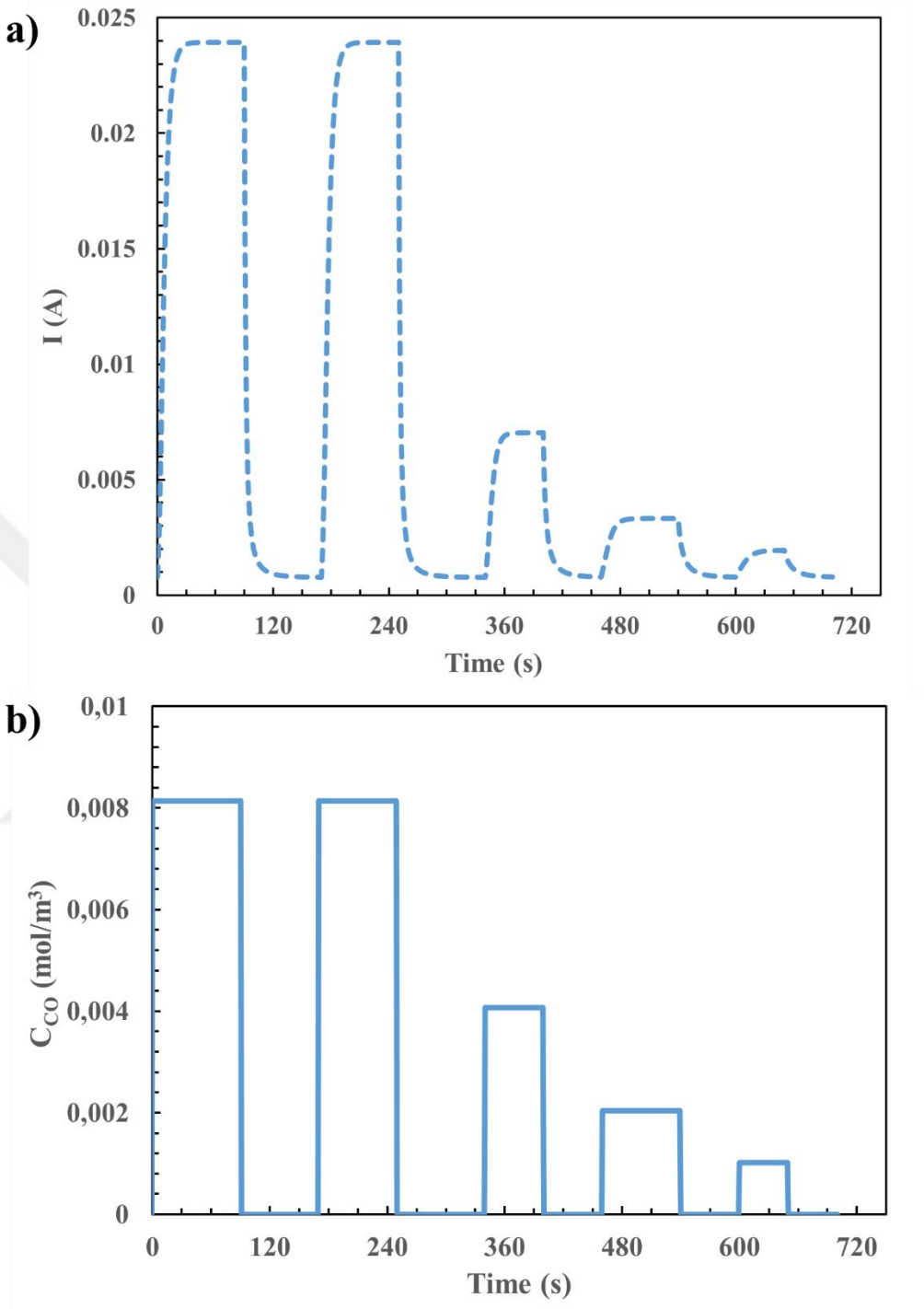


Figure 4-21. Response/recovery analysis of 10µm thick SnO_2 films having 1 nm pore diameter to step changes of carbon monoxide concentration in an excess oxygen ambient at 350 °C.

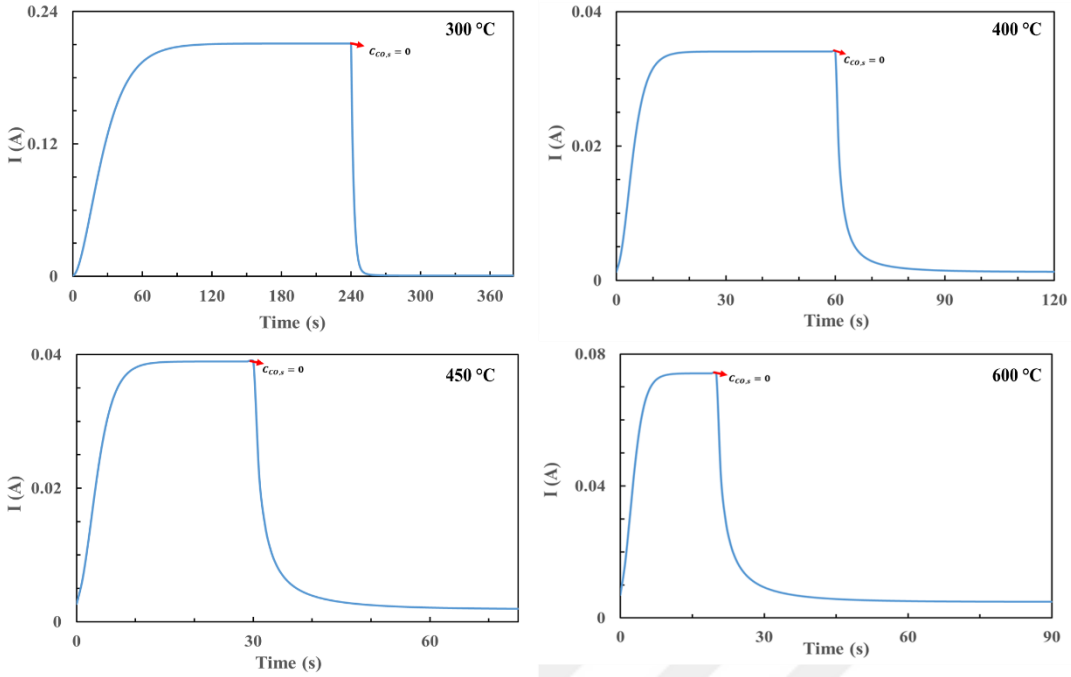


Figure 4-22. The effect of the temperature on the response/recovery dynamics for 10 µm thick SnO_2 film initially exposed to CO concentration of 0.00814 mol/m^3 in an excess oxygen ambient.

The effect of temperature on the sensor response and recovery was examined in 300 – 600 °C temperature range. *Figure 4-22* demonstrates the response and recovery dynamics of 10 µm thick film of SnO_2 with 4 nm pore diameter at different temperatures for the step change of carbon monoxide from 0 to 0.00814 mol/m^3 at t=0 in an excess oxygen ambient. The recovery tests were performed by switching carbon monoxide concentration to zero at the times which are indicated with arrows shown next to the response curves. As stated before when a step change of 0.00814 mol/m^3 was applied to the carbon monoxide concentration at the time that sensor have reached equilibrium with the ambient oxygen, CO concentration at the substrate interphase becomes 72 percent of the surface concentration within a second. So, when a step change to CO concentration from 0.00814 mol/m^3 to 0 mol/m^3 is applied, the carbon monoxide diffuses out from the film within a second. It means that only oxygen

adsorption and ionization steps determines the recovery dynamics, whereas its consumption with carbon monoxide become insignificant. The fast replenishment of the ionized oxygen can be seen in *Figure 4-22* for all cases from the sudden fall in electric current. The rate of consumption of the ionized oxygen with carbon monoxide is significant effect on the replenish of ionized oxygen since it has low activation energy ($E_3 = 5121.42$) and its effect is more pronounced at low temperatures. From *Table 4-5*, one can say that faster responses and recoveries were obtained at higher temperatures and for temperatures higher than 400°C the response and recovery times are same for the same operating temperatures. Since temperature enhances the reaction rates it is an expected situation that recovery and response times get smaller with increasing temperature. The only difference in recovery and response time for the same operating temperature was seen when T=300°C. As stated before at low temperatures the replenish of ionized oxygen is slow and change in the ionized oxygen concentration is high. Therefore, at T=300°C response time is high due to the consumption of ionized oxygen with the carbon monoxide, on the other hand recovery dynamics is fast compared to response dynamics since effect of consumption with carbon monoxide disappear in one seconds. However, at high temperatures that difference between response and recovery times is not seen. The reason of this may be due to the faster replenish of ionized oxygen during response period in which the consumption with carbon monoxide is not dominant as in the low temperatures. This was also seen in *Table 4-2* in which response times are very close to each other at high temperatures. The initial states of the recovery dynamics which is also the steady state responses of the sensor to step change in CO concentration of 0.00814 mol/m^3 in an excess oxygen ambient are different. Hence, the differences in density of ionized oxygen at the initial state (when there is no CO exists in ambient) and steady state density of ionized oxygen which was obtained after exposure to CO can affect the recovery times. As seen in *Figure 4-9* at 300°C the change in ionized oxygen is very high compared to changes at temperatures higher than 400°C which was explained with the slow replenish of ionized oxygen at low temperatures due to relative magnitudes of reaction rates of different steps before. Also at steady states of response

of SnO_2 to continuous exposure to 0.00814 mol/m^3 CO in excess oxygen ambient show that ionized oxygen density distributions are close and change from the initial ionized densities are relatively less. So, the time required to recover of the sensor to its initial state is higher when T=300°C.

Table 4-5. Response and recovery times of SnO_2 film with pore size of 4nm for different temperatures between 300-600°C during step changes in CO concentration in an excess oxygen ambient.

T °C	Response Time (s)	Recovery Time (s)
300	56	14
400	9	9
450	7	7
600	6	7

4.5. Ambient CO Concentration Effect On Response

The ambient concentration of the carbon monoxide was always at the same value for the previously discussed results. At different values of surface concentration of carbon monoxide, the response of the 10 μm SnO_2 based gas sensor for two different pore sizes were simulated. In both *Figure 4-23* and *Figure 4-24* the abscissas show the dimensionless surface concentration values of carbon monoxide and the ordinates show the electrical current output. The θ_s is defined as the ratio of the surface concentration to the specific surface concentration value which was used in all simulations that were analyzed before. Five different surface concentrations which are $C_s/20$, $C_s/8$, $C_s/4$, $C_s/2$ and C_s were used in the simulations to obtain steady state responses. As expected in both gas sensors with pore diameters of 1 nm and 4 nm, the magnitude of the electrical current increases as the surface concentration of carbon monoxide increases. In both plots, it can be seen that at temperatures 300 and $350\ °C$

there is an exponential relation between the surface concentration and the response, however as temperature increases these relations become linear and therefore the difference in responses are small compared to low temperature cases. At low temperatures higher changes in responses were obtained which was explained by primarily with the temperature dependence of activation energies and secondarily with the diffusion effect. That temperature dependence of response change is more pronounced at high surface concentrations for low temperatures.

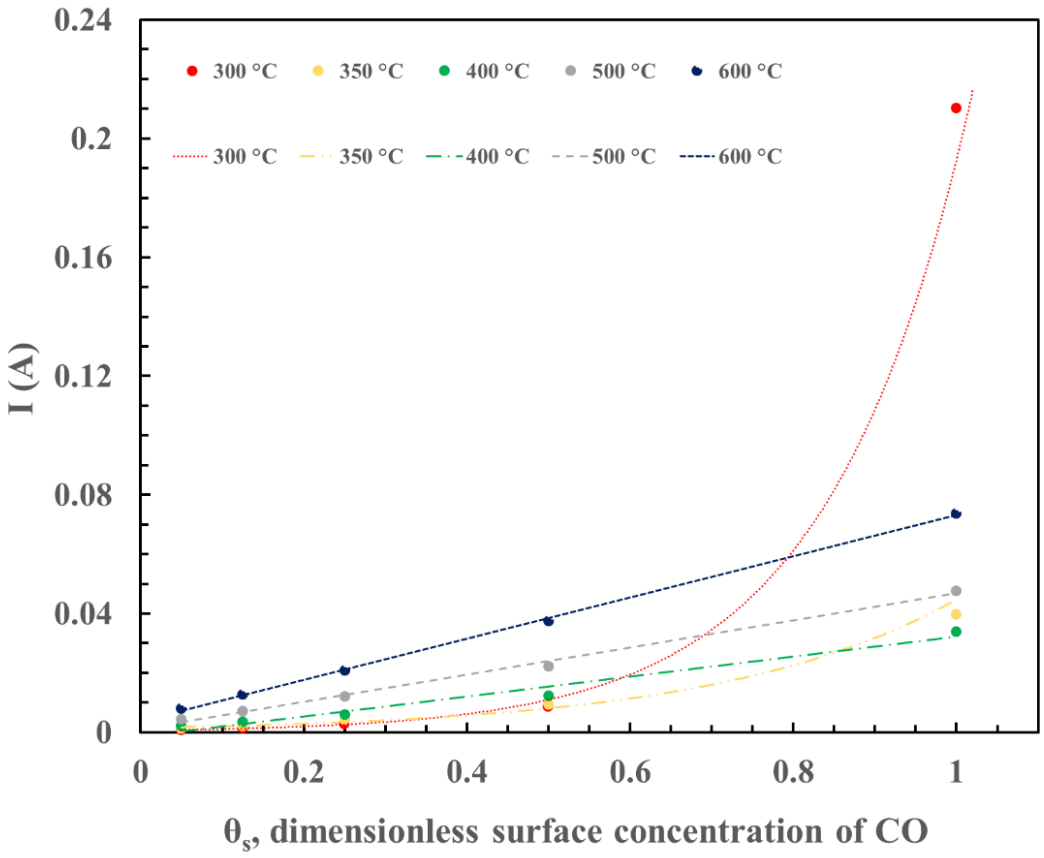


Figure 4-23. The effect of the ambient concentration of carbon monoxide on the steady state electric current response of 10 μm thick SnO_2 gas sensor having pores with 4 nm diameter in an excess oxygen environment.

To analyze the effect of the diffusion, pore diameter was decreased to one quarter of its value. From *Figure 4-24*, it can be seen diffusion effect at same temperature does not influence the exponential dependency however, smaller current values were obtained as pore diameter decreases. Since decreasing pore diameter hinders the diffusion of the carbon monoxide in the film. Thus, mass transfer limitation in the film makes inner regions inefficient compared to the surface and the response changes were decreased. This decrease is more pronounced at low temperatures.

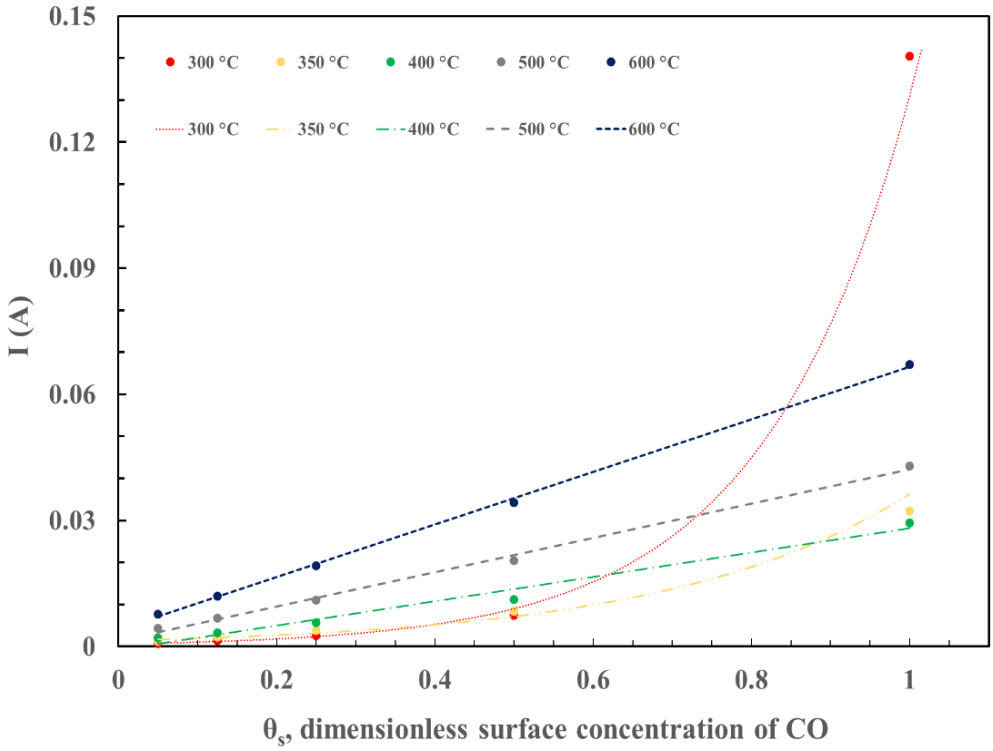


Figure 4-24. The effect of the ambient concentration of carbon monoxide on the steady state electric current response of 10 µm thick SnO_2 gas sensor having pores with 1 nm diameter in an excess oxygen environment.

CHAPTER 5

CONCLUSION

Theoretical study was conducted to analyze the dynamic behavior of n-type metal oxide semiconductor. The results were obtained for an n-type SnO_2 based gas sensor and carbon monoxide as the target gas in an excess oxygen environment. Once the mathematical model was defined in COMSOL Multiphysics® environment, simulations were carried out for analyzing the transient response behavior, the effect of temperature, film thickness and diffusion on the response change and response/recovery time.

The obtained results from simulations showed that diffusion of CO through the SnO_2 film have significant effect on the response. The transient analysis showed that diffusion is fast that the penetration of carbon monoxide from surface to substrate was completed in a few seconds. Therefore, the diffusion time is not the limiting factor the dynamic response time, which is determined by the reaction kinetics. The relative rates of mass transfer and the reaction cause a variation of carbon monoxide concentration along the film thickness. This variation affects the consumption rate of ionized oxygen. Thus, ionized oxygen density variation in the SnO_2 sensing film was seen. Even small differences in ionized oxygen density cause significant variations in conductance and the current density in the film. The response change decreased when the pore size is reduced due to the mass transfer influence. It showed that the control of the pore sizes during synthesis of the sensing films is crucial in order to get higher responses.

One of the most crucial parameter for the gas sensor operation is temperature which was analyzed extensively in this study. The results showed the response/recovery times, magnitude of the response in terms of current and conductance change were

substantially affected from the temperature. Temperature dependence analysis revealed the competitive effect of kinetic parameters, diffusion and conductance. The results of the simulated model provide to gain insight to those complex interactions. The initial equilibrium state of the gas sensor when there is no carbon monoxide exist in the ambient is changed with temperature. It was shown that both ionized oxygen density and the conductance are increased with increase in temperature. This means that when there is no consumption of ionized oxygen with carbon monoxide, the conductance is more sensitive to temperature than the changes in ionized oxygen density. Increase in temperature enhances the reaction between carbon monoxide and the ionized oxygen. Hence, the relative rate of reaction becomes fast compared to kinetics and variations in concentrations of CO and ionized oxygen are more pronounced. This variations cause:

i. Decrease in effectiveness factor.
ii. High ionized oxygen densities and consequently high potential energy barriers in deeper regions of the SnO_2 film.
iii. Significant differences in magnitudes of conductance and current density between regions close to substrate and gas exposed surface.
iv. Lower responses due to relatively unreacted part of the film.

Beside those effects, it was revealed that the most important effect of temperature is on the replenish rate of the ionized oxygen which depends on relative magnitudes of kinetic parameters. The results were analyzed based on how activation energies of the surface reactions are influenced by temperature and it was concluded that:

i. The replenish of ionized oxygen is slow compared to its consumption rate with carbon monoxide.
ii. The difference between replenish and consumption rate of ionized oxygen is more pronounced at low temperatures while, at high temperatures replenish rate become comparable with the consumption rate.
iii. The change in ionized oxygen density

iv. The response in terms of electric current or conductance change is lower at high temperatures since ionized oxygen can be replenished faster.

The increase in operating temperature resulted in the decrease of response times and times required to reach steady state. After 300 °C significant drop in response time was observed. Also the times to reach steady state were closer to each other at high temperatures while the difference in steady state times increases at low temperatures. The faster recovery processes were obtained at high temperatures. On the other hand, almost same response and recovery times were obtained at high temperatures while this difference becomes significant at 300 °C. For temperatures higher than 300 °C, it can be concluded that the replenish rate of the ionized oxygen becomes significant.

The analysis on the film thickness effect on the gas sensor response provided the following conclusions:

i. The limitation of the diffusion can be seen more clearly in thicker films as carbon monoxide and ionized oxygen concentration variations increase which cause significant variations in the potential energy barrier and conductance.
ii. Change in electric current or the average conductance decreases as the film thickness increases.
iii. Deeper regions of the sensing film act as insulator relative to the gas exposed surface in thicker films. This means that the large portion of the film is inefficient in terms of gas sensing. Thus, the selection of the position of the electrodes can be critical in gas sensors in which the diffusion effect is significant.
iv. The lowest response time was obtained in thinnest film and response time decreases slightly as film thickness increases.
v. The change in z component of the current density becomes significant as thickness of the sensing film increases due to the potential difference in z direction.

For various ambient concentrations of carbon monoxide, the response/recovery analyses were also done. It was observed that both response and recovery times slightly increased as the surface concentration decreased. Besides the dynamic analysis, also steady state responses for different ambient concentrations of carbon monoxide were investigated for two different pore diameters. The relation between the surface concentration and the steady state response in terms of electric current was found to be linear at high temperatures and exponential for temperatures lower than 350°C. The same relation found for both cases which means diffusion does not affect surface concentration dependence of the response. However, at the magnitudes were found to be lower in the 1nm pore diameter case due to the effect of the diffusion.

To conclude, the mathematical model successfully demonstrated the complex effect of the parameters on the response behavior. From the simultaneous effects of mass transfer, surface kinetics, charge interactions to electro-physical changes of the microstructure and how those physical and chemical processes affect the conductance and electrical current were extensively discussed. The time dependent simulations provided to get insight the dynamic behavior of the semiconductor gas sensor. The effects of temperature, film thickness, diffusion and ambient concentration of carbon monoxide on the dynamics of response and recovery processes, the current density distribution and the response changes were analyzed in this study.

REFERENCES

1. Moseley, P. T. Solid State Gas Sensors. *Meas. Sci. Technol.* **8**, 223–237 (1997).
2. Kim, I. D., Rothschild, A. & Tuller, H. L. Advances and new directions in gas-sensing devices. *Acta Mater.* **61**, 974–1000 (2013).
3. Righettoni, M., Amann, A. & Pratsinis, S. E. Breath analysis by nanostructured metal oxides as chemo-resistive gas sensors. *Mater. Today* **18**, 163–171 (2015).
4. Sharma, S. & Madou, M. Review article: A new approach to gas sensing with nanotechnology. *Philos. Trans. R. Soc. A* **370**, 2448–2473 (2012).
5. Yamazoe, N. Toward innovations of gas sensor technology. *Sensors Actuators, B Chem.* **108**, 2–14 (2005).
6. Fine, G., Cavanagh, L., Afonja, A. & Binions, R. Metal oxide semiconductor gas sensors in environmental monitoring. *Sensors* **10**, 5469–5502 (2010).
7. Korotcenkov, G., Brinzari, V. & Ham, M. H. Materials Acceptable for Gas Sensor Design: Advantages and Limitations. *Key Eng. Mater.* **780**, 80–89 (2018).
8. Neri, G. First Fifty Years of Chemoresistive Gas Sensors. *Chemosensors* **3**, 1–20 (2015).
9. Wetchakun, K. *et al.* Semiconducting metal oxides as sensors for environmentally hazardous gases. *Sensors Actuators, B Chem.* **160**, 580–591 (2011).
10. Kanan, S. M., El-Kadri, O. M., Abu-Yousef, I. A. & Kanan, M. C. Semiconducting metal oxide based sensors for selective gas pollutant detection. *Sensors* **9**, 8158–8196 (2009).
11. Christopher, K. & Dimitrios, R. A review on exergy comparison of hydrogen

production methods from renewable energy sources. *Energy Environ. Sci.* **5**, 6640–6651 (2012).

12. Korotcenkov, G. Metal oxides for solid-state gas sensors: What determines our choice? *Materials Science and Engineering B* **139**, 1–23 (2007).

13. Capone, S. *et al.* Solid State Gas Sensors: State of the Art and Future Activities. *J. Optoelectron. Adv. Mater.* **5**, 1335–1348 (2003).

14. Barsan, N., Koziej, D. & Weimar, U. Metal oxide-based gas sensor research: How to? *Sensors Actuators B* **121**, 18–35 (2007).

15. Barsan, N., Schweizer-Berberich, M. & Göpel, W. Fundamental and practical aspects in the design of nanoscaled SnO_2 gas sensors: A status report. *Fresenius' Journal of Analytical Chemistry* **365**, 287–304 (1999).

16. Bochenkov, V. E. & Sergeev, G. B. Sensitivity, Selectivity, and Stability of Gas-Sensitive Metal-Oxide Nanostructures. in *Metal Oxide Nanostructures and Their Applications* (eds. Umar, A. & Hahn, Y.-B.) **3**, 31–52 (American Scientific Publishers, 2010).

17. Varma, D. R., Mulay, S. & Chemtob, S. *Carbon Monoxide: From Public Health Risk to Painless Killer*. *Handbook of Toxicology of Chemical Warfare Agents: Second Edition* (Elsevier Inc., 2015). doi:10.1016/B978-0-12-800159-2.00021-X

18. Rahilly, L. & Mandell, D. C. Carbon Monoxide. in *Small Animal Critical Care Medicine* 369–373 (2009). doi:10.1016/B978-1-4160-2591-7.10087-6

19. Figaro Engineering Inc. (2018). Available at: https://www.figaro.co.jp/en/. (Accessed: 6th August 2019)

20. Izawa, K., Ulmer, H., Staerz, A., Weimar, U. & Barsan, N. *Application of SMOX-based sensors*. *Gas Sensors Based on Conducting Metal Oxides* (Elsevier Inc., 2019). doi:10.1016/B978-0-12-811224-3.00005-6

21. Barsan, N. & Schierbaum, K. Introduction. *Gas Sensors Based Conduct. Met. Oxides* 1–11 (2018). doi:10.1016/b978-0-12-811224-3.00014-7

22. Pijolat, C., Sauvan, M., Tournier, G., Lalauze, R. & Pupier, C. Gas detection for automotive pollution control. *Sensors Actuators B Chem.* **59**, 195–202 (1999).

23. Madou, M. J. & Morrison, S. R. *Chemical Sensing with Solid State Devices*. *Chemical Sensing with Solid State Devices* (Academie Press, 1989). doi:10.1016/c2009-0-22258-6

24. Korotcenkov, G. & Cho, B. K. Instability of metal oxide-based conductometric gas sensors and approaches to stability improvement (short survey). *Sensors Actuators B* **156**, 527–538 (2011).

25. Nanto, H., Minami, T. & Takata, S. Zinc-oxide thin-film ammonia gas sensors with high sensitivity and excellent selectivity. *J. Appl. Phys.* **60**, 482–484 (1986).

26. Arshak, K. & Gaidan, I. Development of a novel gas sensor based on oxide thick films. *Mater. Sci. Eng. B* **118**, 44–49 (2005).

27. Penza, M. *et al.* Tungsten trioxide (WO_3) sputtered thin films for a NO_x gas sensor. *Sensors Actuators, B Chem.* **50**, 9–18 (1998).

28. Penza, M., Martucci, C. & Cassano, G. NO_x gas sensing characteristics of WO_3 thin films activated by noble metals (Pd, Pt, Au) layers. *Sensors Actuators, B Chem.* **50**, 52–59 (1998).

29. Aguir, K., Lemire, C. & Lollman, D. B. B. Electrical properties of reactively sputtered WO_3 thin films as ozone gas sensor. *Sensors Actuators, B Chem.* **84**, 1–5 (2002).

30. Gurlo, A. & Riedel, R. Gas Sensors In Situ and Operando Spectroscopy for Assessing Mechanisms of Gas Sensing Angewandte. *Angew. Chemie Int. Ed.* **46**, 3826–3848 (2007).

31. Ding, J., McAvoy, T. J., Cavicchi, R. E. & Semancik, S. Surface state trapping models for SnO2-based microhotplate sensors. *Sensors Actuators, B Chem.* **77**, 597–613 (2001).

32. Lee, J.-H. Technological realization of semiconducting metal oxide–based gas sensors. in *Gas Sensors Based on Conducting Metal Oxides* 167–216 (Elsevier Inc., 2019). doi:10.1016/b978-0-12-811224-3.00004-4

33. Graf, M. *et al.* Metal Oxide-Based Monolithic Complementary Microsystem which comprises for the first time a micro hot plate as. *Anal. Chem.* **76**, 4437–4445 (2004).

34. Bevan, D. J. M. & Anderson, J. S. Electronic conductivity and surface equilibria of zinc oxide. *Discuss. Faraday Soc.* **8**, 238–246 (1950).

35. Wagner, C. The mechanism of the decomposition of nitrous oxide on zinc oxide as catalyst. *J. Chem. Phys.* **18**, 69–71 (1950).

36. Brattain, W. H. & Bardeen, J. Surface Properties of Germanium. *BELL Syst. Tech. J.* **32**, 1–41 (1953).

37. Boudart, M. Electronic Chemical Potential in Chemisorption and Catalysis. *J. Am. Chem. Soc.* **74**, 1531–1535 (1952).

38. Morrison, S. . Surface Barrier Effects in Adsorption, Illustrated by Zinc Oxide. 259–301 (1953).

39. Weisz, P. B. Effects of electronic charge transfer between adsorbate and solid on chemisorption and catalysis. *J. Chem. Phys.* **21**, 1531–1538 (1953).

40. Hauffe, K. The Application of the Theory of Semiconductors to Problems of Heterogeneous Catalysis. *Adv. Catal.* **7**, 213–257 (1955).

41. Heiland, G., Mollwo, E. & Stöckmann, F. Electronic Processes in Zinc Oxide. *Solid State Phys. - Adv. Res. Appl.* **8**, 191–323 (1959).

42. Seiyama, T. & Kagawa, S. Study on a Detector for Gaseous Components Using

Semiconductive Thin Films. *Anal. Chem.* **38**, 1069–1073 (1966).

43. Das, S. & Jayaraman, V. SnO_2: A comprehensive review on structures and gas sensors. *Progress in Materials Science* **66**, 112–255 (2014).

44. Erickson, J. W. & Semancik, S. Surface Conductivity Changes In SnO_2(110): Effects Of Oxygen. *Surf. Sci. Lett.* **187**, 658–668 (1987).

45. Yamazoe, N. & Shimanoe, K. Receptor function and response of semiconductor gas sensor. *J. Sensors* **2009**, 1–21 (2009).

46. Sze, S. M. *Semiconductor Devices: Physics and Technology*. *Wiley* (2002). doi:10.1016/S0026-2692(82)80036-0

47. Bârsan, N., Hübner, M. & Weimar, U. Conduction mechanisms in SnO_2 based polycrystalline thick film gas sensors exposed to CO and H_2 in different oxygen backgrounds. *Sensors Actuators, B Chem.* **157**, 510–517 (2011).

48. Tuller, H. L. Review of electrical properties of metal oxides as applied to temperature and chemical sensing. *Sensors and Actuators* **4**, 679–688 (1983).

49. Barsan, N., Rebholz, J. & Weimar, U. Conduction mechanism switch for SnO_2 based sensors during operation in application relevant conditions; Implications for modeling of sensing. *Sensors Actuators, B Chem.* **207**, 455–459 (2015).

50. Morrison, S. R. *The Chemical Physics of Surfaces*. (Springer US, 1977). doi:10.1007/978-1-4615-8007-2

51. Barsan, N. & Weimar, U. Fundamentals of Metal Oxide Gas Sensors. in *The 14th International Meeting on Chemical Sensors* 618–621 (2012). doi:10.5162/IMCS2012/7.3.3

52. Kohl, D. Surface processes in the detection of reducing gases with SnO2-based devices. *Sensors and Actuators* **18**, 71–113 (1989).

53. Rantala, T. S., Lantto, V. & Rantala, T. T. Rate equation simulation of the height of Schottky barriers at the surface of oxidic semiconductors. *Sensors*

Actuators B **13**–**14**, 234–237 (1993).

54. Korotcenkov, G., Brynzari, V., Golovanov, V. & Blinov, Y. Kinetics of gas response to reducing gases of SnO_2 films, deposited by spray pyrolysis. *Sensors Actuators B* **98**, 41–45 (2004).

55. Hahn, S. H. *et al.* CO sensing with SnO_2 thick film sensors: Role of oxygen and water vapour. in *Thin Solid Films* **436**, 17–24 (2003).

56. Rothschild, A. & Komem, Y. The effect of grain size on the sensitivity of nanocrystalline metal-oxide gas sensors. *J. Appl. Phys.* **95**, 6374–6380 (2004).

57. Yamazoe, N. & Shimanoe, K. Roles of Shape and Size of Component Crystals in Semiconductor Gas Sensors II. Response to NO_2 and H_2. *J. Electrochem. Soc.* **155**, J93–J98 (2008).

58. Yamazoe, N. & Shimanoe, K. Roles of Shape and Size of Component Crystals in Semiconductor Gas Sensors I. Response to Oxygen. *J. Electrochem. Soc.* **155**, J85–J92 (2008).

59. Kida, T., Fujiyama, S., Suematsu, K., Yuasa, M. & Shimanoe, K. Pore and Particle Size Control of Gas Sensing Films Using SnO_2 Nanoparticles Synthesized by Seed-Mediated growth: Design of Highly Sensitive Gas Sensors. *J. Phys. Chem. C* **117**, 17574–17582 (2013).

60. Kocemba, I. & Rynkowski, J. The influence of catalytic activity on the response of Pt/SnO_2 gas sensors to carbon monoxide and hydrogen. *Sensors Actuators, B Chem.* **155**, 659–666 (2011).

61. Hübner, M., Bârsan, N. & Weimar, U. Influences of Al, Pd and Pt additives on the conduction mechanism as well as the surface and bulk properties of SnO_2 based polycrystalline thick film gas sensors. *Sensors Actuators, B Chem.* **171**–**172**, 172–180 (2012).

62. Degler, D. *et al.* Structure and chemistry of surface-doped $Pt:SnO_2$ gas sensing materials. *RSC Adv.* **6**, 28149–28155 (2016).

63. Suematsu, K. *et al.* Role of vanadium oxide and palladium multiple loading on the sensitivity and recovery kinetics of tin dioxide based gas sensors. *RSC Adv.* **6**, 5169–5176 (2016).

64. Gautheron, B., Labeau, M., Delabouglise, G. & Schmatz, U. Undoped and Pd-doped SnO_2 thin films for gas sensors. *Sensors Actuators B* **15**–**16**, 357–362 (1993).

65. Kappler, J., Tomescu, A., Barsan, N. & Weimar, U. CO consumption of Pd doped SnO_2 based sensors. *Thin Solid Films* **391**, 186–191 (2001).

66. Korotcenkov, G. Gas response control through structural and chemical modification of metal oxide films: State of the art and approaches. in *Sensors and Actuators, B: Chemical* **107**, 209–232 (2005).

67. Ahlers, S., Müller, G. & Doll, T. Factors Influencing the Gas Sensitivity of Metal Oxide Materials. in *Encylcopedia of Sensors* (ed. C. A. Grimes, E. C. Dickey, and M. V. P.) 1–35 (American Scientific Publishers, 2006).

68. Schwarz, J. A., Contescu, C. & Contescu, A. Methods for Preparation of Catalytic Materials. *Chem. Rev.* **95**, 477–510 (1995).

69. Binions, R., Carmalt, C. J. & Parkin, I. P. A comparison of the gas sensing properties of solid state metal oxide semiconductor gas sensors produced by atmospheric pressure chemical vapour deposition and screen printing. *Meas. Sci. Technol.* **18**, 190–200 (2007).

70. Becker, T., Ahlers, S., Bosch-v.Braunmühl, C., Müller, G. & Kiesewetter, O. Gas sensing properties of thin- and thick-film tin-oxide materials. *Sensors Actuators B Chem.* **77**, 55–61 (2001).

71. Korotcenkov, G., Han, S. D., Cho, B. K. & Brinzari, V. Grain size effects in sensor response of nanostructured SnO_2- and In_2O_3-based conductometric thin film gas sensor. *Crit. Rev. Solid State Mater. Sci.* **34**, 1–17 (2009).

72. Korotcenkov, G. & Cho, B. K. Thin film SnO_2-based gas sensors: Film

thickness influence. *Sensors Actuators, B Chem.* **142**, 321–330 (2009).

73. Montmeat, P., Lalauze, R., Viricelle, J. P., Tournier, G. & Pijolat, C. Model of the thickness effect of SnO_2 thick film on the detection properties. in *Sensors and Actuators, B: Chemical* **103**, 84–90 (2004).

74. Sukharev, V. Y. Percolation model of adsorption-induced response of the electrical characteristics of polycrystalline semiconductor adsorbents. *J. Chem. Soc. Faraday Trans.* **89**, 559–572 (1993).

75. Ulrich, M., Bunde, A. & Kohl, C. D. Percolation and gas sensitivity in nanocrystalline metal oxide films. *Appl. Phys. Lett.* **85**, 242–244 (2004).

76. McLachlan, D. S., Blaszkiewicz, M. & Newnham, R. E. Electrical Resistivity of Composites. *J. Am. Ceram. Soc.* **73**, 2187–2203 (1990).

77. Scott Kirkpatrick. Percolation Conduction. *Rev. Mod. Phys.* **45**, 15 (1973).

78. Chwieroth, B., Patton, B. R. & Wang, Y. Conduction and Gas-Surface Reaction Modeling in Metal Oxide Gas Sensors. *J. Electroceramics* **6**, 27–41 (2001).

79. Williams, D. E. & Pratt, K. F. E. Microstructure effects on the response of gas-sensitive resistors based on semiconducting oxides. *Sensors Actuators, B Chem.* **70**, 214–221 (2000).

80. Yaghouti Niyat, F. & Shahrokh Abadi, M. H. COMSOL-Based Modeling and Simulation of SnO_2/rGO Gas Sensor for Detection of NO_2. *Sci. Rep.* **8**, 1–12 (2018).

81. Šetkus, A. Heterogeneous reaction rate based description of the response kinetics in metal oxide gas sensors. *Sensors Actuators, B Chem.* **87**, 346–357 (2002).

82. Fort, A., Mugnaini, M., Pasquini, I., Rocchi, S. & Vignoli, V. Modeling of the influence of H_2O on metal oxide sensor responses to CO. *Sensors Actuators, B Chem.* **159**, 82–91 (2011).

83. Brinzari, V. & Korotcenkov, G. Kinetic approach to receptor function in chemiresistive gas sensor modeling of tin dioxide. Steady state consideration. *Sensors Actuators, B Chem.* **259**, 443–454 (2018).

84. Pulkkinen, U., Rantala, T. T., Rantala, T. S. & Lantto, V. Kinetic Monte Carlo simulation of oxygen exchange of SnO_2 surface. in *Journal of Molecular Catalysis A: Chemical* **166**, 15–21 (2001).

85. Zemel, J. N. Theoretical description of gas-film interaction on SnO_x. *Thin Solid Films* **163**, 189–202 (1988).

86. Windischmann, H. & Mark, P. A Model for the Operation of a Thin-Film SnO_x Conductance-Modulation Carbon Monoxide Sensor. *J. Electrochem. Soc. Solid-State Sci. Technol.* **126**, 627–633 (1979).

87. Barsan, N. & Weimar, U. Conduction Model of Metal Oxide Gas Sensors. *J. Electroceramics* **7**, 143–167 (2002).

88. Vilanova, X., Llobet, E., Brezmes, J., Calderer, J. & Correig, X. Numerical simulation of the electrode geometry and position effects on semiconductor gas sensor response. *Sensors Actuators, B Chem.* **48**, 425–431 (1998).

89. Jain, U., Harker, A. H., Stoneham, A. M. & Williams, D. E. Effect of Electrode Geometry on Sensor Response. *Sensors Actuators B. Chem.* **2**, 111–114 (1990).

90. Romppainen, P. & Lantto, V. The effect of microstructure on the height of potential energy barriers in porous tin dioxide gas sensors. *J. Appl. Phys.* **63**, 5159–5165 (1988).

91. Barsan, N., Simion, C., Heine, T., Pokhrel, S. & Weimar, U. Modeling of sensing and transduction for p-type semiconducting metal oxide based gas sensors. *J. Electroceramics* **25**, 11–19 (2010).

92. Rothschild, A. & Komem, Y. Numerical computation of chemisorption isotherms for device modeling of semiconductor gas sensors. in *Sensors and Actuators, B: Chemical* **93**, 362–369 (2003).

93. Nakata, S., Okunishi, H. & Inooka, S. Gas-sensing system based on the cyclic temperature: Further characterization by the second harmonic perturbation. *Anal. Chim. Acta* **517**, 153–159 (2004).

94. Ciobanu, C., Liu, Y., Wang, Y. & Patton, B. R. Numerical calculation of electrical conductivity of porous electroceramics. *J. Electroceramics* **3**, 17–23 (1999).

95. Gardner, J. W. A diffusion-reaction model of electrical conduction in tin oxide gas sensors. *Semicond. Sci. Technol.* **4**, 345–350 (1989).

96. Matsunaga, N., Sakai, G., Shimanoe, K. & Yamazoe, N. Formulation of gas diffusion dynamics for thin film semiconductor gas sensor based on simple reaction-diffusion equation. *Sensors Actuators, B Chem.* **96**, 226–233 (2003).

97. Oprea, A., Degler, D., Barsan, N., Hemeryck, A. & Rebholz, J. Basics of semiconducting metal oxide–based gas sensors. in *Gas Sensors Based on Conducting Metal Oxides* 61–165 (Elsevier Inc., 2019). doi:10.1016/b978-0-12-811224-3.00003-2

98. Clifford, P. K. & Tuma, D. T. Characteristics of Semiconductor Gas Sensors I. Steady State Gas Response. *Sensors and Actuators* **3**, 233–254

99. Clifford, P. K. & Tuma, D. T. Characteristics of semiconductor gas sensors II. transient response to temperature change. *Sensors and Actuators* **3**, 255–281

100. Liu, J. *et al.* The sensor response of tin oxide thin films to different gas concentration and the modification of the gas diffusion theory. *Sensors Actuators, B Chem.* **138**, 289–295 (2009).

101. Yamazoe, N. & Shimanoe, K. Theoretical approach to the gas response of oxide semiconductor film devices under control of gas diffusion and reaction effects. in *Sensors and Actuators, B: Chemical* **154**, 277–282 (Elsevier B.V., 2011).

102. Sakai, G., Matsunaga, N., Shimanoe, K. & Yamazoe, N. Theory of gas-diffusion controlled sensitivity for thin film semiconductor gas sensor. *Sensors*

Actuators, B Chem. **80**, 125–131 (2001).

103. Gardner, J. W. A Non-linear Diffusion-reaction Model of Electrical Conduction in Semiconductor Gas Sensors. 166–170 (1990).

104. Ghosh, A. & Majumder, S. B. Modeling the sensing characteristics of chemi-resistive thin film semi-conducting gas sensors. *Phys. Chem. Chem. Phys.* **19**, 23431–23443 (2017).

105. Gardner, J. W., Iskandarani, M. Z. & Bott, B. Effect of electrode geometry on gas sensitivity of lead phthalocyanine thin films. *Sensors Actuators B. Chem.* **9**, 133–142 (1992).

106. Williams, D. E. & Pratt, K. F. E. Theory of Self-diagnostic Sensor Array Devices using Gas-sensitive Resistors. *J. Chem. Soc. Faraday Trans.* **91**, 1961–1966 (1995).

107. Williams, D. E., Henshaw, G. S. & Pratt, K. F. . Reaction-Diffusion Effects and Systematic Design of Gas-sensitive Resistors based on Semiconducting Oxides. *J. Chem. Soc. Faraday Trans.* **91**, 4299–4307 (1995).

108. Gong, S. *et al.* Gas sensing characteristics of SnO_2 thin films and analyses of sensor response by the gas diffusion theory. *Mater. Sci. Eng. B* **164**, 85–90 (2009).

109. Skafidas, P. D., Vlachos, D. S. & Avaritsiotis, J. N. Modelling and simulation of abnormal behaviour of thick-film tin oxide gas sensors in CO. *Sensors Actuators B. Chem.* **21**, 109–121 (1994).

110. Vilanova, X., Llobet, E., Alcubilla, R., Sueiras, J. E. & Correig, X. Analysis of the conductance transient in thick-film tin oxide gas sensors. *Sensors Actuators, B Chem.* **31**, 175–180 (1996).

111. Gardner, J. W. Electrical conduction in solid-state gas sensors. *Sensors and Actuators* (1989). doi:10.1016/0250-6874(89)87043-X

112. Matsunaga, N., Sakai, G., Shimanoe, K. & Yamazoe, N. Diffusion equation-based study of thin film semiconductor gas sensor-response transient. in *Sensors and Actuators, B: Chemical* **83**, 216–221 (2002).

113. Malagù, C., Guidi, V., Stefancich, M., Carotta, M. C. & Martinelli, G. Model for Schottky barrier and surface states in nanostructured n-type semiconductors. *J. Appl. Phys.* **91**, 808–814 (2002).

114. Yamazoe, N., Shimanoe, K. & Sawada, C. Contribution of electron tunneling transport in semiconductor gas sensor. *Thin Solid Films* **515**, 8302–8309 (2007).

115. Barsan, N. & Weimar, U. Conduction model of metal oxide gas sensors. *J. Electroceramics* (2001). doi:10.1023/A:1014405811371

116. Brynzari, V., Korotchenkov, G. & Dmitriev, S. Simulation of thin film gas sensors kinetics. *Sensors Actuators, B Chem.* **61**, 143–153 (1999).

117. Ahlers, S., Müller, G. & Doll, T. A rate equation approach to the gas sensitivity of thin film metal oxide materials. *Sensors Actuators, B Chem.* **107**, 587–599 (2005).

118. Brynzari, V., Korotchenkov, G. & Dmitriev, S. Theoretical study of semiconductor thin films gas sensors. Attempt to consistent approach. *Electron Technol.* **33**, 225–235 (2000).

119. Fort, A. *et al.* CO sensing with SnO_2-based thick film sensors : Surface state model for conductance responses during thermal-modulation. *Sensors Actuators B Chem.* **116**, 43–48 (2006).

120. Fort, A. *et al.* Simplified models for SnO_2 sensors during chemical and thermal transients in mixtures of inert, oxidizing and reducing gases. *Sensors Actuators, B Chem.* **124**, 245–259 (2007).

121. Ionescu, R. *et al.* Response model for thermally modulated tin oxide-based microhotplate gas sensors. in *Sensors and Actuators, B: Chemical* **95**, 203–211

(2003).

122. Koziej, D., Thomas, K., Barsan, N., Thibault-Starzyk, F. & Weimar, U. Influence of annealing temperature on the CO sensing mechanism for tin dioxide based sensors-Operando studies. *Catal. Today* **126**, 211–218 (2007).

123. Emiroglu, S., Bârsan, N., Weimar, U. & Hoffmann, V. In situ diffuse reflectance infrared spectroscopy study of CO adsorption on SnO_2. *Thin Solid Films* **391**, 176–185 (2001).

124. Ionescu, R., Vasilescu, V. & Vancu, A. Conduction-concentration relationship in chemoresistive thick-film SnO_2 gas sensors. *Sensors Actuators B. Chem.* **8**, 151–154 (1992).

125. Chai, S. *et al.* Effect of phase interaction on catalytic CO oxidation over the SnO_2 /Al_2O_3 model catalyst. *Appl. Surf. Sci.* **402**, 12–20 (2017).

126. Kröger, F. A. & Vink, H. J. Relations between the Concentrations of Imperfections in Crystalline Solids. *Solid State Phys. - Adv. Res. Appl.* **3**, 307–435 (1956).

127. Fuller, M. J. & Warwick, M. E. The catalytic oxidation of carbon monoxide on tin(IV) oxide. *J. Catal.* **29**, 441–450 (1973).

128. Jaffe, L. S. Ambient carbon monoxide and its fate in the atmosphere. *J. Air Pollut. Control Assoc.* **18**, 534–540 (1968).

129. Tsang, W. & Hampson, R. F. Chemical Kinetic Data Base for Combustion Chemistry. Part I. Methane and Related Compounds. *J. Phys. Chem. Ref. Data* **15**, 1087–1279 (1986).

130. Pisani, L. Simple Expression for the Tortuosity of Porous Media. *Transp. Porous Media* **88**, 193–203 (2011).

131. Mirkelamoglu, B. & Karakas, G. CO oxidation over palladium- And sodium-promoted tin dioxide: Catalyst characterization and temperature-programmed

studies. *Appl. Catal. A Gen.* **281**, 275–284 (2005).

132. Mcaleer, J. F., Moseley, P. T., Norris, J. 0 W. & Williams, D. E. Tin Dioxide Gas Sensors. *J. Chem. Soc. Faraday Trans. I* **83**, 1323–1346 (1987).